Final Report

February 1971

Ed file

AVALANCHE DIODE OSCILLATOR CIRCUIT WITH TUNING AT MULTIPLE FREQUENCIES

By: DON PARKER CLARENCE M. ABLOW ROBERT E. LEE
ARTHUR KARP DONALD R. CHAMBERS

Prepared for:

DEPARTMENT OF TRANSPORTATION
TRANSPORTATION SYSTEMS CENTER
55 BROADWAY
CAMBRIDGE, MASSACHUSETTS 02142

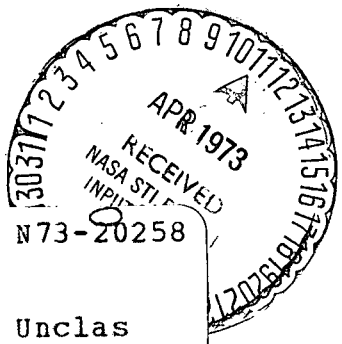

STANFORD RESEARCH INSTITUTE
Menlo Park, California 94025 · U.S.A.

TECHNICAL REPORT STANDARD TITLE PAGE

1. Report No.	2. Government Accession No.	3. Recipient's Catalog No.

4. Title and Subtitle	5. Report Date
AVALANCHE-DIODE OSCILLATOR CIRCUIT WITH TUNING AT MULTIPLE FREQUENCIES	February 1971
	6. Performing Organization Code: Electromagnetic Techniques Laboratory
7. Author(s): Don Parker, Clarence M. Ablow, Robert E. Lee, Arthur Karp, Donald R. Chambers	8. Performing Organization Report No.: SRI Project 8327
9. Performing Organization Name and Address: Stanford Research Institute, Menlo Park, California 94025	10. Work Unit No.
	11. Contract or Grant No.: DOT-TSC-6
12. Sponsoring Agency Name and Address: Department of Transportation, Transportation Systems Center, 55 Broadway, Cambridge, Massachusetts 02142	13. Type of Report and Period Covered: Final Report, 4 December 1969 to 4 December 1970
	14. Sponsoring Agency Code

15. Supplementary Notes

This work was initiated by NASA Electronics Research Center under Contract NAS 12-2231

16. Abstract

Detailed theoretical analysis of three different modes or types of high-efficiency oscillation in a PIN diode are presented. For the TRAPATT mode in a PIN diode, it is shown that a traveling avalanche zone is not necessary to generate a dense "trapped" plasma. An economical computer program for TRAPATT oscillations in a PIN diode is described. Typical results of diode power, dc-to-RF conversion efficiency, and required circuit impedances are presented for several different current waveforms.

A semianalytical solution for a second type of high-efficiency mode in a PIN diode is derived assuming a rectangular current waveform.

A quasi-static approximation is employed to derive a semianalytical solution for the voltage across a PIN diode in a third mode, where avalanching occurs during a major portion of a half cycle. Calculations for this mode indicate that the power increases proportionally to the magnitude of the drive current with a small decrease in efficiency relative to the ordinary TRAPATT mode.

An analytical solution is also given for a PIN diode, where it is assumed that the ionization coefficient is a step function. It is shown that the step-ionization approximation permits one to draw possible patterns of avalanche regions in the depletion layer as a function of time. A rule governing admissible patterns is derived and an example solution given for one admissible pattern.

Preliminary experimental results on the high-efficiency oscillations are presented and discussed. Two different experimental circuits, which used channel-dropping filters to provide independent harmonic tuning, are described. Simpler circuits used to produce high-efficiency oscillations are discussed. Results of experiments using inexpensive Fairchild FD300 diodes are given.

17. Key Words	18. Distribution Statement
Avalanche Diodes High Efficiency Oscillations TRAPATT Oscillations	

19. Security Classif. (of this report)	20. Security Classif. (of this page)	21. No. of Pages	22. Price
UNCLASSIFIED	UNCLASSIFIED	144	9.45

Form DOT F 1700.7 (8-69)

PREFACE

Theoretical and experimental results of high-efficiency oscillations in an avalanche diode are reported. Detailed theoretical analyses of three different modes or types of high-efficiency oscillation in a PIN diode are presented. The results for TRAPATT oscillations in a PIN diode are the most extensive.

The characteristics of TRAPATT oscillations in a PIN diode are discussed and an approximate semianalytical solution for the diode voltage waveform is derived when the diode current is a squarewave. It is shown that a traveling avalanche zone is not necessary to generate a dense "trapped" plasma and that the boundary conditions prevent the trapped plasma from completely filling the depletion layer. Typical voltage waveforms and corresponding diode power, efficiencies, and impedances at the fundamental and higher harmonics are presented. When the diode current is a square wave, the diode does not necessarily exhibit a negative resistance at all higher harmonics.

A computer program for TRAPATT oscillations in a PIN diode is described. Its running time is two or three orders of magnitude less than more exact time-domain computer analyses. Typical results of diode power, dc-to-RF conversion efficiency, and required circuit impedances are presented for several different current waveforms, which are composed of up to the seventh harmonic of a square wave and the first two harmonics of a half-wave sine wave. It is shown that high-efficiency oscillations are possible with diode currents composed of only the fundamental or the fundamental and one higher harmonic.

A second high-efficiency mode is discussed. It is distinguished from the ordinary TRAPATT mode by the fact that, at the beginning of a cycle, the diode voltage is above avalanche and the diode current is small or assumed to be zero, whereas in the ordinary TRAPATT mode the diode voltage is initially high but below avalanche and the diode current is large. A semianalytical solution for this second high-efficiency mode in a PIN diode is derived, assuming a rectangular current waveform. No calculations of diode operating parameters are reported for this mode. This mode is believed to be more representative of the high-efficiency oscillations observed experimentally than is the ordinary TRAPATT mode, when the fundamental frequency is 1/2, 1/3, or 1/4 of the diode transit time frequency.

The third mode of high-efficiency oscillations discussed in this report is similar to the ordinary TRAPATT mode, except that avalanching occurs throughout a major portion of a half cycle rather than only once at the beginning of a cycle to form the "trapped plasma." A quasi-static approximation is employed to derive a semianalytical solution for the voltage across the diode during the multiple avalanche portion of the cycle. This result is then pieced together with the solution for the other portions of a cycle that are similar to the ordinary TRAPATT mode to obtain analytical expressions for the voltage waveform. The current waveform is assumed to be essentially a square wave except the transitions from maximum current to minimum current are not instantaneous.

Preliminary calculations for this mode in a PIN diode indicate that the power increases proportionally to the magnitude of the drive current with a small decrease in efficiency. Since this mode is characterized by large external currents, the optimum circuit impedance for the diode will be less than for the ordinary TRAPATT mode.

An analysis is also given for a PIN diode, where it is assumed that the ionization coefficient is a constant above a critical E-field and is zero for values of E less than the critical field. This approximate analysis permits one to draw possible patterns of avalanche regions in the depletion layer as a function of time. A rule governing admissible patterns is derived; use of this rule has shown that many suggested patterns are inadmissible. One useful family of admissible patterns has been found. It is further shown that, for a given admissible pattern, there are some portions of a cycle where there is a great deal of freedom in the waveshape of the external current. In these time regions the current can be chosen to optimize the dc-to-RF conversion efficiency.

Preliminary experimental results on the high-efficiency oscillations are presented and discussed. Two different experimental circuits, which used channel-dropping filters to provide independent harmonic tuning, are described. These circuits proved to be inadequate for high-efficiency operation because of excessive circuit losses. Simpler circuits used to produce high-efficiency oscillations are discussed. The effects of harmonic tuning in these circuits were determined indirectly from impedance measurements. Inexpensive Fairchild FD300 diodes were used and efficiencies comparable with those obtained by Chaffin and EerNisse were observed. The impedance measurements made on these circuits indicated that these diodes wanted to see a circuit impedance with a small real part at all higher harmonics. These results do not correspond with the theoretical cases considered in the report, where the impedance presented to the diode should be infinite at some of the higher harmonics.

These results tend to substantiate that there are several possible voltage and current waveforms which all give relatively high efficiencies.

Some circuits required for high-efficiency operation are more easily realized than are others.

The authors wish to thank A.I. Grayzel for many stimulating discussions and helpful suggestions during the initial phases of this work.

CONTENTS

ILLUSTRATIONS

TABLES

1. INTRODUCTION

The purpose of this contract was to determine theoretically the operating characteristics of an avalanche diode oscillator when several currents, harmonically related, are flowing in the diode. Emphasis was placed on the high-efficiency modes of oscillation.[1-4] A secondary purpose was to design, construct, and test an avalanche diode experimental circuit that would permit independent tuning of at least two harmonically related frequencies.

Most of the objectives of this contract were accomplished. Significant theoretical results were obtained for the TRAPATT[3,4] mode of oscillation in a PIN diode. A PIN diode was considered because it was felt that the high-efficiency modes were not critically dependent upon the depletion layer doping distribution and the PIN diode simplified the analyses. Indeed it is shown that TRAPATT oscillation can exist in PIN diodes with voltage and current waveforms similar to those calculated by others[3,4] for P^+NN^+ structures. Two other modes or types of high-efficiency oscillations are discussed in this report. It appears that these modes have not been discussed previously in the literature. Approximate semianalytical solutions are given for each of these modes. Whereas considerable calculations were made for various operating characteristics of the TRAPATT mode only preliminary calculations were made for these other high-efficiency modes. Two technical papers based on the theoretical results of this report have already been accepted for publication and a third one is in preparation.[16,17]

The results of the experimental circuits originally intended in this contract were inconclusive. It was hoped that by proper filtering,

a few of the low-order harmonics could be tuned independently to optimize the efficiency. The circuits constructed met the design goal of providing independent tuning but circuit losses and an improper bias supply prevented high-efficiency oscillations from occurring. Simpler circuits were also constructed in which several harmonic currents could flow but could not be controlled independently. The effects of the higher harmonics were determined indirectly by measuring the circuit impedances as viewed from the diode terminals. These experimental results indicate that the observed oscillations do not correspond to the same sets of voltage and current waveforms considered theoretically. The difference between theory and experiment tends to substantiate the fact that there are several distinct operating conditions (hence, different circuit configurations) that lead to high-efficiency operation. Also some circuit impedances are easier to realize than are others when multiple harmonics are involved. Specifically those circuits with a zero real part at higher harmonics are easier to build at microwave frequencies than are those circuits that are open-circuited at higher harmonics.

This report is organized into eight sections including the introduction, conclusion, and recommendations. In the second section we derive a semianalytical solution for TRAPATT oscillations in a PIN diode. Equal ionization coefficients and equal velocities are assumed for both holes and electrons. These assumptions cause the E-field to be symmetrical about the center of the depletion layer of a PIN diode. This in turn simplifies the analysis without changing the essential characteristics of TRAPATT oscillations. These assumptions also made it possible to develop a time-domain computer program for TRAPATT oscillations that is two or three orders of magnitude faster than more exact computer programs. Voltage waveforms for the diode were computed for several different current waveforms using this program. Typical waveforms and computer powers and impedances are given in Section 2.

Section 3 contains a description of a second type of high-efficiency mode. A trapped plasma is generated in this mode as in the ordinary TRAPATT mode. However, in this case, the voltage is driven into avalanche by the diode current, which then drops to zero (or to a small value) while the high field generates sufficient charge to drop the voltage and increase the current again. A semianalytical solution for the diode voltage waveform is derived for a rectangular current waveform. No specific calculations of efficiency or required circuit impedances have been made for this mode. However, it is believed that many experimental observations of high efficiency oscillation may be representative of this mode of operation.

In Section 4 we discuss a third type of high-efficiency oscillation in a PIN avalanche diode. The mode is characterized by very large drive current densities and corresponding avalanching over a major portion of a half cycle of oscillation. In the modes described in Section 2 and 3, it is assumed that the drive current does not exceed a maximum value so that an avalanche does not occur more than once during a cycle. In Section 4 it is shown that if the current is significantly larger than the maximum current mentioned after the initial trapped plasma is partially removed, the diode will break down again. Within a small fraction of a cycle the diode may reach a quasi-static state of continuous breakdown at the edges of the depletion layer while the dense trapped plasma in the center is being removed. When the plasma is removed, the current decreases and the voltage increases for the second half of the cycle. Preliminary calculations of this mode show that the output power increases proportional to the diode current with a small decrease in efficiency compared to the ordinary TRAPATT mode.

Section 5 does not necessarily discuss a different mode of operation, but contains another potentially useful analytical analysis for

moderately high-efficiency oscillations in a PIN diode. By assuming a step function for the ionization coefficient and saturated velocities for the charge carriers, it is possible to divide the depletion layer into avalanching regions and nonavalanching regions. Correspondingly, by an appropriate choice of dependent variable, the telegraphers equation and the wave equation respectively describe the device dynamics. An analytical solution for one admissible pattern in the time-space plane of the junction is given in Section 5. It is shown that the efficiency can be optimized by an appropriate choice of the current waveform in certain portions of a cycle.

A review of the experimental results is contained in Section 6. The several different circuits used are described and their relative merits are discussed.

2. TRAPATT OSCILLATIONS IN A PIN DIODE

The anomalous mode of oscillation in avalanche diodes was first reported by Prager et al.[1*] This mode was characterized by high-efficiency (60 percent) oscillations at frequencies considerably below the diode avalanche frequency. Detailed computer simulations of a high-efficiency mode made by Johnston et al.[2] showed that during part of a cycle of oscillation, a plasma was created in the diode depletion layer and was "trapped" by the low electric field. This mode was called TRAPATT, for Trapped Plasma Avalanche Triggered Transit.

Approximate analytical solutions for the TRAPATT mode in a P^+NN^+ diode have been developed.[3,4] These analyses show that a high-field avalanche "zone" propagates through the diode and fills the depletion layer with a dense plasma of electrons and holes which become trapped in the low-field region behind the "zone." In this section we present an approximate solution for the voltage waveform in a PIN diode that is oscillating in the TRAPATT mode.[†] It is shown that the traveling avalanche "zone" is not essential to generate a trapped plasma. We also show that the boundary conditions confine the trapped plasma to the central portion of the depletion region.

---

*References are listed at the end of the report.

†It has been shown by Muller and Guckel that the dc negative resistance in a PIN diode gives rise to an instability that tends to lead to the formation of current filaments.[5] The oscillations discussed in this section result from a dynamic negative resistance that can be considerably larger than the dc negative resistance and the current filaments should not form.

An approximate solution for the voltage of a PIN diode operating in the TRAPATT mode is derived assuming a square-wave current. A square-wave current was chosen for mathematical convenience although it leads to high-efficiency operation. Expressions for the diode voltage are developed for each of seven separate portions of a cycle as shown in Figure 2-1. The voltage waveform is very similar to that for a P^+NN^+

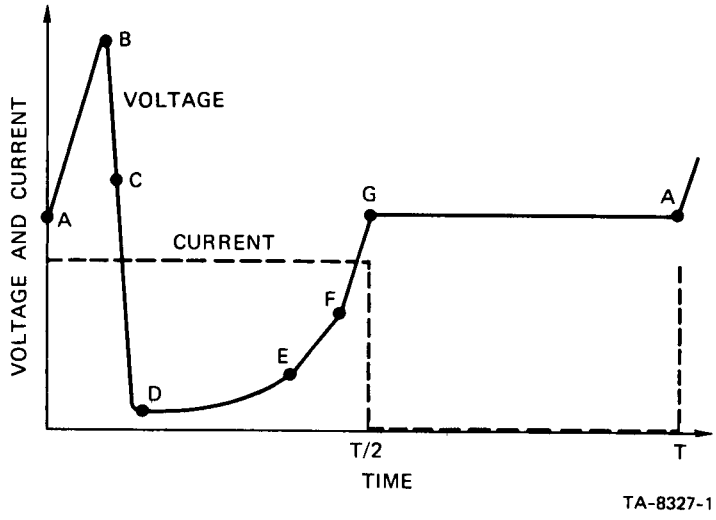

FIGURE 2-1 TYPICAL VOLTAGE WAVEFORM FOR THE TRAPATT MODE OF AN AVALANCHE DIODE ASSUMING A SQUARE-WAVE CURRENT DRIVE

diode.[3] At point A, the E-field is uniform throughout the sample, and its magnitude is large but less than the value required for avalanche breakdown. At this instant, the diode current is turned on. Since the only charge carriers present are those due to thermal generation, the diode initially charges up like a linear capacitor, driving the magnitude of the E-field above the value required for avalanche. When a sufficient number of carriers are generated, the particle current exceeds the external current, and the E-field is depressed throughout the depletion region, causing the voltage to decrease. This portion of the cycle is shown by the curve from point B to point C. During this time

interval, the E-field is sufficiently large for avalanche to continue, and a dense plasma of electrons and holes is created. As some of the electrons and holes drift out of the ends of the depletion layer, the field is further depressed and "traps" the remaining plasma. The voltage decreases to point D. A long time is required to remove the plasma because the total plasma charge is large compared to the charge per unit time in the external current.

At point E the plasma is removed, but a residual charge of electrons remains in one side of the depletion layer and a residual charge of holes in the other side. As the residual charge is removed, the voltage increases from point E to point F. At point F, all the charge that was generated internally has been removed. This charge must be greater than or equal to that supplied by the external current or the voltage will exceed that at point A. This places a limit on the allowable magnitude of the diode current to prevent a second avalanche within the same period. From point F to point G, the diode charges up again like a fixed capacitor. At point G, the diode current goes to zero for half a period, and the voltage remains constant at V_A until the current comes back on and the cycle repeats. The plasma extraction, residual charge extraction, and final charge-up phases of the cycle are as described by others except that $N_D - N_A = 0$ in a PIN diode.

In Sections 2-A through 2-G, approximate expressions for the voltage are derived for each portion of the waveform. These results are used to compute the diode power, impedance, and conversion efficiency at the fundamental and at several harmonics as a function of the diode saturation current and the magnitude of the drive current. The results are only indicative of the diode operation rather than exact calculations of the diode operating characteristics. Equal ionization coefficients for holes and electrons and the same functional dependence on E

for electron and hole velocities were assumed. The essential features of the TRAPATT mode are not obscured by these assumptions.

A time-domain analysis computer program has also been written to model TRAPATT oscillations in a PIN avalanche diode when the current is not a square wave. This program has a running time two or three orders of magnitude less than more exact time-domain computer analyses but exhibits all the essential diode terminal characteristics. The results of the approximate model are compared with those of a more exact computer model over portions of a TRAPATT cycle, and it is shown that the approximate model is relatively accurate. The computer model is used to study several different diode current waveforms. Typical results for diode power, dc-to-RF conversion efficiency, and required circuit impedances are presented for different current waveforms. The obvious advantage of this simplified model is that parametric studies can be made relatively economically.

A. Basic Equations

The electric field, E, the electron density, n, and the hole density, p, in the depletion region of a P-N junction are related by the continuity equations and Poisson's equation. In normalized units these equations are written as follows:*

$$\frac{\partial n}{\partial t} = \frac{\partial J_n}{\partial x} + \alpha v \, [n + p] \qquad (2\text{-}1)$$

$$\frac{\partial p}{\partial t} = -\frac{\partial J_p}{\partial x} + \alpha v \, [n + p] \qquad (2\text{-}2)$$

---

*The normalization is given in Appendix A.

$$\frac{\partial E}{\partial x} = N_D - N_A + p - n \quad , \tag{2-3}$$

where $J_n = vn$, $J_p = vp$, and $\alpha(E)$ is the ionization coefficient and v is the particle velocity. The total external current density, J, can be derived from Eqs. (2-1), (2-2), and (2-3):

$$\frac{\partial E}{\partial t} = - (J_n + J_p) + J \quad . \tag{2-4}$$

The boundary conditions at the edges of the depletion layer are

$$J_p(0) = J_p(x)\Big|_{x=0} = J_s \quad , \tag{2-5a}$$

$$J_n(1) = J_n(x)\Big|_{n=1} = J_s \quad . \tag{2-5b}$$

In a PIN diode, $N_D - N_A$ is zero, and in the absence of internal charge, the E-field is uniform. When the charge density is small or moderate and the average value of the field is high, the E-field is still essentially uniform. When the depletion layer is filled with a plasma, the E-field is uniform throughout the plasma except for a finite gradient near the edges. Therefore, over certain portions of a TRAPATT cycle it is useful to write the equations for a PIN diode under the assumption that the E-field is uniform. To account for the removal of charge by the carriers drifting out of the depletion region, we will introduce a charge relaxation.

Equations (2-1) and (2-2) can be combined to give

$$\frac{\partial \bar{Q}}{\partial t} = \frac{\partial}{\partial x} (J_p - J_n) + 2 \alpha v \bar{Q} \quad , \tag{2-6}$$

where $\bar{Q} = n + p$ and is equal to the total charge density. Integrating with respect to x, and taking α and v outside the integral since E is effectively uniform, we obtain

$$\frac{dQ}{dt} = -(J_p - J_n)\Big|_0^1 + 2\alpha v Q \quad , \tag{2-7}$$

where $Q = \int_0^1 \bar{Q} dx$. If the E-field were exactly uniform, $J_p - J_n$ would be zero, but due to the boundary conditions, $J_p(0) = J_n(1) = J_s$. We approximate $J_p(1)$ and $J_n(0)$ by avQ, where a is some proportionality constant:*

$$\frac{dQ}{dt} = 2v(\alpha - a)Q + 2J_s \quad . \tag{2-8}$$

The charge removed by drift from the depletion layer has been modeled by a relaxation of the total charge. Obviously, this is not strictly correct because all the charges could drift out and J_n and J_p would be zero or J_s.

If we neglect J_s, the solution of Eq. (2-8) is

$$Q = Q_0 \exp\left\{2\int_0^t v(\alpha - a)\, dt\right\} \quad , \tag{2-9}$$

where Q_0 is the charge density at t = 0. Integrating Eq. (2-4) with respect to x and assuming a uniform E-field yields:

---

*It can be shown on a small-signal basis that a more exact approximation for $J_p(1)$ and $J_n(0)$ would be $avQ(t - \tau)$, where τ corresponds to a drift time. For the TRAPATT mode, however, the former approximation is adequate and somewhat simpler.

$$\frac{dE}{dt} = - vQ + J \quad . \tag{2-10}$$

Note that for a uniform field, the normalized terminal voltage is equal to the magnitude of the E-field. Most of the characteristics of the TRAPATT mode for a PIN diode are exhibited by the simple model of an avalanche diode given by Eqs. (2-8) and (2-10). This model is inadequate only during that portion of a cycle when the trapped plasma is being extracted. Since the model assumes that the plasma is removed uniformly across the sample, it does not account for the electric field being larger in those regions of the depletion layer where the plasma has been removed. In Appendix B we show how to correct for the plasma removed from the ends of the depletion layer, and a computer program is described that numerically integrates Eqs. (2-8) and (2-10). Results from this computer program have shown that the proportionality constant, a, is approximately unity in order for all the charge generated during avalanche to equal the integral of the external current over one cycle.

B. Initial Charge-Up Phase

In Figure 2-1, the E-field that corresponds to the voltage at point A is uniform and just below avalanche. Initially the charge density is small, so Eqs. (2-8) and (2-10) can be used to describe the field and the voltage from point A to point B. For an applied constant current density J, the E-field initially increases linearly with time:

$$E = E_A + Jt \quad . \tag{2-11}$$

It continues to increase approximately linearly until vQ equals J, and the voltage has reached its maximum value. From Eq. (2-9) we can

determine the time, t_m, when the voltage reaches its maximum value, if we use an exponential function for α:

$$\alpha = \alpha_o e^{\lambda E} \quad . \tag{2-12}$$

The constants α_o and λ are chosen by fitting the exponential function at two points (say, at $1.5E_A$ and $2E_A$) to the experimental data.[6] Figure 2-2 shows a fit to the data for electrons in silicon.

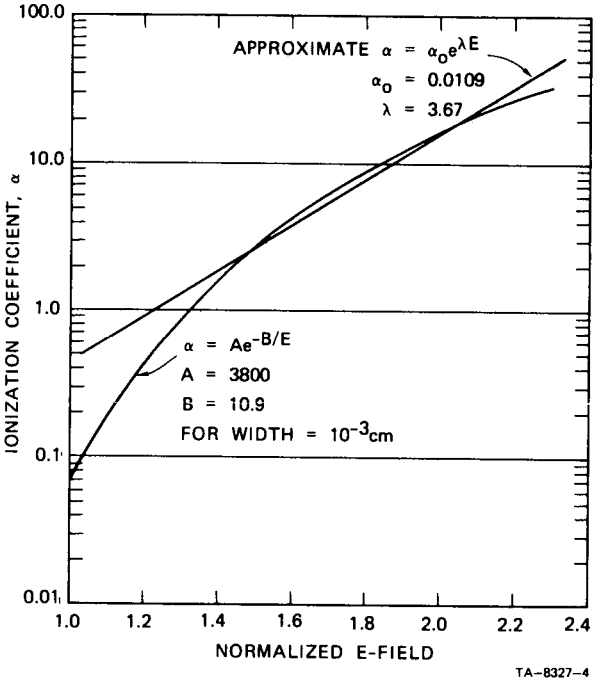

FIGURE 2-2 COMPARISON OF EXPONENTIAL APPROXIMATION OF THE IONIZATION COEFFICIENT FOR ELECTRONS IN SILICON WITH A MORE EXACT FORM

Substituting Eq. (2-11) into Eq. (2-12) and using the result in Eq. (2-9), we obtain

$$Q = Q_s \exp\left\{\frac{2v_s\alpha}{\lambda J}\left[e^{\lambda J t} - 1\right] - 2v_s t\right\} \quad , \tag{2-13}$$

where $Q_s = J_s/v_s$ and $\alpha_A = \alpha(E_A)$. According to our normalization, $v_s = 1$; we retain v_s in our equations for completeness and clarity. We have set the constant, a, equal to unity for the reason discussed earlier. We obtain a transcendental equation for t_m by setting $Q = J/v_s$:

$$t_m = \frac{1}{\lambda J} \ell n \left\{ 1 + \frac{\lambda J}{\alpha_A} \left[t_m + 1/(2v_s) \ell n (J/J_s) \right] \right\} \quad . \qquad (2\text{-}14)$$

An iterative procedure is used to evaluate t_m. Initially, t_m is set equal to zero in the argument of the logarithm, and a first approximation for t_m is obtained. This value is used to obtain a better approximation. Two or three iterations are sufficient if the ratio J/J_s is large.

The voltage from point A to point B is approximately

$$V(t) = V_A + Jt \quad , \quad 0 \leq t \leq t_m \quad . \qquad (2\text{-}15)$$

C. Plasma Generation

During the time from point B to point C in Figure 2-1, a large concentration of holes and electrons is generated in the depletion layer. An accurate calculation of the total charge generated and the corresponding spatial distribution of the E-field requires a computer program that integrates the partial differential equations (2-1), (2-2), and (2-3). We have written such a program, and it will be referred to as UNSAT. Examination of some computer simulations shows that during the short time from point B to point C, the E-field is effectively uniform across the sample except near the boundaries. Therefore, Eqs. (2-9) and (2-10) can also be used during this portion of the TRAPATT cycle.

To obtain an analytical solution for Eqs. (2-9) and (2-10) over the time interval, t_g (from point B to point C), we assume that α is equal to a constant $\alpha_m = \alpha(E_{max})$ for values of E greater than some critical field value, E_c, and is zero for $E < E_c$. This approximation is similar to that used in the analytical solutions of a P^+NN^+ diode.[3,4]

The solution to Eq. (2-8) for constant α and $v = v_s$ is

$$Q(t) = Q_m e^{2v_s(\alpha_m - 1)t} , \qquad (2\text{-}16)$$

where $Q_m = J/v_s$ is the charge density at maximum E-field. Substituting Eq. (2-16) into Eq. (2-10), we obtain for E:

$$E = E_m + J(t-t_m) - \frac{J}{2v_s(\alpha_m - 1)} \left[e^{2v_s(\alpha_m - 1)(t-t_m)} - 1 \right] , \quad t_m \le t \le t_g + t_m . \qquad (2\text{-}17)$$

When $E = E_c$, α is zero, and the avalanche process stops. The time, t_g, required to go from point B to point C can be found from Eq. (2-17) by setting $E = E_c$, and $t = t_m + t_g$:

$$t_g = \frac{1}{2v_s(\alpha_m - 1)} \ell n \left\{ 1 + \frac{2v_s(\alpha_m - 1)}{J} \left[E_m - E_c + Jt_g \right] \right\} . \qquad (2\text{-}18)$$

One can solve for t_g numerically by iteration, as explained earlier for t_m.

It we use the right-hand side of Eq. (2-18) in Eq. (2-16) we obtain an expression for the total charge, Q_p, in the plasma filling the depletion layer:

$$Q_p = Q_m + 2(\alpha_m - 1)\left[E_m - E_c + Jt_g\right] \quad . \tag{2-19}$$

The total number of holes or electrons generated in the time t_g is G:

$$G = \int_{t_m}^{t_g + t_m} v\alpha Q dt \quad . \tag{2-20}$$

Equation (2-20) can be written as

$$G = \alpha_m\left[E_m - E_c + Jt_g\right] \quad . \tag{2-21}$$

An additional negative or positive charge of 1/2 Q_m was generated while the E-field was increasing to its maximum value.

The importance of G is that it must equal the integral of the external current over one period. This condition is used as a check that the times calculated in the approximate solution all add up to the correct period for a square wave. This condition is even more useful for the non-square-wave current waveforms discussed later.

D. Field Depression and Partial Plasma Extraction

We can rewrite Eq. (2-19) in the following form:

$$Q_p = 2G - 2\left[E_m - E_c + Jt_g\right] \quad . \tag{2-22}$$

This equation shows that the plasma charge density throughout the depletion layer is equal to the total charge generated less a quantity

equal to the charge that has drifted out of the depletion layer. It is the drifting charges that actually depress the E-field and stop the avalanche process. The amount of charge that drifts out is equal to that amount required at the edges of the depletion region to drop the field from E_m to E_c plus the charge in the external current during generation.

Beginning at point C in the cycle, we can no longer use the assumption of a uniform E-field. The boundary conditions do not permit a uniform E-field throughout the depletion layer in the presence of large charge densities. At the left boundary the hole current is equal to the saturation current, while the electron current has a large finite value and vice versa at the right-hand boundary. On the other hand, the field inside the plasma region is uniform and equal to some small value determined by the plasma velocity. These two conditions are satisfied simultaneously by the charge carriers in the plasma near the boundaries leaving the depletion layer. A residual charge of one carrier type remains in each end of the depletion layer sufficient to satisfy Poisson's equation and the total current equation.

Initially, when the E-field is still high the carriers in the plasma move at saturated velocity. As the field decreases, the carrier velocity decreases until it reaches the plasma velocity, v_p, given by

$$v_p = J/Q_p \quad , \tag{2-23}$$

where Q_p is given by Eq. (2-22). In the plasma the total change in the E-field is $E_c - E_p$, where E_p is the plasma field. If t_d is the time required for the E-field to change by this amount, then we have,

$$E_c - E_p + Jt_d = \text{Total charge removed during } t_d \quad . \tag{2-24}$$

We assume that all the charge is removed from the ends of the depletion layer within a depth, x_d, from each boundary. The number of holes per unit distance removed near the left boundary is $1/2\ Q_p$; the number of electrons per unit distance removed near the same boundary is $(1/2\ Q_p - n_r)$, where n_r is the residual electron density; thus from Eq. (2-24) we have:

$$E_c - E_p + Jt_d = \int_0^{x_d} (Q_n - n_r)dx \quad . \tag{2-25}$$

The residual charge would be equal to

$$n_r = \frac{1}{v}\left[J - \frac{\partial E}{\partial t}\right] \quad , \tag{2-26}$$

which is a function of both time and position. Only the final value of the residual charge density and the value of x_d when the field in the plasma has dropped to E_p are of primary interest because this phase of the TRAPATT cycle happens quickly. These quantities determine the minimum voltage at point D and the amount of charge that must be removed at the plasma velocity. We assume that at point D, n_r is uniform in the region from the boundary to the plasma. Then the E-field has the following distribution at the left edge of the depletion layer:

$$E = E_p + n_r(x_d - x) \ , \quad 0 \le x \le x_d \quad . \tag{2-27}$$

A similar expression can be written for the E-field at the right boundary.

Since $x_d = v_p t$, the partial derivative with respect to time of Eq. (2-27) when substituted into Eq. (2-26) gives

$$n_r = J/(v + v_p) \quad . \tag{2-28}$$

The velocity, v, depends upon the E-field, which in turn is a function of n_r. We will assume $v = v_s$ as a first approximation; then Eq. (2-26) becomes

$$E_c - E_p + Jt_d = \left[Q_p - \frac{1}{(v_s + v_p)}\right] x_d \quad . \tag{2-29}$$

An estimate of t_d can be obtained from the fact that the holes traverse the distance x_d with some average velocity, v_a. The initial velocity is v_s and the final velocity at point D is v_p; we use a simple average as a first approximation:

$$t_d = \frac{2x_d}{v_s + v_p} \tag{2-30}$$

and

$$x_d = \frac{E_c - E_p}{Q_p - \dfrac{3J}{(v_s + v_p)}} \quad . \tag{2-31}$$

We have not developed an expression for the voltage during the transition from point C to point D. This time is short and the voltage variation large; we assume simply a linear relationship:

$$V(t) = V_c - (V_c - V_p) \frac{t-(t_m + t_g)}{t_d} \quad , \quad t_m + t_g \leq t \leq t_m + t_g + t_d \quad , \tag{2-32}$$

where

$$V_p = E_p + n_r x_d^2 \quad .$$

This approximation should not affect any low-frequency components of the voltage waveform.

E. Plasma Extraction

The plasma is extracted by the external current as the voltage moves from point D to point E. During this time, the E-field inside the plasma is time-invariant and uniform. The edges of the plasma move toward the center of the depletion layer with the velocity v_p and leave a residual charge of electrons on one side of the depletion layer and of holes on the other side. The plasma exists until the right- and left-hand edges of the plasma meet at the center of the depletion layer. The time, t_p, required to remove the plasma is

$$t_p = \frac{Q_p(0.5 - x_d)}{J} \quad . \tag{2-33}$$

As the plasma is extracted, the electric field between the left edge of the depletion layer and the left edge of the plasma, x_p, is given by

$$E = E_p + n_r(x_p - x) \quad , \quad 0 \le x \le x_p \quad , \tag{2-34}$$

and the voltage across the device is

$$V = E_p + n_r x_p^2 \quad . \tag{2-35}$$

The distance, $x_p = v_p t$, increases linearly with time until it equals 0.5. If $t_1 = t_m + t_g + t_d$ and $t_2 = t_1 + (0.5 - x_d)/v_p$, then the voltage is

$$V(t) = E_p + \frac{Jx_d^2}{v_s + v_p} + \frac{Jv_p^2}{v_s + v_p}(t-t_1), \quad t_1 \le t \le t_2 \quad , \tag{2-36}$$

while the plasma is being removed.

It was assumed for the voltage waveform shown in Figure 2-1 that avalanche occurred only once during a cycle. To prevent a second avalanche, the current J must not exceed a maximum value, J_{max}.* The maximum current can be obtained from a consideration of Eq. (2-34). At x = 0, E cannot exceed E_A, the value of the field at the beginning of the cycle, or

$$E_A - E_p \ge \frac{Jx_p}{(v_s + v_p)} \quad . \tag{2-37}$$

The field reaches its peak value when $x_p = 0.5$; thus,

$$J \le 2 (E_A - E_p) (v_s + v_p) \quad , \tag{2-38}$$

which agrees with DeLoach and Scharfetter.[4]

F. Residual Charge Extraction

When the plasma is completely removed at point E, a residual charge of electrons exists on the left-hand side of the depletion layer and a similar residual charge of holes exists on the right half of the depletion layer. The time required to remove the residual charge is of the

---

*This second avalanche is the same as the "premature avalanche" discussed by Clorfeine et al.[3]

order of half a transit time. As the residual charge is removed, the field in the center increases. From Eq. (2-34) and the fact that $x_p = 0.5$ when the voltage is at point E, we can write for the field on the left side of the depletion region:

$$E(x) = E_p + n_r(0.5 - x) \quad , \quad 0 \leq x \leq x_r \quad , \tag{2-39}$$

where x_r is the extent of the residual charge from the left boundary. The value of x_r decreases linearly with time:

$$x_r = 0.5 - v_s(t-t_2) \quad , \quad t_2 \leq t \leq t_3 \quad , \tag{2-40}$$

where $t_3 = t_2 + 1/2v_s$. The corresponding terminal voltage is

$$V(t) = E_p + \frac{J(1 + 2v_s(t-t_2))}{4(v_s + v_p)} \quad , \quad t_2 \leq t \leq t_3 \quad . \tag{2-41}$$

The voltage increases linearly with a slope approximately equal to one-half that for a charge-free region.

G. Final Charge-Up Phase

At point F all the charge is removed and the field is uniform across the sample again. Since the field is below avalanche breakdown, the diode charges up like a linear capacitor. The voltage is

$$V(t) = E_p + \frac{J}{2(v_s + v_p)} + J(t-t_3) \quad , \quad t_3 \leq t \leq T/2 \tag{2-42}$$

The time required for this final charge-up phase depends on the value of the voltage at point F. When J equals the maximum allowable current, the voltage reaches V_A just as the last of the residual charge leaves the depletion layer and no additional time is required. For smaller currents, additional external charge is necessary to charge the diode back up to V_A.

H. Calculations

The semianalytical solution has been used to calculate the performance of a PIN diode with a 10-micron-wide depletion layer. The normalized low-field velocity, v, was assumed to be ten times the electric field. The expression of Scharfetter and Gummel for the electron ionization coefficient in silicon was assumed to correspond to the experimental data for the ionization coefficient.[6]

Figure 2-3 shows the normalized fundamental impedance of a PIN diode operating in a TRAPATT mode for three levels of a square-wave drive current. The different levels of the saturation current correspond to different thermal generation rates of carriers in the diode; the lower the level of the saturation current, the smaller the thermal generation. It is evident from Figure 2-3 that the higher the level of the drive current, the smaller the variation in the fundamental impedance over several orders of magnitude of the saturation current.

Tables 2-1, 2-2, and 2-3 show the normalized period, T, power, P_i, and impedance, Z_i, corresponding to the results shown in Figure 2-3. The fundamental frequency for each data point is different; in fact, for a given drive current, the frequency varies over an octave, with the range of saturation currents shown. Also, the diode impedances at higher harmonics change appreciably. These results for a square-wave current indicate that at the higher harmonics, the diode furnishes

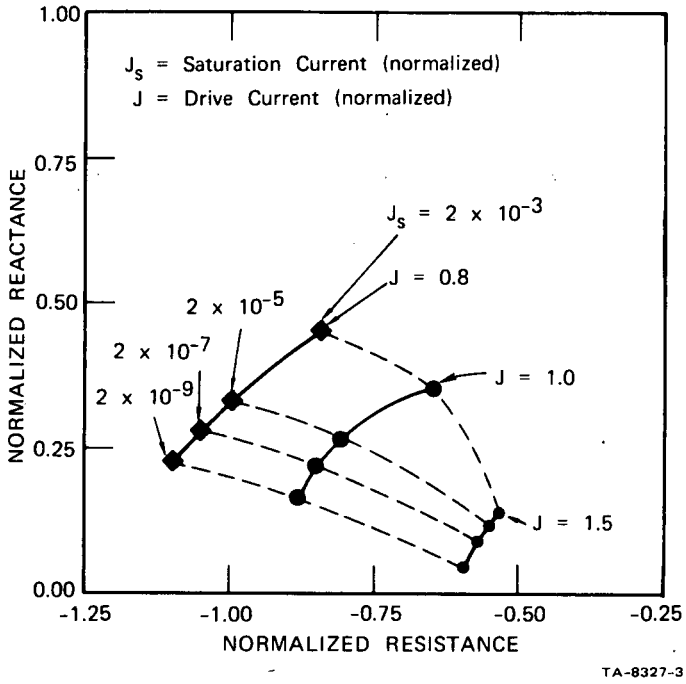

FIGURE 2-3 NORMALIZED FUNDAMENTAL IMPEDANCE OF PIN DIODE OPERATING IN A TRAPATT MODE WITH A SQUARE-WAVE CURRENT DRIVE

power for small saturation currents and high drive levels, but that ac power must be furnished to it for large saturation currents and low drive currents. The choice of a square-wave drive current was arbitrary and made to simplify the analysis in the analytical solution. In practice, the diode would always be placed in a passive circuit, and the diode impedances would change accordingly.

The results shown in Figure 2-3 and Tables 2-1, 2-2, and 2-3 are based upon a particular choice of parameter values used in the semi-analytical solution.

The parameter, R, is the ratio of the maximum value of the ionization coefficient, α_m, to that value of the ionization coefficient, α_c, below which we assume that avalanche stops and the ionization coefficient drops to zero. By comparing the results of a more exact computer

Table 2-1

NORMALIZED PERIOD, T, POWERS, P_i, AND IMPEDANCES, Z_i, FOR A PIN AVALANCHE DIODE OPERATING IN THE TRAPATT MODE, WITH A SQUARE-WAVE CURRENT DRIVE, AS COMPUTED BY THE ANALYTICAL SOLUTION

($J = 1.5$, $E_A = 1.0$, $R = 2.5$)

Normalized Parameter	$J_s = 2 \times 10^{-9}$	$J_s = 2 \times 10^{-7}$	$J_s = 2 \times 10^{-5}$	$J_s = 2 \times 10^{-3}$
Period	25.5	20.0	15.4	10.0
P_0	0.473	0.483	0.500	0.535
P_1	-0.266	-0.263	-0.255	-0.234
P_3	-0.019	-0.015	-0.009	+0.005
P_5	-0.002	-0.001	+0.006	+0.011
P_7	+0.002	-0.004	+0.006	+0.005
Z_0	0.840	0.858	0.888	0.951
Z_1	-0.584 + j 0.058	-0.576 + j 0.080	-0.560 + j 0.112	-0.513 + j 0.168
Z_3	-0.374 + j 0.306	-0.304 + j 0.336	-0.176 + j 0.360	+0.105 + j 0.316
Z_5	-0.083 + j 0.406	+0.070 + j 0.383	+0.310 + j 0.275	+0.630 - j 0.120
Z_7	+0.252 + j 0.346	+0.447 + j 0.206	+0.657 - J 0.110	+0.534 - j 0.707

Table 2-2

NORMALIZED PERIOD, T, POWERS, P_i, AND IMPEDANCES, Z_i, FOR A PIN AVALANCHE DIODE OPERATING IN THE TRAPATT MODE, WITH A SQUARE-WAVE CURRENT DRIVE, AS COMPUTED BY THE ANALYTICAL SOLUTION

($J = 1.0$, $E_A = 1.0$, $R = 2.4$)

Normalized Parameter	$J_s = 2 \times 10^{-9}$	$J_s = 2 \times 10^{-7}$	$J_s = 2 \times 10^{-5}$	$J_s = 2 \times 10^{-3}$
Period	23.9	19.6	15.0	10.6
P_0	0.323	0.333	0.349	0.384
P_1	-0.177	-0.172	-0.162	-0.134
P_3	-0.008	-0.004	+0.003	+0.014
P_5	+0.003	+0.005	+0.007	+0.006
P_7	+0.004	+0.004	+0.003	-0.002
Z_0	1.291	1.331	1.398	1.53
Z_1	-0.875 + j 0.182	-0.849 + j 0.218	-0.797 + j 0.271	-0.659 + j 0.353
Z_3	-0.365 + j 0.537	-0.185 + j 0.54	+0.118 + j 0.471	+0.636 + j 0.109
Z_5	+0.327 + j 0.454	+0.611 + j 0.242	+0.910 - j 0.219	+0.710 - j 1.052
Z_7	+0.879 - j 0.060	+1.000 - j 0.525	+0.755 - j 0.193	-0.481 - j 0.973

Table 2-3

NORMALIZED PERIOD, T, POWERS, P_i, AND IMPEDANCES, Z_i, FOR A PIN AVALANCHE DIODE OPERATING IN THE TRAPATT MODE, WITH A SQUARE-WAVE CURRENT DRIVE, AS COMPUTED BY THE ANALYTICAL SOLUTION

($J = 0.8$, $E_A = 1.0$, $R = 2.4$)

Normalized Parameter	$J_s = 2 \times 10^{-9}$	$J_s = 2 \times 10^{-7}$	$J_s = 2 \times 10^{-5}$	$J_s = 2 \times 10^{-3}$
Period	25.0	20.5	16.0	11.2
P_0	0.259	0.266	0.278	0.303
P_1	-0.142	-0.138	-0.130	-0.111
P_3	-0.006	-0.003	+0.002	+0.011
P_5	+0.003	+0.004	+0.006	+0.005
P_7	+0.003	+0.001	+0.002	-0.002
Z_0	1.617	1.664	1.740	1.893
Z_1	-1.096 + j 0.238	-1.064 + j 0.276	-1.005 + j 0.330	-0.852 + j 0.412
Z_3	-0.404 + j 0.657	-0.188 + j 0.643	+0.167 + j 0.546	+0.765 + j 0.138
Z_5	+0.505 + j 0.467	+0.821 + j 0.190	+1.136 - j 0.348	+0.914 - j 1.271
Z_7	+1.147 - j 0.282	+1.220 - j 0.822	+0.861 - j 1.467	-0.587 - j 1.226

simulation (UNSAT) with those of the analytical solution, over the initial charge-up and generation phases of a TRAPATT cycle, we found that the value of R differs for different drive currents. Figure 2-4(a), (b), and (c) compare the amount of total charge generation as a function of the saturation current as calculated by the computer simulation (UNSAT) and by the analytical solution. Note that for J = 0.9, R is 2.4; whereas for J = 1.0 and 1.5, R is 2.4 and 2.5, respectively. Since the diode fundamental period of oscillation for a square-wave drive current is equal to twice the generation divided by the current magnitude, Figure 2-4 can be used to determine the frequency.

We have also made a comparison of the diode voltage as a function of time as computed by the approximate analytical solution and by the exact computer simulation (UNSAT) over the initial charge-up and charge generation phases of the TRAPATT cycle. These results are shown in Figure 2-5(a) and (b) for two different drive levels. The results from the approximate analytical solution are quite good. A comparison was not made over a longer portion of the cycle because of the excessive running times required for the exact computer simulation.

I. Nonsquare-Wave Current Waveforms

Several other current waveforms were investigated using the computer program modified SMPAL described in Appendix B. For example, current waveforms composed of the first few nonzero harmonics of a square-wave were used. The relative magnitudes and phases of the harmonics were the same as for a square wave. Figures 2-6 and 2-7 show the normalized voltage waveforms for currents composed of the first and third harmonics and of the first, third, and fifth harmonics, respectively.

Table 2-4 lists the powers and diode impedances corresponding to Figures 2-6 and 2-7. Comparison of Table 2-4 with Tables 2-1 and 2-2

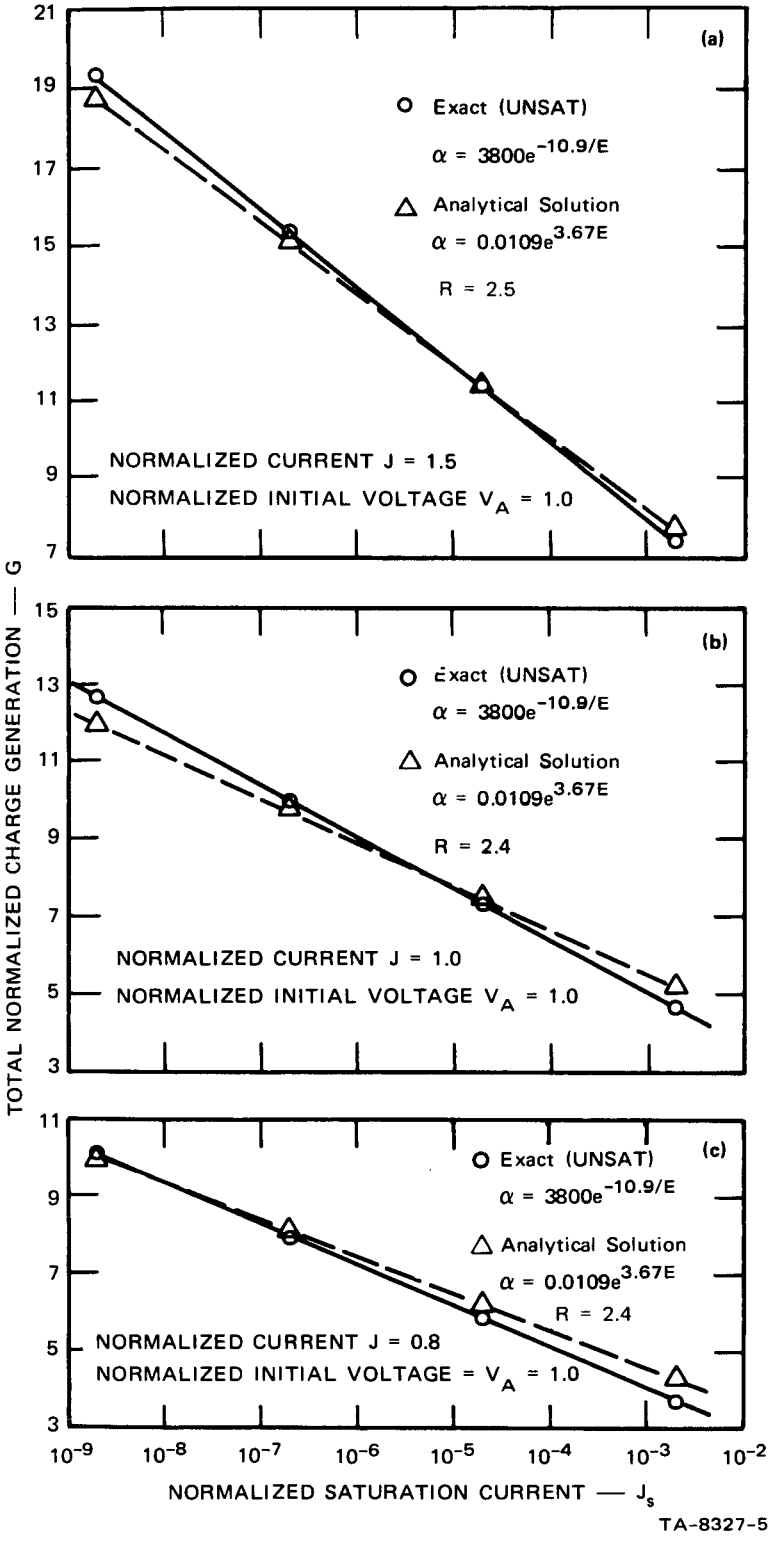

FIGURE 2-4 TOTAL NORMALIZED CHARGE GENERATION DURING ONE CYCLE OF THE TRAPATT MODE IN A PIN DIODE

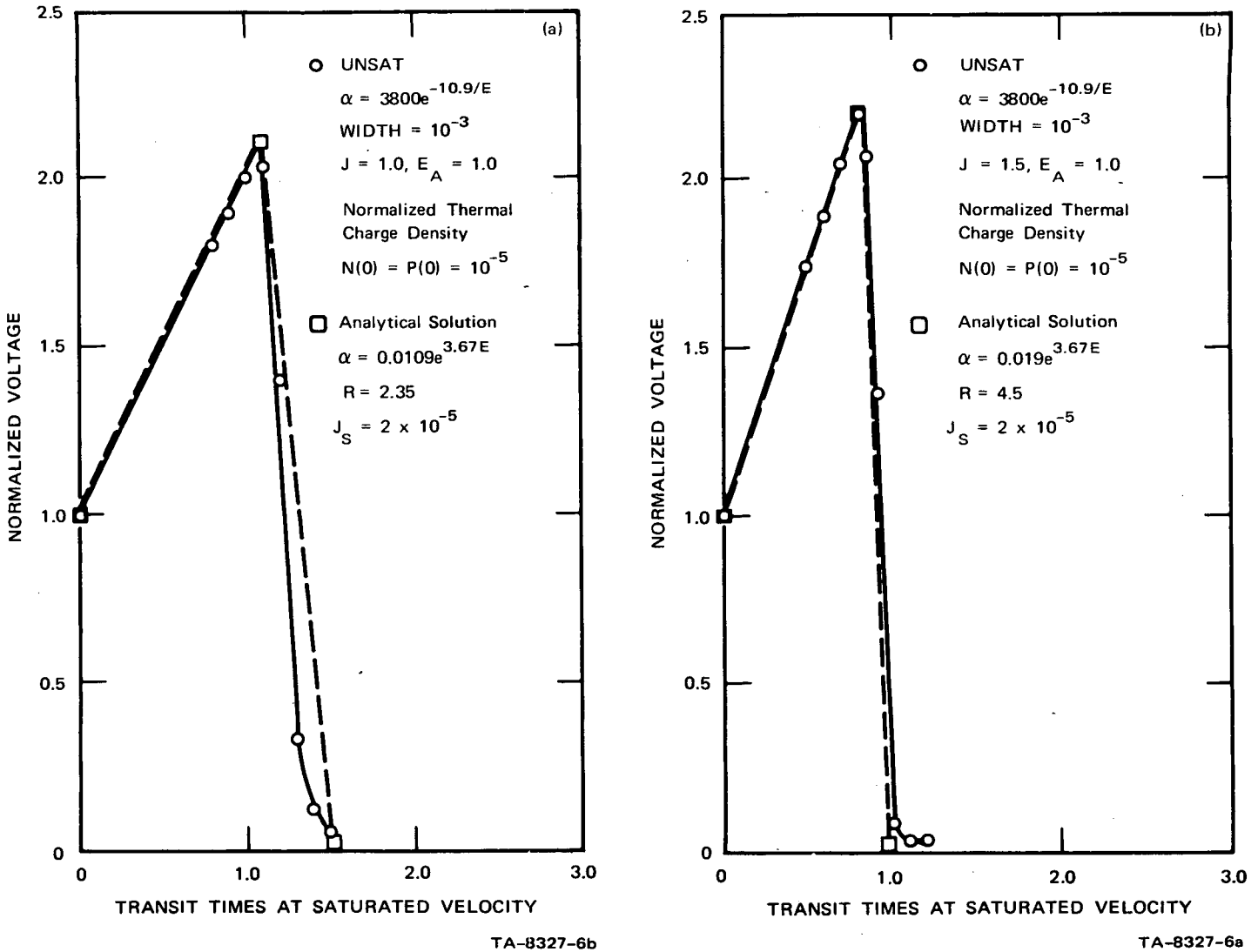

FIGURE 2-5 COMPARISON OF THE NORMALIZED VOLTAGE DURING THE INITIAL CHARGE-UP AND GENERATION PHASES OF THE TRAPATT MODE IN A PIN DIODE, AS COMPUTED BY UNSAT AND BY THE ANALYTICAL SOLUTION

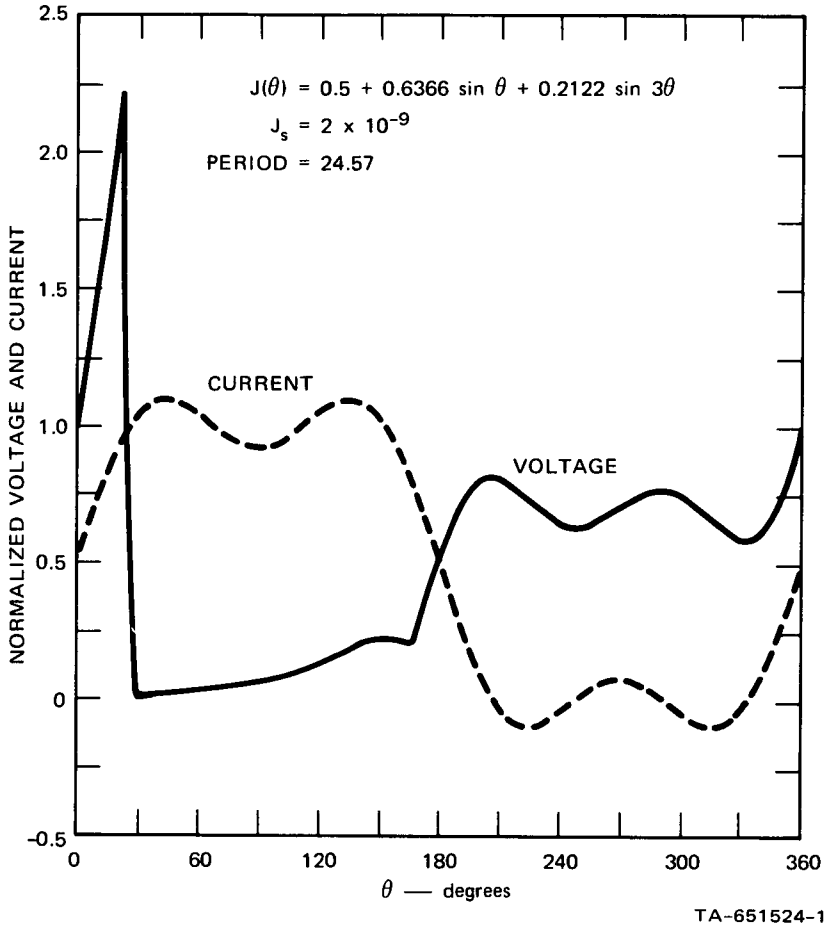

FIGURE 2-6 NORMALIZED VOLTAGE AND CURRENT WAVEFORMS FOR THE TRAPATT MODE WITH A CURRENT USING THE FIRST AND THIRD HARMONICS OF A SQUARE WAVE

shows that for the same J_s and J, the fundamental period is about the same for the nonsquare-wave waveform. This is a consequence of the fact that the currents in Figures 2-6 and 2-7 do charge the diode up about as rapidly as does a squarewave current. For the assumed operating conditions in Figures 2-6 and 2-7, power must be fed to the diode at the third and fifth harmonics.

Table 2-4

NORMALIZED PERIOD, T, POWERS, P_i, AND IMPEDANCES, Z_i, FOR A PIN AVALANCHE DIODE FOR A NORMALIZED DRIVE CURRENT USING UP TO THE SEVENTH HARMONICS OF A SQUARE WAVE, AS COMPUTED BY MODIFIED SMPAL

($V_A = 1.0$, $J_s = 2 \times 10^{-9}$)

$J = A[0.5 + 0.6366 \sin\theta + 0.2122 \sin 3\theta + 0.1273 \sin 5\theta + 0.0909 \sin 7\theta]$

Normalized Parameter	Three Harmonics A = 1.0	Five Harmonics A = 1.5	Seven Harmonics A = 1.5
Period	24.57	24.90	26.4
P_0	0.26	0.383	0.41
P_1	-0.10	-0.15	-0.16
P_3	+0.004	-0.0002	-0.006
P_5	--	+0.007	+0.004
P_7	--	--	+0.005
Z_0	1.04	0.68	0.73
Z_1	-0.51 + j 0.24	-0.32 + j 0.08	-0.35 + j 0.04
Z_3	+0.17 + j 0.66	-0.003 + j 0.40	-0.11 + j 0.44
Z_5	--	+0.40 + j 0.43	+0.20 + j 0.44
Z_7	--	--	+0.50 + j 0.32

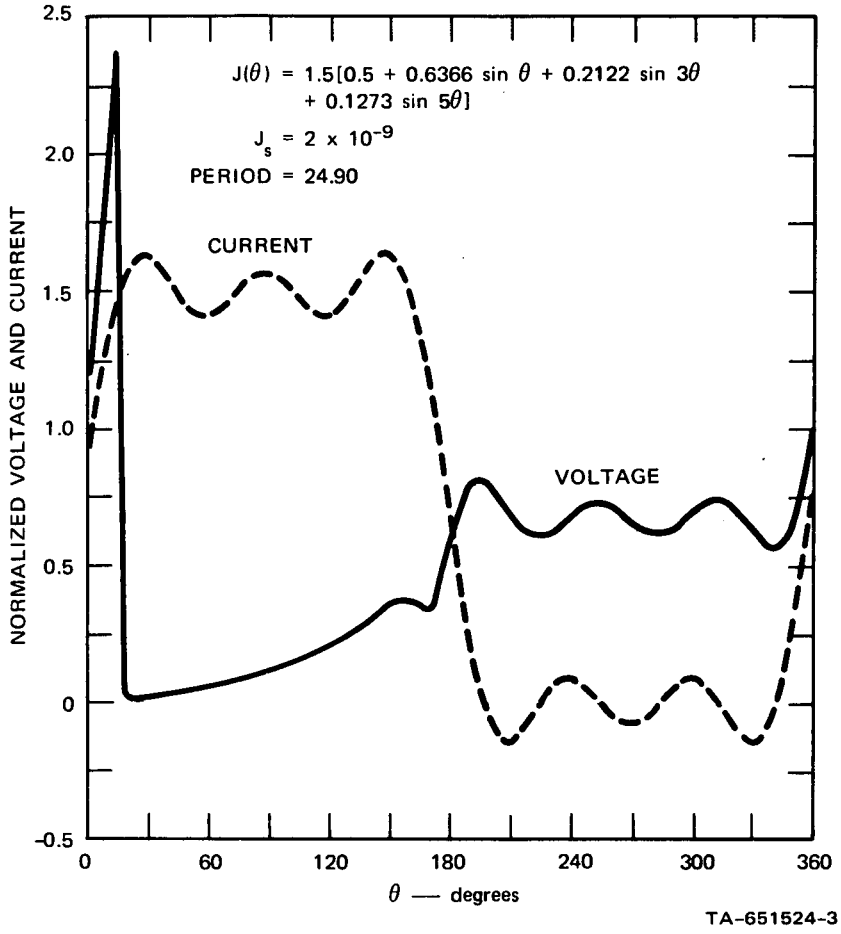

FIGURE 2-7 NORMALIZED VOLTAGE AND CURRENT WAVEFORMS FOR THE TRAPATT MODE WITH A CURRENT USING THE FIRST, THIRD, AND FIFTH HARMONICS OF A SQUARE WAVE

The efficiency has also decreased appreciably from that for a square wave. This is primarily a consequence of the voltage not being as high in the second half of the cycle as in the case of a square wave. The voltage is less in this region because the charge necessary to bring the voltage back up to the original starting value is supplied by the current at the end of the cycle.

The efficiency can be improved if the entire current waveform is shifted to the right and all other parameters remain the same. This is shown in Figure 2-8 for the case of a current composed of the first and third harmonics of a square wave. Note that the normalized voltage during the last half of the cycle now oscillates around unity instead of about 0.8. The dc-to-RF conversion efficiency in the fundamental is 50 percent, and the real part of the diode impedance at the third harmonic is negative. Similar shifts have been made for current waveforms using up to the fifth and up to the seventh harmonics of a square wave. These

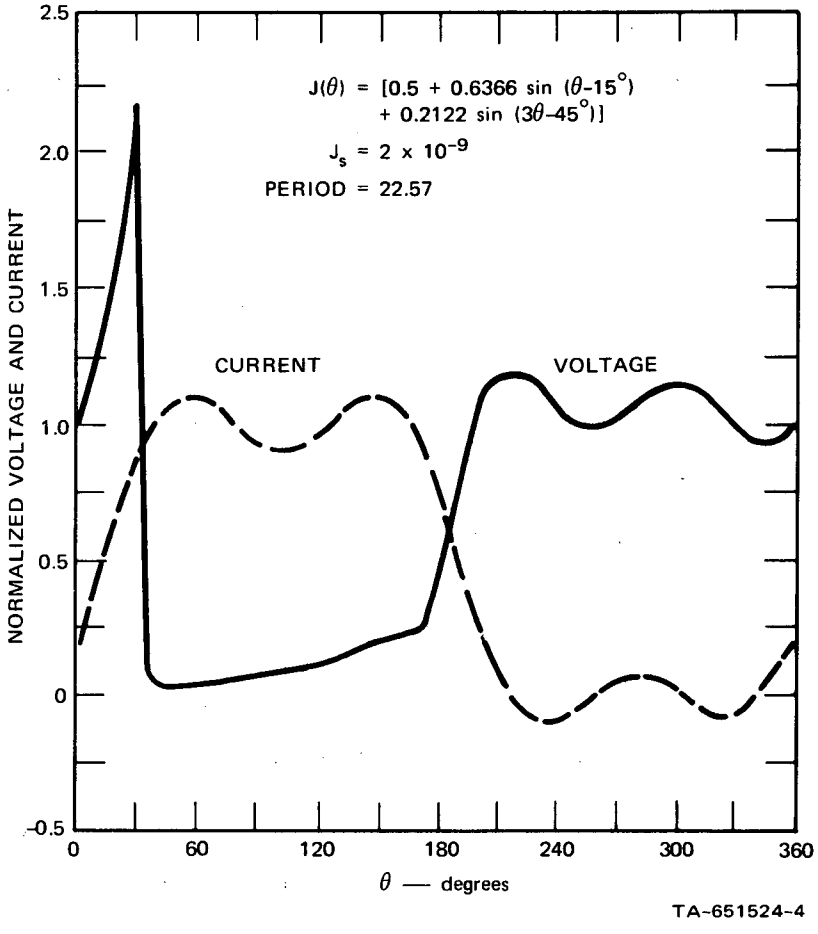

FIGURE 2-8 NORMALIZED VOLTAGE AND CURRENT WAVEFORMS FOR THE TRAPATT MODE WITH A CURRENT USING THE FIRST AND THIRD HARMONICS OF A SQUARE WAVE SHIFTED 15 DEGREES

results are tabulated in Tables 2-5 and 2-6. The efficiency has increased over the corresponding results for the unshifted curves. The impedances at the higher harmonics either are effectively reactive or have a small negative real part except for the case of the seventh harmonic.

The shifting of the current waveform is equivalent to changing the impedance of a passive circuit. These results indicate, therefore, that by proper tuning of the circuit, 50-percent efficiency should be possible with just the first few harmonics of a square-wave current. This is in agreement with the results for a P^+NN^+ diode.[3]

If the initial voltage, V_A, at time t = 0, were increased, the effect would be similar to shifting the current waveform to the right. The two effects would be exactly equivalent if the initial charge were also increased above the thermal generation value to account for the amount of generation that occurs from $V_A = 1.0$ to the increased value of voltage.

Other current waveforms were tried where for the assumed operating conditions a trapped plasma occurred, but the diode exhibited no negative resistance. In each of these cases, too much of the charge required from the external current to neutralize the avalanche charge occurred during the second half of a period. Thus, the voltage remained low after avalanche until the very last portion of the cycle. The higher harmonics are very important in shaping the current waveform so that it is nearly zero over the entire last half of a cycle.

The half-wave rectified sine wave was considered as a drive current waveform because the current is zero over the second half of a cycle. Also, there are no discontinuities in this waveform, so the higher harmonics are less important than in a square wave. In fact the first and second harmonics are the most significant. A normalized current density of the following form was used:

Table 2-5

NORMALIZED PERIOD, T, POWERS, P_i, AND IMPEDANCES, Z_i, FOR A PIN AVALANCHE DIODE OPERATING IN THE TRAPATT MODE

$J = A[0.5 + 0.6366 \sin(\theta - 15^\circ) + 0.2122 \sin(3\theta - 45^\circ)]$, $V_A = 1.0$

$J_s = 2 \times 10^{-9}$

Parameter	A = 1.0	A = 1.5	A = 2.0
Period	22.5	20.28	18.84
P_0	0.35	0.52	0.71
P_1	-0.17	-0.26	-0.32
P_3	-0.005	-0.01	-0.02
Z_0	1.42	0.93	0.71
Z_1	-0.86 + j 0.19	-0.57 + j 0.06	-0.40 + j 0.01
Z_3	-0.22 + j 0.63	-0.30 + j 0.39	-0.24 + j 0.28

$J_s = 2 \times 10^{-3}$

Period	10.9	10.1	9.5
P_0	0.4	0.59	0.76
P_1	-0.13	-0.21	-0.27
P_3	+0.013	+0.009	+0.004
Z_0	1.59	1.04	0.76
Z_1	-0.62 + j 0.26	-0.45 + j 0.12	-0.33 + j 0.05
Z_3	+0.58 + j 0.29	+0.18 + j 0.33	+0.04 + j 0.28

Table 2-6

NORMALIZED PERIOD, T, POWERS, P_i, AND IMPEDANCES, Z_i, FOR A PIN AVALANCHE DIODE FOR A NORMALIZED DRIVE CURRENT USING UP TO FIFTH AND UP TO SEVENTH HARMONICS OF A SQUARE WAVE SHIFTED 1/36 PERIOD TO THE RIGHT

$V_A = 1.0, \quad A = 1.5, \quad J_s = 2 \times 10^{-9}$

Parameter	Five Harmonics	Seven Harmonics
Period	23.0	24.70
P_0	0.52	0.52
P_1	-0.26	-0.26
P_3	-0.015	-0.018
P_5	0.001	-0.001
P_7	--	0.002
Z_0	0.92	0.91
Z_1	-0.57 + j 0.05	-0.58 + j 0.04
Z_3	-0.30 + j 0.36	-0.36 + j 0.32
Z_5	0.06 + j 0.46	-0.07 + j 0.45
Z_7	--	0.27 + j 0.43

$$J(t) = A\left[0.318 + 0.5 \sin\left(\frac{2\pi t}{T}\right) + 0.212 \sin\left(\frac{4\pi t}{T} + 270^{o}\right)\right]. \qquad (2\text{-}43)$$

Figure 2-9 shows a typical voltage waveform for a current given by Eq. (2-43) as computed by modified SMPAL. Three different values of the current drive level, A, and four different levels of the saturation current were considered. These results are summarized in Table 2-7. The diode exhibits a negative resistance at both frequencies over the

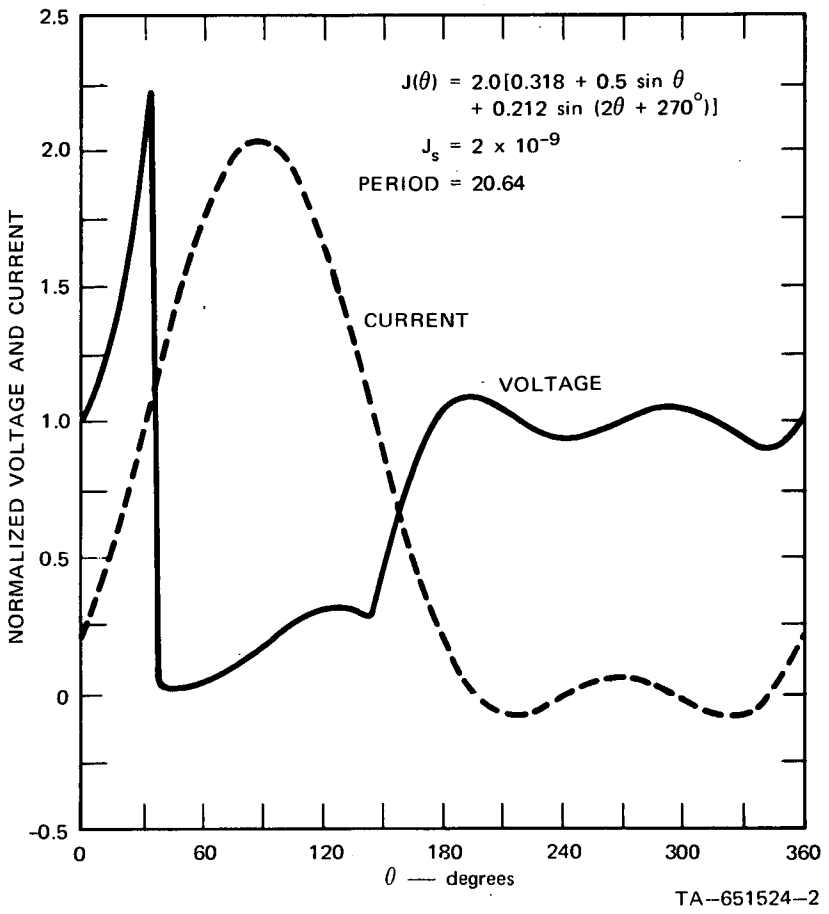

FIGURE 2-9 NORMALIZED VOLTAGE AND CURRENT WAVEFORMS FOR THE TRAPATT MODE WITH A CURRENT USING THE FIRST AND SECOND HARMONICS OF A HALF-WAVE RECTIFIED SINE WAVE

Table 2-7

NORMALIZED PERIOD, T, POWERS, P_i, AND IMPEDANCES, Z_i, FOR A PIN AVALANCHE DIODE OPERATING IN THE TRAPATT MODE FOR A DRIVE CURRENT USING THE FIRST AND SECOND HARMONICS OF A HALF-WAVE RECTIFIED SINE WAVE

Parameter	A = 2.0	A = 1.5	A = 1.0
$J_s = 2 \times 10^{-9}$			
T	20.64	22.49	25.41
P_o	0.500	0.375	0.251
P_1	-0.20	-0.15	-0.096
P_2	-0.06	-0.05	-0.031
Z_o	1.24	1.65	2.48
Z_1	-0.406 + j 0.112	-0.540 + j 0.174	-0.765 + j 0.300
Z_2	-0.660 + j 0.226	-0.905 + j 0.390	-1.37 + j 0.756
$J_s = 2 \times 10^{-7}$			
T	17.65	19.22	21.72
P_o	0.500	0.380	0.258
P_1	-0.187	-0.137	-0.084
P_2	-0.028	-0.045	-0.029
Z_o	1.24	1.67	2.55
Z_1	-0.375 + j 0.114	-0.491 + j 0.186	-0.703 + j 0.304
Z_2	-0.658 + j 0.248	-0.905 + j 0.442	-1.33 + j 0.813
$J_s = 2 \times 10^{-5}$			
T	14.41	15.68	17.66
P_o	0.519	0.395	0.268
P_1	-0.169	-0.123	-0.075
P_2	-0.059	-0.044	-0.028
Z_o	1.28	1.75	2.64
Z_1	-0.338 + j 0.118	-0.441 + j 0.183	-0.602 + j 0.307
Z_2	-0.655 + j 0.288	-0.869 + j 0.48	-1.23 + j 0.887
$J_s = 2 \times 10^{-3}$			
T	10.74	11.63	13.03
P_o	0.550	0.418	0.287
P_1	-0.130	-0.088	-0.046
P_2	-0.054	-0.036	-0.020
Z_o	1.36	1.84	2.85
Z_1	-0.259 + j 0.120	-0.316 + j 0.187	-0.371 + j 0.306
Z_2	-0.598 + j 0.36	-0.731 + j 0.578	-0.871 + j 1.01

the complete range of parameters used. The reactive component of the impedance at each frequency is inductive. As the saturation current increases from 2×10^{-9} to 2×10^{-3}, the fundamental frequency increases by approximately a factor of two, and the efficiency decreases by about the same factor.

If a sinusoidal current waveform is shifted in phase and all other parameters kept the same, high-efficiency oscillations are possible. We have considered normalized diode current waveforms of the form

$$J(\theta) = 1.5[0.5 + 0.55 \sin (\theta - \varphi)] \tag{2-44}$$

and computed the corresponding voltage, power, efficiencies, and impedances of a PIN avalanche diode using the computer program, modified SMPAL. Figure 2-10 shows the current and voltage waveforms when $\varphi = 45^{o}$. The theoretical efficiency of this case is 44 percent. Results for current waveforms with other phase angles are summarized in Table 2-8, where the saturation current was assumed to be $J_s = 2 \times 10^{-9}$.

It is unlikely that this mode has been observed experimentally because it is difficult to construct a microwave circuit that allows current to flow at only a single frequency.

Current waveforms of avalanche diodes operating in a high-efficiency mode have been measured by Snapp et al.[7] We have Fourier analyzed the measured current waveform for one diode that Snapp reported to be oscillating at 49-percent efficiency. This current was then used as the driving current in the computer program, modified SMPAL, to compute the corresponding voltage, powers, efficiencies, and impedances. Figures 2-11 and 2-12 show the normalized voltages and current waveforms where the current was composed of the first three harmonics and first ten harmonics, respectively. Table 2-9 summarizes the operating

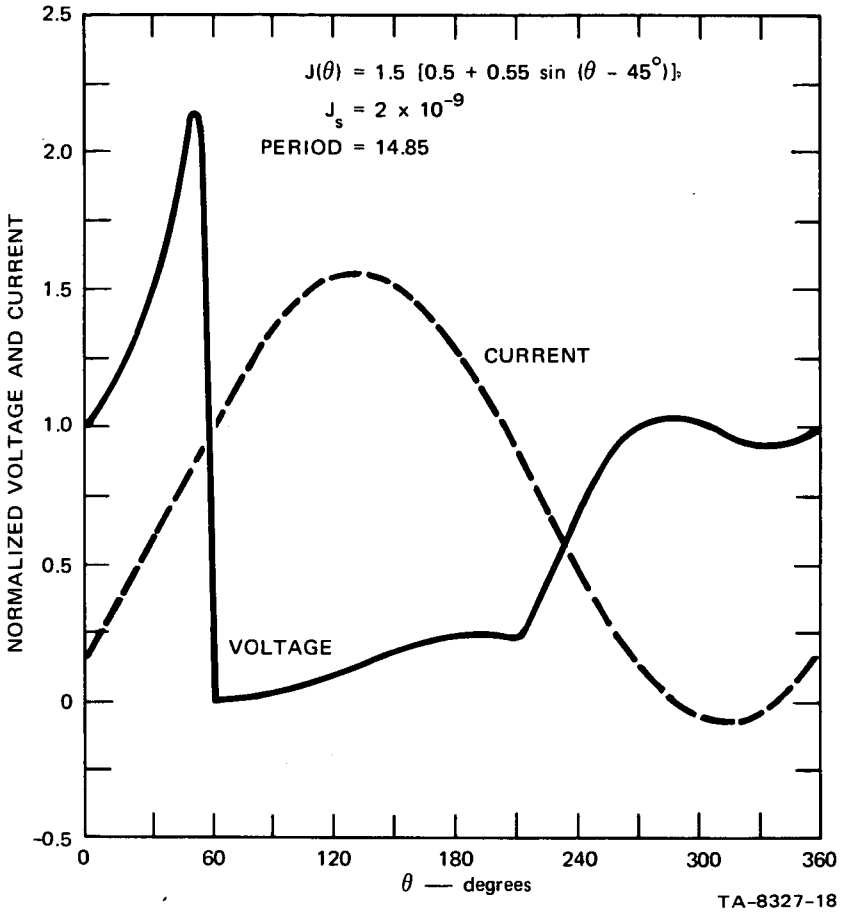

FIGURE 2-10 NORMALIZED VOLTAGE AND CURRENT WAVEFORM IN A PIN AVALANCHE DIODE WHERE THE CURRENT HAS A dc AND A FUNDAMENTAL COMPONENT

Table 2-8

NORMALIZED PERIOD, T, POWERS, P_i, AND IMPEDANCES, Z_i FOR A PIN AVALANCHE DIODE OPERATING IN THE TRAPATT MODE FOR A SINUSOIDAL DRIVE CURRENT

φ	T	P_0	P_1	Z_0	Z_i
0	18.98	0.19	+0.037	0.35	+0.11+j0.34
20^o	16.56	0.37	-0.12	0.65	-0.35+j0.33
45^o	14.85	0.49	-0.22	0.87	-0.64+j0.28
65^o	14.49	0.51	-0.23	0.91	-0.68+j0.26

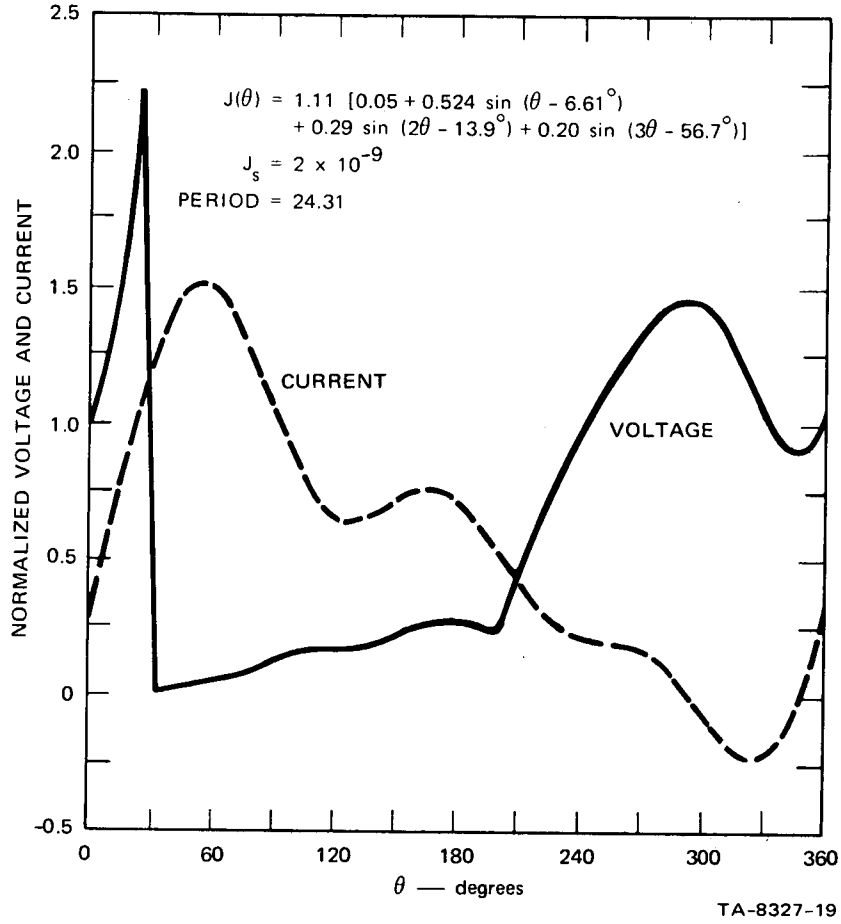

FIGURE 2-11 NORMALIZED VOLTAGE AND CURRENT WAVEFORMS FOR THE TRAPATT MODE IN A PIN DIODE WITH A DRIVE CURRENT USING THREE HARMONICS OF A WAVEFORM REPORTED BY SNAPP, et al.[7]

characteristics for these two cases. The normalized thermal generation was 2×10^{-9}. It is evident from these results that only the first three harmonics of the current are significant. From a circuit point of view this is encouraging because it is difficult to control more than a few harmonics of current or voltage.

The theoretical results for the current waveforms in Figures 2-11 and 2-12 predict efficiencies comparable to that reported by Snapp et al.[7] The period of oscillation is about double. There are several

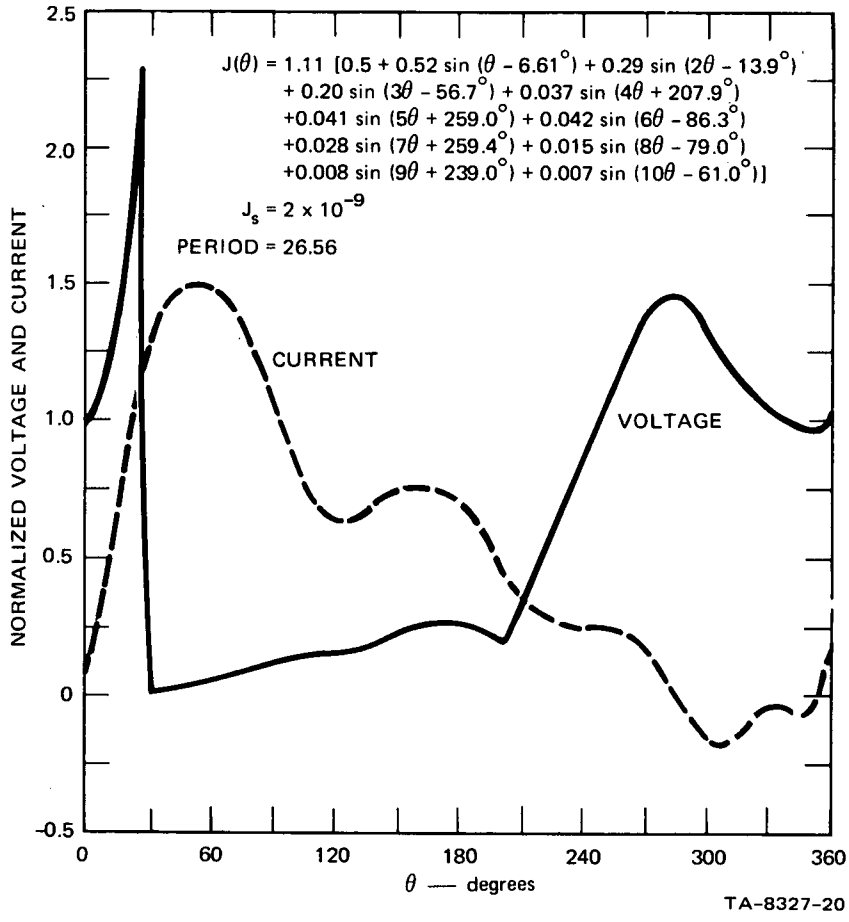

FIGURE 2-12 NORMALIZED VOLTAGE AND CURRENT WAVEFORMS FOR THE TRAPATT MODE IN A PIN DIODE WITH A DRIVE CURRENT USING TEN HARMONICS OF A WAVEFORM REPORTED BY SNAPP, et al.[7]

possible explanations for this difference. First, we assumed a 10-micron-wide depletion layer whereas the depletion width of the experimental diode was reported to be less. Second, the electrons and holes were assumed to have equal ionization coefficients, which should lead to the generation of more charge and a corresponding increased period of oscillation. Third, we chose a small thermal generation rate whereas the experimental diode may have been at a higher temperature.

Table 2-9

NORMALIZED PERIOD T, POWERS, P_i, AND IMPEDANCES, Z_i,
FOR A PIN AVALANCHE DIODE OPERATING IN THE TRAPATT MODE

$$J = 1.11(0.5 + 0.52 \sin(\theta - 6.61^\circ) + 0.29 \sin(2\theta - 13.9^\circ) + 0.20 \sin(3\theta - 56.7^\circ) + 0.037 \sin(4\theta + 207.9^\circ) + 0.041 \sin(5\theta + 259^\circ) + 0.042 \sin(6\theta - 86.3^\circ) + 0.028 \sin(7\theta + 259.4^\circ) + 0.015 \sin(8\theta + 79^\circ) + 0.008 \sin(9\theta + 239^\circ) + 0.007 \sin(10\theta - 61^\circ)]$$

$$J_s = 2 \times 10^{-9}$$

Parameter	Three Harmonics	Ten Harmonics
T	24.31	26.56
P_o	0.365	0.351
P_1	-0.167	-0.162
P_2	-0.018	-0.023
P_3	+0.00008	+0.002
Z_o	1.183	1.128
Z_1	-0.987 + j 0.558	-0.961 + j 0.582
Z_2	-0.343 - j 0.044	-0.414 - j 0.065
Z_3	0.003 + j 0.788	0.065 + j 0.795

The significance of our theoretical results are that we can predict, at least qualitatively, the performance of avalanche diodes oscillating in the TRAPATT mode for arbitrary current waveforms.

3. ANALYTICAL SOLUTION FOR A SECOND HIGH-EFFICIENCY MODE

A. Description of a Second High-Efficiency Mode

There are modes of oscillation other than the TRAPATT mode described in Section 2 which provide efficient dc-to-RF energy conversion. Figure 3-1 shows a set of voltage and current waveforms that are representative of one of these modes of oscillation. In this section an approximate analytical solution for the voltage waveform for this mode is derived for a rectangular-wave current. First, the essential characteristics of this mode of operation are briefly described.

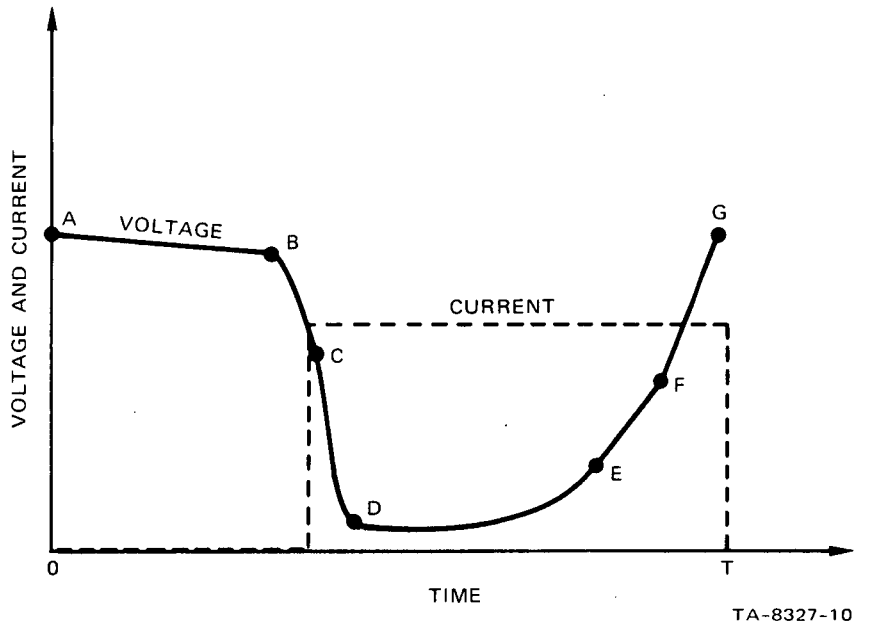

FIGURE 3-1 VOLTAGE WAVEFORM OF A HIGH-EFFICIENCY MODE OF AN AVALANCHE DIODE FOR A RECTANGULAR DRIVE CURRENT

This mode is distinguished from the TRAPATT mode described in Section 2 by the fact that at the beginning of a cycle the diode voltage is above avalanche and the external current is assumed to be zero, whereas in the ordinary TRAPATT mode the diode voltage is initially high but below avalanche and the external current is charging up the diode. At Point A in Figure 3-1, the voltage is above breakdown, but there is very little particle current in the depletion layer. The charge density builds up owing to the avalanche process and drifts out, thereby depressing the internal E-field and the terminal voltage. Since the initial internal charge is so small, considerable time is required to generate sufficient charge to depress the E-field. At Point B enough charge has built up that the ionization process acts very rapidly, and a large amount of charge is generated during the short time between Points B and C. At Point C the field has been depressed sufficiently to stop further ionization of charge carriers. We assume that at this point the external current begins to flow. The exact instant of time is somewhat arbitrary and depends upon the external circuit. For the present discussion it is sufficient to assume that the external current comes on when the E-field drops to the critical value E_c below which the avalanche process stops.

As more charge drifts out the ends of the depletion region, the field in the center is further depressed. The voltage drops to Point D, and the plasma is "trapped" in the middle of the depletion region. This portion of the cycle and the portions over to Point F are the same as the corresponding portions in the ordinary TRAPATT mode if the plasma density is sufficiently large. Thus from Point D to Point E the plasma is extracted by the external current, and several transit times will be required for large charge densities.

At Point E the plasma has been extracted, leaving a residual charge of electrons in one half of the depletion layer and a residual charge of holes in the other half. As the residual charge is removed, the voltage increases more or less linearly from Point E to Point F. At Point F all the charge that has been generated internally has been removed from the depletion layer. This charge must be greater than or equal to that supplied by the external current or the voltage will exceed that at Point A. For analysis it is convenient to assume that Point F lies below the critical field required for avalanche. Then all the charges except those due to thermal generation will have been swept out before the diode is charged back up to Point G. The assumption that only a background of thermally generated charges exists at Point F enables one to calculate the charges generated in going from Point F to Point G. The charge in the depletion layer at Point G must be the same as that at Point A to have a periodic solution.

As in the case of our analysis of the ordinary TRAPATT mode, we assume that we have a PIN diode with equal ionization coefficients, α, and equal velocities, v, for both electrons and holes. We showed in Section 2 that, when the charge density is small or when the depletion region is filled with a plasma, the E-field is effectively uniform. These conditions are satisfied over certain portions of a cycle of the high-efficiency mode discussed here.

B. Initial Avalanche and Generation Phase

During that portion of the cycle from Point A to Point B in Figure 3-1 the internal charge is small, and there is no external current. The operation of the diode over this portion of the cycle is described by Eqs. (2-9) and (2-10). Between Points B and C a large plasma is generated by the avalanche process. As the charges in this plasma

drift, they depress the E-field. However, the avalanche process is essentially uniform across the depletion layer, and the E-field remains relatively uniform. We assume as a first approximation that E remains uniform between Points A and C. At Point B, Q has increased from a small value to a magnitude of about 0.1; during this time E is nearly constant and equal to E_m. Similarly, α is equal to α_m, a maximum value corresponding to E_m. Between Point B and Point C, Q increases rapidly. The E-field begins to decrease, forcing α to decrease. Since the mathematics becomes very complicated for α not a constant, we let $\alpha = \alpha_m$ until E reaches a critical value, E_c, at Point C. For values of E less than E_c, we assume $\alpha = 0$. This assumption is similar to the one used in analytical solutions for the ordinary TRAPATT mode. The validity of these assumptions and the value of E_c can be established from a computer program such as UNSAT.

Using the above assumptions, we can write the equations for the charge density and the electric field during the initial avalanche and generation phases of the high-efficiency mode:

$$\frac{dE}{dt} = -v_s Q \quad , \tag{3-1}$$

$$Q = Q_A e^{2v_s(\alpha_m - 1)t} \quad , \tag{3-2}$$

where Q_A is the initial charge density at Point A, v_s is the saturated velocity and α_m is the ionization coefficient corresponding to the maximum field at Point A. Substituting Eq. (3-2) into Eq. (3-1) and integrating, we obtain

$$E(t) - E_A = \frac{J_A}{2v_s(\alpha_m - 1)} \left[e^{2v_s(\alpha_m - 1)t} - 1 \right] \qquad 0 < t < t_g \quad , \tag{3-3}$$

where $J_A = v_s Q_A$ is the small particle current at the beginning of the cycle, t_g is the time when E drops to the critical field E_c, and the generation phase is complete. We solve for t_g from the above equation by setting $E = E_c$:

$$t_g = \frac{1}{2v_s(\alpha_m - 1)} \ln \left\{ 1 + \frac{2v_s(\alpha_m - 1)}{J_A} (E_A - E_c) \right\} \quad . \tag{3-4}$$

The time for the generation phase is a function of both E_A and J_A. Since J_A can vary over several orders of magnitude, it can have a dominant effect on the generation time. The voltage over this portion of the cycle is just equal to E(t), since we have assumed a uniform electric field. By substituting the value of t_g back into Eq. (3-2), we can calculate the magnitude of the plasma charge, Q_p, in the depletion region at the end of the generation phase:

$$Q_p = Q_A + 2(\alpha_m - 1)(E_A - E_c) \quad . \tag{3-5}$$

The plasma charge is a function of only the ionization coefficient and the difference between the magnitude of the E-field at Point A and that at Point C.

By analogy with Eqs. (2-20) and (2-21), the total positive or negative charge generated in one cycle, G, is equal to the following:

$$G = \alpha_m (E_A - E_c) + \frac{1}{2} Q_A \quad . \tag{3-6}$$

The integral of the external current over one period must equal G, the total charge generated internally, for the oscillations to be periodic. This sets a limit on the maximum value of J to prevent a second avalanche within the same period.

We can rewrite Eq. (3-5) for the total charge at Point C as a function of the generation:

$$Q_p = 2G - 2(E_A - E_c) \quad . \tag{3-7}$$

As in the ordinary TRAPATT mode, the plasma charge density is equal to the total charge generated less those charges that have drifted out of the depletion layer. It is the drifting charges that actually depress the E-field and stop further ionization.

C. Field Depression and Charge Removal

The operation of the device over those portions of a cycle from Point C to Point F in this high-efficiency mode is the same as that in the ordinary TRAPATT mode described in Section 2 if $Q_p \gg J$. The discussions and corresponding equations are the same if Eq. (2-22) in Section 2 is replaced by Eq. (3-7) above. If $Q_p \lesssim J$, then different expressions for the voltage during the field-depression and charge-removal phases of a cycle must be derived. Since the latter inequality corresponds to a less efficient mode, it is not considered in this report.

D. Final Charge-up Phase

If the drive current has not exceeded the value that would cause second avalanche, all the charge will be removed from the depletion region at Point F (Figure 3-1). The E-field will again be uniform across the sample. From Eq. (2-42) the voltage at Point F is V_F:

$$V_F = E_p + \frac{J}{2(v_s + v_p)} \quad . \tag{3-8}$$

The diode charges up like a linear capacitor until the field reaches the point where significant avalanche occurs, i.e., where the normalized ionization coefficient approaches unity. During this time the charge density will remain at a small value, determined by the diode back-biased saturation current, J_s:

$$Q_s = \frac{J_s}{v_s} \ll 1 \quad . \tag{3-9}$$

The external current will continue to drive the field higher into avalanche until the voltage reaches the value at Point G. Since the charge density is small throughout this portion of the cycle, the time required for the final charge-up phase is given by the following:

$$t_c = (E_A - E_F)/J \quad , \tag{3-10}$$

where $E_A = E_G$ owing to periodicity.

To calculate the charge, Q_A, we must assume a particular functional dependence on E for α. We choose an exponential function, for mathematical convenience, as done in Section 2.

$$\alpha = \alpha_o \, e^{\lambda E} \quad . \tag{3-11}$$

Since we have assumed that the E-field increases linearly with the external current, we can solve for the charge from Eq. (2-9) during the final charge-up phase of the cycle:

$$Q(t) = Q_s \exp\left\{\frac{2v_s\alpha_1}{\lambda J}\left[e^{\lambda Jt} - 1\right] - 2v_s t\right\} \quad , \tag{3-12}$$

where α_1 is the value of the ionization coefficient when avalanche starts and hence is equal to one; Q_s is the charge due to thermal generation and corresponds to the diode saturation current. To find Q_A we must substitute for t, the time required for the field to increase from E_1 to E_A, where E_1 is the value corresponding to $\alpha_1 = 1$. Thus we have $t = (E_A - E_1)/J$ and

$$Q_A = Q_s \exp\left\{\frac{2v_s\alpha_1}{\lambda J}\left[e^{\lambda(E_A - E_1)}\right] - \frac{2v_s}{J}(E_A - E_1)\right\} \quad . \tag{3-13}$$

For a self-consistent solution, Q_A should be used in Eq. (3-3) for the electric field during the generation phase of the cycle. The only quantity in our semianalytical solution that is arbitrary is E_c in Eqs. (3-4), (3-5), and (3-6). As mentioned earlier, we can determine E_c by comparing our results for the generation as computed by Eq. (3-6) with those obtained by using a computer program such as UNSAT.

No specific calculations of diode parameters for this mode of operation have been computed as yet. We can, however, make a few general comments. The higher the diode is driven above avalanche before the diode current is turned off, the shorter the time before the subsequent plasma is created, the field depressed, and the external current increased. This results in a rectangular current waveform rather than a square wave and decreases the magnitude of the fundamental component of current. On the other hand, if the diode is not driven very far into avalanche, the density of the generated plasma will be small. A

smaller plasma results in a shorter period of oscillation and tends to decrease the efficiency. But the duration of the high-voltage state is increased, resulting in a more symmetrical waveform, which tends to increase the fundamental efficiency. The interaction of these various trade-offs is not clearly understood at this time. Additional investigation of this mode of oscillation is required. This mode may be more representative of the high-efficiency oscillations observed experimentally where the fundamental frequency is 1/2, 1/3, or 1/4 the transit time frequency.

4. TRAPATT OSCILLATOR WITH MULTIPLE AVALANCHE PER CYCLE

A. Introduction

In this section the behavior of a TRAPATT PIN diode is analyzed under the condition of multiple avalanche per cycle of oscillation. Previous analysis of TRAPATT oscillations have avoided this possibility by assuming the diode current to be below a certain threshold value (see Section 2 and Refs. 3 and 4). The results of this section are an approximate solution for the voltage and current waveforms over an entire cycle of oscillation. The problem considered can be summarized as follows. A dense plasma is formed uniformly throughout the depletion region of the PIN diode by avalanche ionization, as in the ordinary TRAPATT mode. Part of the trapped plasma is removed near the ends of the depletion layer by the external current, leaving a residual charge of electrons at the left side of the plasma and a residual hole concentration on the right side. The residual charge outside the plasma causes the electric field to increase toward either boundary. Since the magnitude of the residual charge, and hence the boundary value of the electric field, is proportional to the external current during this segment of the cycle, the E-field near the edges will exceed the value for avalanche breakdown for sufficiently large currents [see Eq. (2-38)]. The electrons created at the left boundary by this second avalanche exit, but the holes drift to the right toward the slowly receding plasma, and increase the residual charge density in that region. Similarly, holes created at the right boundary by the second avalanche exit, and the electrons drift to the left toward the plasma.

The dynamics of this second avalanche, and any subsequent avalanche, are not completely understood at this time. We will assume that the transients associated with this avalanche are short lived (on the order of one transit time) and allow the diode to reach a new quasi-steady state. The new field configuration and charge distributions are determined from a quasi-static approximation to the continuity equations and an assumed constant external current that exists over the majority of the first half of the cycle. This current decreases near mid-cycle to hold the voltage just below uniform avalanche and then drops to zero over the last half cycle. The quasi-static approximation is based upon the assumption that the only time variations in electron and hole distributions are caused by the slowly moving boundaries of the trapped plasma. Since the plasma velocity is much less than the saturated velocity, this approximation seems reasonable.

B. Initial Charge-up and Plasma Generation

We shall assume that initially a PIN diode is biased just below avalanche with a uniform electric field, E_A, over the depletion layer and a constant current, J, applied to the device. The form of the solution is the same as given before in Eq. (2-11):

$$V(t) = V_A + Jt \quad , \quad 0 \leq t \leq t_m \quad . \tag{4-1}$$

As the current increases, the rate of voltage growth increases, but the time over which this formula applies, t_m, decreases. The peak value that the voltage attains increases about two fold for a ten-fold increase in drive current.

The plasma generation sequence then follows in which the carriers generated by the avalanche reduce the field across the depletion region

rapidly from its maximum value E_m to the value E_p within the dense plasma. The total charge filling the depletion layer Q_p is given by Eq. (2-19)

$$Q_p = Q_m + 2(\alpha_m - 1)\,[E_m - E_c + Jt_g] \quad , \tag{4-2}$$

where $Q_m = J/v_s$, v_s = the saturated velocity, α_m is the ionization coefficient corresponding to the field E_m, and t_g is the time of this process given by Eq. (2-18). The voltage drops rapidly from the maximum E_m to E_p as the dense plasma removal begins. The velocity at which the dense plasma is removed is the plasma velocity $v_p = J/Q_p$ correspondong to the low plasma field, E_p. So far the diode behavior is similar to the lower current case in the ordinary TRAPATT mode.

As the dense plasma is removed, its boundary moves toward the center of the depletion region at v_p, and the electric field increases in the region outside the plasma. This continues until the field at the boundary reaches the avalanche value E_c. In the region of residual charge the field is given by

$$E(x) = E_p + n_r\,(x_p - x) \quad , \quad 0 \le x \le x_p \quad , \tag{4-3}$$

where $x_p = v_p t$ is the position of the plasma boundary and n_r is the residual charge density. The time, t_c, it takes for the field at the edge to reach the avalanche value is given as

$$t_c = \frac{E_c - E_p}{v_p J}\,(v_s + v_p) \quad . \tag{4-4}$$

At this time the second avalanche is established near the depletion layer's edge. To determine the field when this occurs, we invoke a

quasi-static approximation. The normalized static continuity equations for static fields can be combined with Poisson's equation (neglecting diffusion) to yield a second-order nonlinear equation for E:

$$v \frac{\partial^2 E}{\partial x^2} = 2 \alpha J - v' \left(\frac{\partial E}{\partial x} \right)^2 \quad . \tag{4-5}$$

Here we have also assumed equal hole, electron ionization rates, α, and equal carrier velocities, v.

J, the external current, equals $J_n + J_p$, the sum of electron and hole currents, and v' equals $(\partial V/\partial E)$. The boundary conditions on the left side of the junction are

$$\left. \frac{\partial E}{\partial x} \right|_{x=0} = J \tag{4-6}$$

and

$$E = E_p \quad \text{at} \quad x = x_p \quad . \tag{4-7}$$

The field profile will be symmetrical about the middle of the depletion region, with the E-field continuous throughout this zone.

Since both α and v are functions of E, one method of solution for Eqs. (4-5), (4-6), and (4-7) is to separate the problem into two regions. In one region the field is above the critical field E_c for avalanche and the other below, so α may be neglected. Near the boundary, in the second avalanche zone v equals v_s and Eq. (4-5) reduces to

$$\frac{\partial^2 E}{\partial x^2} = 2 \alpha J \tag{4-8}$$

over the range $0 \leq x \leq x_c$, where x_c is the position at which the field equals E_c. The power representation of the ionization coefficient dependence on field will be assumed

$$\alpha(E) = \alpha_o \left(\frac{E}{E_c}\right)^6 \tag{4-9}$$

as suggested by McKay,[8] where α_o is a constant ≈ 0.2 for silicon. This form of the ionization coefficient is used rather than the exponential for mathematical convenience. Equation (4-8) can be written as

$$\frac{d^2E}{dx^2} = \left(\frac{2\,\alpha_o J}{E_c^6}\right) E^6 \tag{4-10}$$

and has a solution given by

$$E(x) = \frac{1}{(2Ax + 2C)^{1/2}} \quad , \qquad 0 \leq x \leq x_c \quad , \tag{4-11}$$

where

$$A = \sqrt{\frac{2\,\alpha_o J}{E_c^6}} \quad ,$$

and using the boundary condition

$$\frac{dE}{dx} = J \quad \text{at } x = 0 \quad ,$$

$$C = \sqrt[3]{\frac{\alpha_o}{4E_c^6 J}} \quad .$$

Setting $E(x) = E_c$ and solving for the position x_c yields

$$x_c = \frac{E_c}{2}\left(\frac{1}{\sqrt{2\,\alpha_o J}} - \frac{1}{\sqrt[6]{2\,\alpha_o J^5}}\right) \quad . \tag{4-12}$$

The region over which second avalanche occurs ($0 \le x \le x_c$) is not a strong function of J, x_c being about 0.22 for currents just large enough to cause second avalanche; x_c decreases to about 0.18 at four times this threshold current.

The electric field at the boundary is

$$E(0) = E_c\left(\frac{J}{2\,\alpha_o}\right)^{1/6} \tag{4-13}$$

and also is seen to be a slowly varying function of the current. The voltage across the second avalanche region is quickly established, in a fraction of a transit time, and then remains constant so long as the extracted current is constant. The time-dependent voltage is

$$V(t) = \left[\frac{(2Ax_c + C)^{1/2}}{A} - \frac{(2C)^{1/2}}{A}\right]\frac{t}{t_a} = V_s\frac{t}{t_a}\,, \quad 0 \le t \le t_a\,, \tag{4-14}$$

where t_a is the time for a carrier to traverse the second avalanche zone $t_a = x_c/v_s$, and A and C were given above. Between the second avalanche region (ending at $x = x_c$) and the dense plasma region (starting at $x = x_p$), there is a region sufficiently below avalanche that α in Eq. (4-8) is neglectable, but of high enough field that $v \approx v_s$ over most of its range. Equation (4-5) thus reduces to

$$\frac{\partial^2 E}{\partial x^2} = 0 \quad , \tag{4-15}$$

whose solution is linear in space

$$E(x) = E_c - \left[\frac{x - x_c}{x_p - x_c}\right](E_c - E_p) \quad , \; x_c \leq x \leq x_p \quad . \tag{4-16}$$

The voltage across this region is

$$V(t) = \left[E_c x_p - E_p x_c - \left(\frac{E_c - E_p}{x_p - x_c}\right)\left(\frac{x_p^2}{2} - \frac{x_c^2}{2}\right)\right] \quad . \tag{4-17}$$

Since $x_p = v_p t$, x_c = constant, and $E_c \gg E_p$, we have

$$V(t) \approx V_s + \frac{E_c}{2}(v_p t - x_c) \quad , \quad t_c \leq t \leq \frac{0.5}{v_p} \quad . \tag{4-18}$$

Thus the total voltage for the plasma extraction segment under second avalanche is the sum of the voltage across each region, given by Eqs. (4-14) and (4-18):

$$V(t) = V_s + \frac{E_c}{2}(v_p t - x_c) \quad , \tag{4-19}$$

where

$$t_c + \frac{x_c}{v_s} \leq t \leq \frac{0.5}{v_p} \quad ,$$

and is linear with time over this range.

The final step is to remove the sparse plasma left behind from the original avalanche, and from the continuing second avalanche. The field within the second avalanche region is a complex quantity somewhat different than in the region $x_c \leq x \leq 0.5$. Analysis has shown, however, that a linear approximation to the field E(x) over the entire depletion region (this approximation accounts for the extra charge generated within the second avalanche and matches the slope at $x = x_c$) yields reasonable results for the excess charge removal phase. Figure 4-1 shows the normalized field distribution in the presence of second avalanche. The total excess charge is $n_r^* \approx (E(0) - E_p)/0.5$ and the field throughout the depletion region is

$$E(x) = E_p + n_r^* (0.5 - x) \quad , \quad 0 \leq x \leq x_r \quad , \tag{4-20}$$

where x_r is the extent of the residual charge measured from the left boundary. The value of x_r decreases linearly with time:

$$x_r = 0.5 - v_s t \quad , \quad 0 \leq t \leq t_i \quad , \tag{4-21}$$

where t_i will be given below. The corresponding terminal voltage is

$$V(t) = E_p + \frac{E(0) - E_p}{2} (1 + 2v_s t) \quad , \quad 0 \leq t \leq t_i \quad . \tag{4-22}$$

This phase of the cycle continues until the terminal voltage reaches its initial value. The current must be decreased at this time to prevent the voltage from overshooting its initial value. Hence we will require that J decrease in such a way that V(t) is equal to V_A over the final segment of the cycle. The time t_i corresponds to the voltage reaching its initial value V_A,

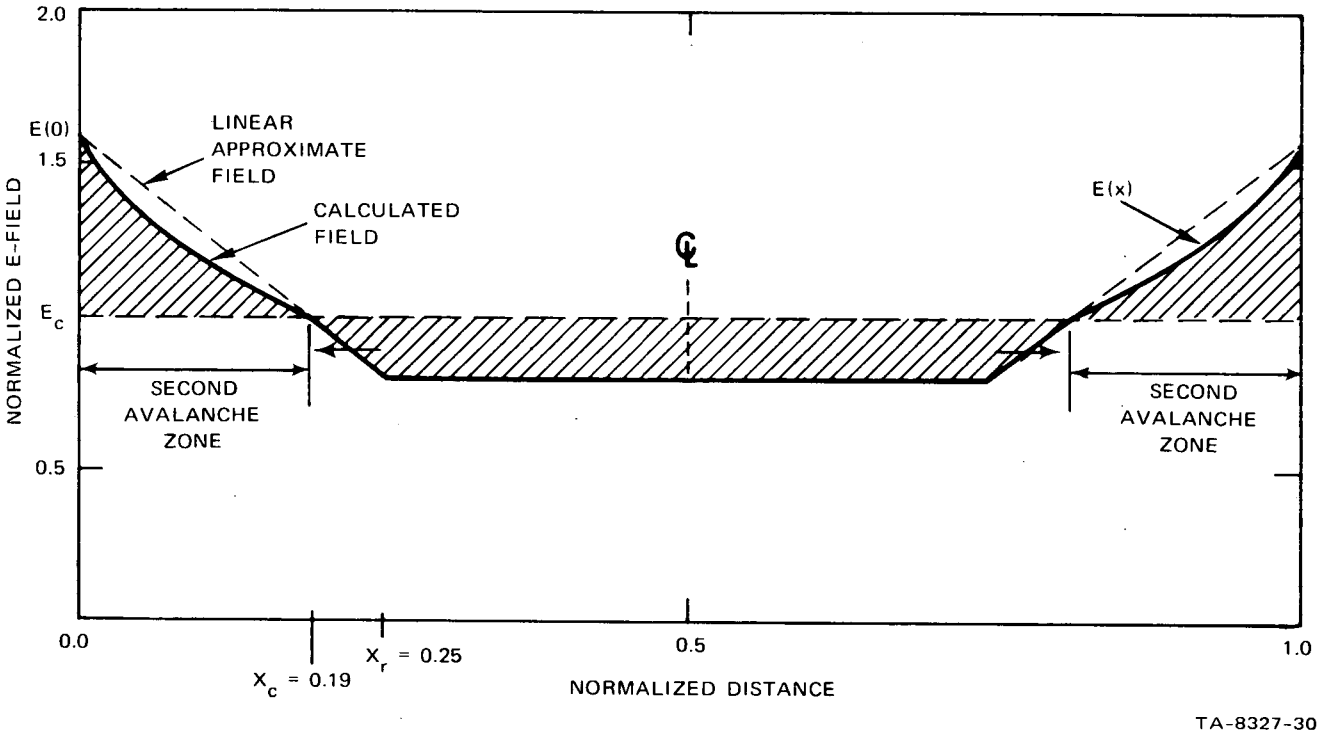

FIGURE 4-1 NORMALIZED FIELD DISTRIBUTION WITHIN A PIN DIODE UNDER SECOND AVALANCHE AT THE TIME t_i

$$t_i = \frac{2E_c - E_o - E_p}{2E_o v_s} \quad . \tag{4-23}$$

At this time the area below E(x) and E_c to the left of x_c must equal the area above the E(x) and E_c to the right, until x = 0.5. From the time t_i until $t = 0.5/v_s$ the current decreases at a rate that keeps the two areas equal (see Figure 4-1), and the current time dependence will be

$$J(t) = J\left\{1 - \left[\frac{1 - \frac{2\alpha_o}{J}}{t_i - \frac{0.5}{v_s}}\right](t_i - t)\right\}, \quad t_i \leq t \leq \frac{0.5}{v_s} \quad . \tag{4-24}$$

It is seen that this portion of the cycle lasts only a fraction of a transit time, and at its conclusion the current is reduced to zero, which maintains the voltage at its high initial value ready for the start of the next cycle.

Multiple avalanche thus has two effects on the total device performance. The power output increases almost linearly with increasing drive current whereas the dc-to-RF efficiency decreases only slightly. For example, calculations indicate a relative decrease in efficiency of 10 percent for a four-fold increase in current, over the threshold value for second avalanche, and a corresponding four-fold power output increase.

5. ANALYSIS OF THE UNIFORM, SYMMETRIC, AVALANCHE DIODE IN THE HIGH-FIELD STEP-IONIZATION APPROXIMATION

A. Introduction

A qualitative understanding of the transient and oscillatory behavior of a PIN diode as it moves in and out of avalanche ionization is sought by approximating the variation of ionization with field as a step from none to a fixed level of ionization at a critical field value. This critical value is assumed high enough so that electrons and holes move at saturated velocities.

In this section it is shown that a solution can be computed when a pattern of regions with field values above and below critical has been prescribed. A rule governing admissibility of patterns has been derived. The rule has shown that many suggested patterns are inadmissible; one family of useful admissible patterns has been found.

In the approximation, electrons and holes move at the same constant speed, electrons to the left and holes to the right, according to assumed sign conventions. In the (x,t) plane the electron and particle paths are straight characteristic lines. The density of electrons, n, has the small thermal value ϵ at the right edge of the diode, is continuous along a characteristic running to the left, is constant in regions with no ionization, and increases in regions with ionization. Hole density, p, satisfies the same conditions on each right-running characteristic.

The requirement that the field be above its critical value in regions with ionization, and below in regions without, leads to the following rule:

If a boundary segment between regions in the (x,t) plane with and without ionization is horizontal, a line of constant t, then p = n along the segment. If the boundary segment is not horizontal and the region with ionization is to the left, then near the segment in both regions $p < n$. If the region with ionization is to the right, $p > n$.

The approximate analysis is used to indicate possible patterns of avalanche regions in the space-time plane for the simplest case of a uniform PIN diode. Qualitative results for the variation of current and voltage drop across the diode are deduced.

B. Basic Equations

The basic equations are those presented in Section 2 in the normalized form they read

$$\begin{aligned} n_t + (v_n n)_x &= \alpha|v_n|n + \beta|v_p|p, \\ p_t + (v_p p)_x &= \alpha|v_n|n + \beta|v_p|p, \\ E_x &= N_D - N_A + p - n \\ E_t &= J + v_n n - v_p p, \end{aligned} \tag{5-1}$$

where E is the field strength, n is electron density, p is hole density, v_n is electron velocity, v_p is hole velocity, α and β are ionization rates, N_D and N_A are donor and acceptor densities, and J is the external current density. Subscripts x and t denote partial differentiation.

The boundary conditions become

$$p = \epsilon \quad \text{at } x = -\tfrac{1}{2} \quad ,$$
$$n = \epsilon \quad \text{at } x = \tfrac{1}{2} \quad , \tag{5-2}$$

where ϵ is the small charge due to thermal generation and the origin has been taken for convenience in the central plane of the diode. Note that in Sections 2 and 3 the origin was chosen at the left-hand edge of the depletion region.

Introduce function F defined by

$$F = E - \int_{x_0}^{x} (N_D - N_A)\, dx - \int_{t_0}^{t} J\, dt \quad , \tag{5-3}$$

where t_0 is a convenient fixed time and x_0 is a fixed location. One finds

$$F_x = p - n \quad , \qquad F_t = v_n n - v_p p \quad ,$$

so that

$$n = (v_p F_x + F_t) / (v_n - v_p) \quad ,$$
$$p = (v_n F_x + F_t) / (v_n - v_p) \quad . \tag{5-4}$$

The system is represented by the single differential equation

$$\left(\frac{v_p F_x + F_t}{v_n - v_p} \right)_t + \left(v_n \frac{v_p F_x + F_t}{v_n - v_p} \right)_x = \alpha |v_n| \frac{v_p F_x + F_t}{v_n - v_p} + \beta |v_p| \frac{v_n F_x + F_t}{v_n - v_p} \tag{5-5}$$

with boundary conditions

$$\frac{v_p F_x + F_t}{v_n - v_p} = \varepsilon \qquad \text{at } x = \tfrac{1}{2} \quad ,$$

$$\frac{v_n F_x + F_t}{v_n - v_p} = \varepsilon \qquad \text{at } x = -\tfrac{1}{2} \quad . \tag{5-6}$$

Since only derivatives of F appear in the differential equation and boundary conditions, if F is a solution so is F + C a solution for any constant, C.

C. High-Field Step-Ionization Approximation

To obtain qualitative understanding of the avalanche process, we have simplified the equations as follows. Near avalanche the field will be so high that electron and hole velocities are essentially saturated. In the normalized units, this means,

$$v_p = -v_n = 1 \quad . \tag{5-7}$$

The ionization rates are taken to be equal. Their sharp variation from a low value to a high one at a critical value of E is taken to be a step change from zero to a constant value α_0. The step is taken to occur at E = 1; this corresponds to the critical value E_c used in Sections 2 and 3:

$$\alpha = \beta = \begin{cases} 0 & E < 1 \\ \alpha_0 & E \geq 1 \end{cases} \quad . \tag{5-8}$$

The resulting approximate equations for F are the wave equation when $E < 1$ and a variant of the telegrapher's equation when $E > 1$:

$$\begin{aligned} F_{tt} - F_{xx} &= 0 \qquad \text{for } E < 1 \quad , \\ F_{tt} - F_{xx} &= 2\alpha_0 F_t \qquad \text{for } E > 1 \quad , \end{aligned} \tag{5-9}$$

with boundary conditions

$$\begin{aligned} F_t + F_x &= -2\epsilon \quad \text{at } x = \tfrac{1}{2\epsilon} \quad , \\ F_t - F_x &= -2\epsilon \quad \text{at } x = -\tfrac{1}{2\epsilon} \quad . \end{aligned} \tag{5-10}$$

Convenient characteristic coordinates are

$$r = t + x \quad , \quad s = t - x \quad . \tag{5-11}$$

One finds

$$\begin{aligned} F_x &= F_r - F_s \quad , \qquad F_t = F_r + F_s \quad , \\ F_{rs} &= (\alpha/2)(F_r + F_s) \quad , \\ F_r &= -\epsilon \qquad \text{at} \quad r - s = 1 \quad , \\ F_s &= -\epsilon \qquad \text{at} \quad r - s = -1 \quad . \end{aligned} \tag{5-12}$$

Since

$$\begin{aligned} n &= -F_r \quad , \\ p &= -F_s \quad , \end{aligned} \tag{5-13}$$

useful solutions of F have negative partial derivatives. From the general theory for hyperbolic equations, one knows that F is continuous with continuous first partial derivatives, except that F_r and n may have a jump in value across a characteristic line s = constant and F_s and p may jump at an r = constant line.

D. Solution Forms

Where $E < 1$, function F satisfies the wave equation and therefore is given by

$$F = f(r) + g(s) \tag{5-14}$$

for arbitrary functions f and g. These functions are to be chosen so that F is continuous and fits the boundary conditions.

Where $E > 1$, function F satisfies the telegrapher's equation. The value of F at a point :: (r_0, s_0) is found by appropriate integrations involving the Riemann function R, which depends on P and a variable point (r,s). In the present case R is only a function of the two variables $(r - r_0)$ and $(s - s_0)$:

$$R = R(r - r_0, s - s_0) \tag{5-15}$$

with

$$R(y,z) = e^{-\alpha_0 (y + z)/2} I_0 (\alpha_0 \sqrt{yz})$$

where I_0 is the modified Bessel function of the first kind.

In particular, if F is known along two intersecting characteristic lines, r = constant and s = constant, as AC and BC in Figure 5-1, F

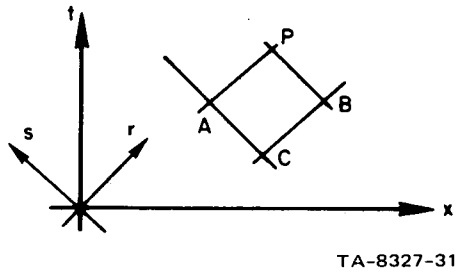

FIGURE 5-1 CHARACTERISTIC INITIAL-VALUE PROBLEM

can be found at P from the formula

$$F(P) = F(A)R(A) + F(B)R(B) - F(C)R(C) - \int_C^A F(R_z + \alpha_0 R/2)\, ds - \int_C^B F(R_y + \alpha_0 R/2)\, dr \quad . \tag{5-16}$$

Similar formulas hold when the data are given in other ways.[9]

Two solutions are F_1 and F_2:

$$F_1 = e^{\alpha_0 (r + s)} = e^{2 \alpha_0 t} \quad , \tag{5-17}$$

$$F_2 = e^{\alpha_0 (r+s)/2} I_0(\alpha_0 \sqrt{rs}) = e^{\alpha_0 t} I_0\left(\alpha_0 \sqrt{t^2 - x^2}\right) \quad . \tag{5-18}$$

In a useful solution, with neither n nor p negative, F_1 or F_2 would appear with a negative coefficient.

E. Avalanche Regions

A solution to the equations may be computed when initial conditions, $(N_D - N_A)$, and J are given. For simplicity, the case of a PIN diode,

with equal donors and acceptors, $N_D - N_A = 0$, is considered here. By Eq. (5-3) we have,

$$E = F + Q \quad , \qquad Q_J = \int_{t_0}^{t} J \, dt \quad . \tag{5-19}$$

One way of specifying J or Q_J is to assign regions of avalanche and no avalanche in the (x,t) plane. For then F can be computed by solving the differential equation and boundary conditions in set of Eqs. (5-12). And, since E = 1 on the boundaries separating the regions, Q can be found; and this gives E everywhere.

Let a region with avalanche ionization be an A-region and one without, a W-region, the letter W being a reminder that the wave equation is controlling in such regions. Since holes and electrons are neither created nor destroyed in a W-region, the value of p is constant along each characteristic running to the right; the value of n is constant along a characteristic running to the left. In an A-region the value of p is increased by the ionization as one follows a right-running characteristic, while n increases along those running to the left.

Consider a segment of boundary between an A-region and a W-region. On the segment, E equals 1. If the segment has slope zero in the (x,t) plane--i.e., follows a line of constant t--then Q and F are constant along it. If the segment has nonzero slope, it is crossed by lines of constant t. On such a traversal in the A-region E falls as it approaches the boundary and continues to decrease as one leaves the boundary in the W-region. Thus, whether there are discontinuities in derivatives at the boundary or not, E_x has a negative sign on both sides of a boundary with the A-region to the left; it has a positive sign if the A-region is to the right. By Poisson's equation, the third equation in set (5-1), and Eq. (5-13), the following rule is established:

$p < n$ or $F_r < F_s$, if the A-region is to the left,

$p > n$ or $F_s < F_r$, if the A-region is to the right,

$p = n$ or $F_r = F_s$, if the boundary has constant t.

The condition at the left edge of the diode, $x = -\frac{1}{2}$, is $p = \epsilon$. If there is a W-region adjacent to this edge, then $p = \epsilon$ along any characteristic starting from that edge. Where the characteristic reaches a boundary with an A-region, in which n will be greater than ϵ, by the rule above, the A-region is to be to the left. Since the characteristic line has slope 1, the boundary has to have zero or positive slope less than one. The same restriction holds with a change of sign at the right edge. In more graphic terms, as time increases, the boundary of a W-region adjacent to an edge of the depletion layer overtakes characteristics issuing from that edge in the W-region.

F. The Characteristic Pattern

If F and F_t and their first derivatives with x are continuous at $t = 0$ across the diode, $-\frac{1}{2} \leq x \leq \frac{1}{2}$, then any discontinuities in solution can only be along characteristic lines originating at the edges of the diode together with their reflections from the edges. These characteristics are shown in the sketch, Figure 5-2. It seems reasonable to seek a solution in which these characteristic lines separate the A-regions from the W-regions. However, this attempt fails, as the following arguments show.

If triangle $A_1C_1A_2$ is a W-region, the whole strip $A_1A_2B_3B_2$ is also, since none of the assumed boundaries are overtaking. For the same reason, strip $B_2B_3A_4A_3$ is also a W-region. If triangle $A_2C_2A_3$ is a W-region, the

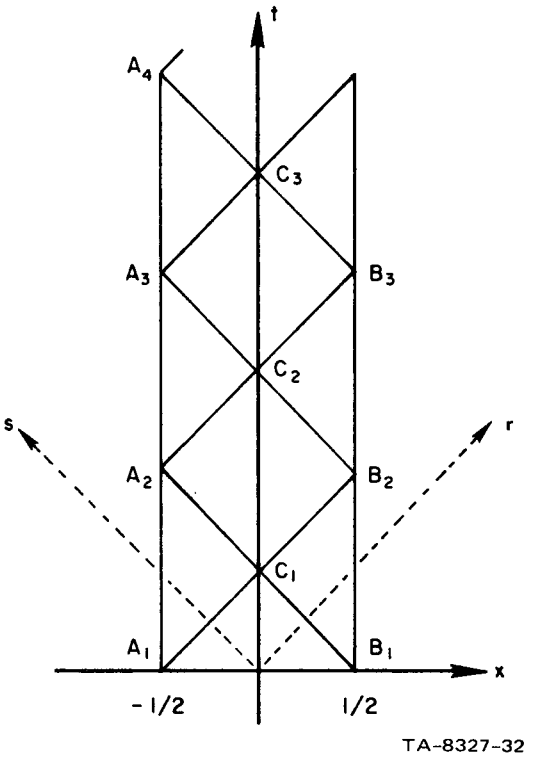

FIGURE 5-2 POSSIBLE LINES OF DISCONTINUITY IN AN INITIALLY SMOOTH SOLUTION

whole diode remains without ionization, a case of no interest here. If triangle $A_2C_2A_3$ is an A-region, it is to the left of a W-region in which $n = \epsilon$. This violates the rule.

Since the various triangles are symmetrically placed, the argument of the above paragraph shows that no triangle can be a W-region. The possibility that quadrilateral $C_1B_2C_2A_2$ is a W-region is now explored.

Triangle $A_1C_1A_2$ is an A-region in which the hole density p is ϵ along edge A_1A_2, and increases along boundary A_1C_1 to a larger positive value at C_1. The hole density increases in the same way along other characteristics parallel to A_1C_1 in the triangle but for shorter periods of time. Thus along C_1A_2, p has a positive value at C_1 and decreases to ϵ at A_2. These values are carried across the quadrilateral W-region

unchanged so that p decreases from a positive value at B_2 to ϵ at C_2. Along the characteristic B_2C_2 in the triangular A-region $B_2C_2B_3$, n increases from ϵ at B_2 to a larger positive value at C_2. Thus, near C_2, n is positive and reasonably large, whereas p is near ϵ. This violates the rule $p > n$ when the A-region $B_2C_2B_3$ is to the right. Thus no solutions exist with only the characteristic lines of the figure as region boundaries.

G. An Admissible Pattern

A pattern satisfying the rules is shown in Figure 5-3. Time intervals a and b are variable on their ranges: $0 \leq a \leq \frac{1}{2}$, $0 \leq b$. The whole pattern is periodic with period (2 + b) transit times. The type of each region is marked on the figure.

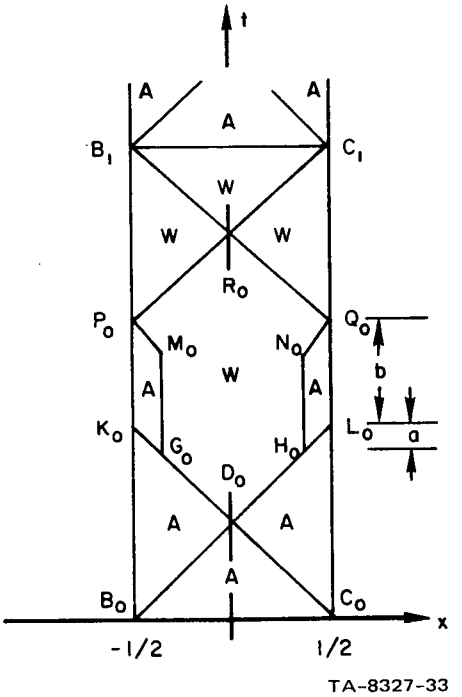

FIGURE 5-3 ADMISSIBLE PATTERN

On constant time line $B_o C_o$, F is constant and $p = n = \epsilon$. One may readily check that the left-running characteristics to points near boundary $D_o G_o M_o P_o$ have a longer run in A-regions than the right-running ones do. Thus, n is greater than p along this boundary with an A-region to the left in accordance with the rule. The rule is also observed on $D_o H_o N_o Q_o$ by symmetry. In the remainder of the time, the electrons and holes are swept away so that their densities are again near zero on $B_1 C_1$. The pattern can repeat.

The two characteristics reaching a point in triangle $B_o C_o D_o$ have equal length back to their crossings of $B_o C_o$, where p or n is zero. Thus p equals n in the triangle and E_x is zero. On each constant t line cutting the traingle, E is constant across the triangle and increases outside the triangle at both ends toward the diode edges, as in Figure 5-4. The value of E on x = 0, E(0,t) is determined from E(0,)) = 1 and by the last of Eqs. (5-1)

$$E_t = J - (p + n) \quad . \tag{5-20}$$

There is great freedom in choosing J so that E(0,0) = 1 and $E(0,\frac{1}{2}) = 1$, and $E(0,t) > 1$, for $0 < t < \frac{1}{2}$.

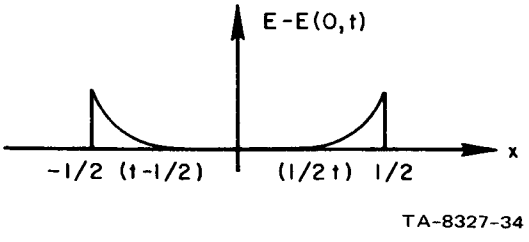

FIGURE 5-4 FIELD VARIATION ACROSS THE DIODE, $0 \leqslant t \leqslant \frac{1}{2}$

Current J is fixed on $\frac{1}{2} \leq t \leq 1 + b$ by the requirement that $E = 1$ on the boundaries between A-regions and W-regions. At a typical value of t on $\frac{1}{2} \leq t \leq 1 + b - a$, the variation of E would be as in Figure 5-5. On $1 + b - a \leq t \leq 1 + b$, the points at which $E = 1$ move to $x = \pm \frac{1}{2}$.

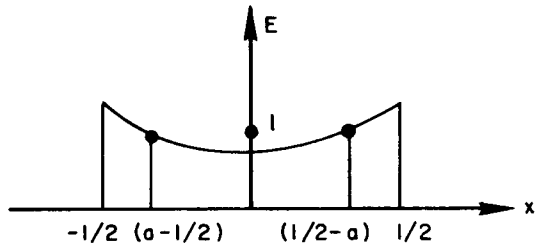

TA-8327-35

FIGURE 5-5 FIELD VARIATION ACROSS THE DIODE, $\frac{1}{2} \leq t \leq 1 + b - a$

In the interval, $1 + b \leq t \leq 2 + b$, maximum values of E occur at each time at the diode edges with some decrease in value to a minimum in the center. During the last half transit time, E is constant at each time across the central section in triangle $R_o C_1 B_1$. Here also J may be chosen quite arbitrarily except that $E < 1$ in the time interval, and $E = 1$ at $t = 2 + b$.

H. Analytic Solution of a Special Case

At time zero, only thermally excited electrons and holes are present. The initial condition is

$$p = n = \epsilon$$

with ϵ a small constant. For function F, we have,

$$F = 0 \quad , \quad F_t = -2\epsilon \quad , \quad t = 0 \quad ,$$

where the initial constant value of F has been taken to be zero.

The solution in the initial A-region, $B_o C_o L_o D_o K_o B_o$ of Figure 5-3, is the same as it would be if the diode were in avalanche for all time. This suggests applying Laplace transform techniques to obtain the solution.

The solution process is simplified if function F is replaced by G:

$$G = e^{-\alpha_o t} F \quad . \tag{5-21}$$

The differential equation and side conditions for G read:

$$G_{tt} - G_{xx} = \alpha_o^2 G \quad ,$$

$$\begin{aligned} G = 0 \quad , \quad G_t = -2\epsilon \qquad & \text{at } t = 0 \quad , \\ G_t + g_x + \alpha_o G = -2\epsilon e^{-\alpha_o t} \qquad & \text{at } t = \tfrac{1}{\epsilon} \quad , \\ G_x = 0 \qquad & \text{at } x = 0 \quad . \end{aligned} \tag{5-22}$$

The Laplace transform of G is $\bar{G}$:

$$\bar{G} = \int_0^\infty e^{-\mu t} G \, dt \quad . \tag{5-23}$$

Conditions on $\bar{G}$ become

$$\bar{G}_{xx} - q^2 \bar{G} = 2\epsilon \quad , \qquad q^2 = \mu^2 - \alpha_o^2 \quad ,$$

$$\mu\bar{G} + \bar{G}_x + \alpha_o \bar{G} = -\frac{2\epsilon}{\mu + \alpha_o} \qquad \text{at } x = \tfrac{1}{2} \quad , \tag{5-24}$$

$$\bar{G}_x = 0 \qquad \text{at } x = 0 \quad .$$

From these one readily finds

$$\bar{G} = -\frac{2\epsilon}{q^2} \left\{ 1 - \frac{2\alpha_o \cosh qx}{[(\mu+\alpha_o) \cosh (q/2) + q \sinh (q/2)]} \right\} \quad . \tag{5-25}$$

The first term, $-2\epsilon\, q^{-2}$, has the inverse transform

$$(\epsilon/\alpha_o)\left(e^{-\alpha_o t} - e^{\alpha_o t}\right) \quad ,$$

so the corresponding part of F is F_I:

$$F_I = (\epsilon/\alpha_o)(1 - e^{2\alpha_o t}) \quad . \tag{5-26}$$

Thus, F_I is a multiple of the solution $F = F_1$ found in a previous section plus a constant.

The second term of $\bar{G}$ may be expanded in a series of exponentials:

$$\bar{G} = \sum_{k=0}^{\infty} (\bar{G}_{k+} + \bar{G}_{k-}) \quad ,$$

$$\bar{G}_{k\pm} = \frac{4\epsilon\alpha_o}{q^2 (p+\alpha_o+q)} \left(-\frac{\mu+\alpha_o-q}{\mu+\alpha_o+q} \right)^k e^{-q(k+1\mp 2x)/2} \quad . \tag{5-27}$$

It can be shown that the inverse transform of $\bar{G}_{k\pm}$ is zero for times t less than $(k + 1 \mp 2x)/2$. Thus, no terms of this series contribute to the solution in triangle of $B_o C_o D_o$ of Figure 5-3: $F = F_I$ in this triangle.

Only the inverse of $\bar{G}_{0+}$ contributes in $C_o D_o L_o$, while only the inverse of $\bar{G}_{0-}$ is used in $B_o D_o K_o$. These inverses have the same form except for the sign of x. Now

$$\bar{G}_{0+} = \frac{4\varepsilon\alpha_o}{q^2 (\mu+\alpha_o+q)} \; e^{-q(1-2x)/2}$$

may be written

$$\bar{G}_{0+} = \frac{2\varepsilon}{q^2}\left[\frac{\alpha_o}{q} - (\mu/q - 1)\right] \; e^{-q(1-2x)/2} \quad , \tag{5-28}$$

where the first factor and each term in the brackets with the exponential function appears in transform tables.[10] The inverse transform is

$$\bar{G}_{0+} = 2\varepsilon \int_0^t \sinh \alpha_o (t - t') \, C(t') \, dt' \quad , \tag{5-29}$$

where

$$C(t) = H\left[I_o(\alpha_o y_1 y_2) - \frac{y_1}{y_2} I_1(\alpha_o y_1 y_2)\right] \quad ,$$

$$y_1 = \sqrt{t - (1 - 2x)/2} \quad , \tag{5-30}$$

$$y_2 = \sqrt{t + (1 - 2x)/2} \quad ,$$

and H is the Heaviside function, which is zero for t less than $(1 - 2x)/2$, and one for t greater than that value.

Finally, in triangle $C_o D_o L_o$, we have,

$$F = F_I + G_{0+} \quad . \tag{5-31}$$

In triangle $B_o D_o K_o$, function F has the same form with x replaced by (-x).

The simplest special case with $a = b = 0$ is considered here; it is sketched in Figure 5-6. On $D_o L_o$, t equals $x + \frac{1}{2}$, so s equals $\frac{1}{2}$. It follows that

$$t = (r + \tfrac{1}{2})/2 \quad , \quad x = (r - \tfrac{1}{2})/2 \quad \text{on } D_o L_o \quad . \tag{5-32}$$

Let function F, as given in Eq. (5-31) but with these values substituted for x and t, be f(r).

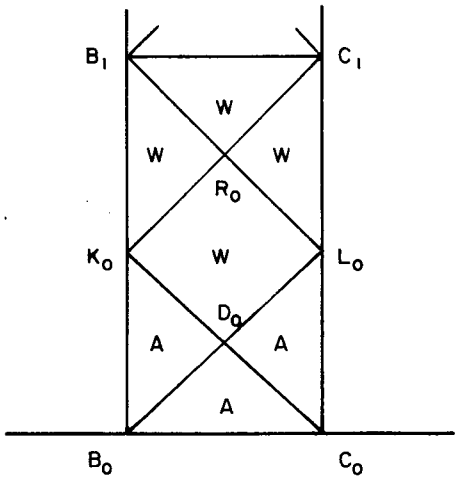

TA-8327-36

FIGURE 5-6 PATTERN WITH a = b = 0

On $D_{oo}K_{oo}$, t + x equals $\frac{1}{2}$ so r equals $\frac{1}{2}$. It follows that

$$t = (\tfrac{1}{2} + s)/2 \quad , \quad x\ (\tfrac{1}{2} - x)/2 \quad \text{on } D_{oo}K_{oo} \quad . \tag{5-33}$$

Now function F is given, in triangle $B_{ooo}D_{oo}K_{oo}$, by Eq. (5-31) with x replaced by (-x). Hence, on $D_{oo}K_{oo}$, F equals f(s) with the same function f as before.

In the characteristic quadrilateral $D_{oooo}L_{oo}R_{oo}K_{oo}$, function F is given by

$$F = f(r) + f(s) - f(\tfrac{1}{2}) \qquad \text{in } D_{oooo}L_{oo}R_{oo}K_{oo} \tag{5-34}$$

since $r = s = \frac{1}{2}$ at D_{o}.

The solution in triangle $R_{oo}L_{oo}C_{o1}$ is F = f(s) + g(r), for some function g. The boundary condition along $L_{oo}C_{o1}$ is $F_{r} = -\epsilon$. Hence, g is $-\epsilon r$ plus a constant chosen so that F will be continuous across $R_{oo}L_{oo}$, where r = 3/2:

$$F = f(s) + f(3/2) - f(\tfrac{1}{2}) - \epsilon(r - 3/2) \quad \text{in } R_{oo}L_{oo}C_{o1} \quad . \tag{5-35}$$

By the symmetry, we have

$$F = f(r) + f(3/2) - f(\tfrac{1}{2}) - \epsilon(s - 3/2) \quad \text{in } R_{oo}K_{oo}B_{o1} \quad . \tag{5-36}$$

Finally, in triangle $R_{o1}B_{o1}C_{o1}$ the solution matching the known values on $R_{o1}B_{o1}$ and $R_{o1}C_{o1}$ is

$$F = 2\ f(3/2) - f(\tfrac{1}{2}) - \epsilon(r + s - 3) \qquad \text{in } R_{o1}B_{o1}C_{o1} \quad . \tag{5-37}$$

I. Current and Voltage

The total external current density J is to be chosen so that $E > 1$ in A-regions and $E < 1$ in W-regions. The relation between E and F, Eq. (5-19) may be written

$$E = F + Q_J + 1 \quad , \quad Q_J = \int_0^t J \, dt \quad . \tag{5-38}$$

This is derived from Eq. (5-19) by noting that parameter t_o should be chosen so that $E = 1$ and $F = 0$ at $t = 0$.

For $t < \frac{1}{2}$, the requirement is that $Q_J + F > 0$. Since Q_J is constant for each value of t while F varies, this inequality is satisfied by taking

$$Q_J > - \min_x F \quad , \quad 0 < t < \tfrac{1}{2} \quad . \tag{5-39}$$

Since $E = 1$ on $K_o D_o L_o$, we have,

$$Q_J = - f(r) \quad , \quad \tfrac{1}{2} \leq t \leq 1 \quad . \tag{5-40}$$

A further requirement is that $(F + Q_J)$ is negative inside the angle $K_o D_o L_o$ and positive outside it. The requirement is shown to be satisfied in two particular cases: Put $F = F(x,t)$. Then one instance of the requirement is

$$F(0,\tfrac{1}{2}) < F(\tfrac{1}{2},\tfrac{1}{2}) \quad .$$

Substitution from Eq. (5-31) and some simplification give

$$0 < e^{\alpha_o/2} - I_o(\alpha_o/2) \quad .$$

But this is a known inequality,[11] so the requirement is satisfied.

If $\alpha_o < 4$, the whole line $t = \frac{1}{2}$ satisfies the condition because the inequality

$$F(0,\tfrac{1}{2}) < F(x,\tfrac{1}{2}) \quad , \quad 0 < x \leq \tfrac{1}{2} \quad ,$$

readily reduces to

$$0 < e^{\alpha_o x} - I_o(\alpha_o y) + [C] \quad , \quad y^2 = x(1 - x) \quad ,$$

where [C] stands for the integral term containing C. This inequality holds provided it does so when positive [C] is dropped and $I_o(\alpha_o y)$ is replaced by the larger quantity,* $\exp(\alpha_o^2 y^2/4)$:

$$0 < e^{\alpha_o x} - e^{\alpha_o^2 x(1-x)/4} \quad .$$

This inequality is satisfied if

$$\alpha_o(1 - x)/4 < 1 \quad .$$

Since $0 < x \leq \frac{1}{2}$, this requires $\alpha_o < 4$. Note that $\alpha_o < 4$ is sufficient for the requirement to hold, but may not be necessary.

In the second half of the period, the whole diode is out of avalanche. The restriction on the current reads

---

*Reference 11, Section 2.11.

$$Q_J < - \max_x F \qquad 1 < t < 2 \quad . \tag{5-41}$$

The voltage drop, V, is the integral of the field. From Eq. (5-20) V_t is given by:

$$V_t = J - \int_{-\frac{1}{2}}^{\frac{1}{2}} (p + n)\, dx \quad . \tag{5-42}$$

Since $p + n = - F_t$, this may be integrated over time to obtain

$$V - V_o = Q_J + M \quad , \quad M = \int_{-\frac{1}{2}}^{\frac{1}{2}} F\, dx \quad , \tag{5-43}$$

where V_o is the diode voltage at time zero.

From the analytic solution forms given above, one may compute F and M. As a guide to the computations and to an understanding of the solution, a qualitative sketch of (-M) is given in Figure 5-7. In Figure 5-7, curve OABC is a sketch of the other functions needed on the various time intervals: (- min F), (-f), and (- max F).

The curve for Q_J in Figure 5-7 would be a continuous curve lying above OA, running along AB, and falling below BC. Two extreme cases are shown: the dashed curve OABC itself, and the dotted curve, ODABGC, departing a "large" distance from OABC. Corresponding sketches of $(V - V_o)$ and J are given in Figure 5-8.

If Q_J follows its boundary curve OABC, the resulting variations of $(V - V_o)$ and J appear from Figure 5-8 to be roughly in phase, a condition of low efficiency. Higher efficiencies are obtainable by following an appropriate curve ODABGC with large departure from the boundary curve.

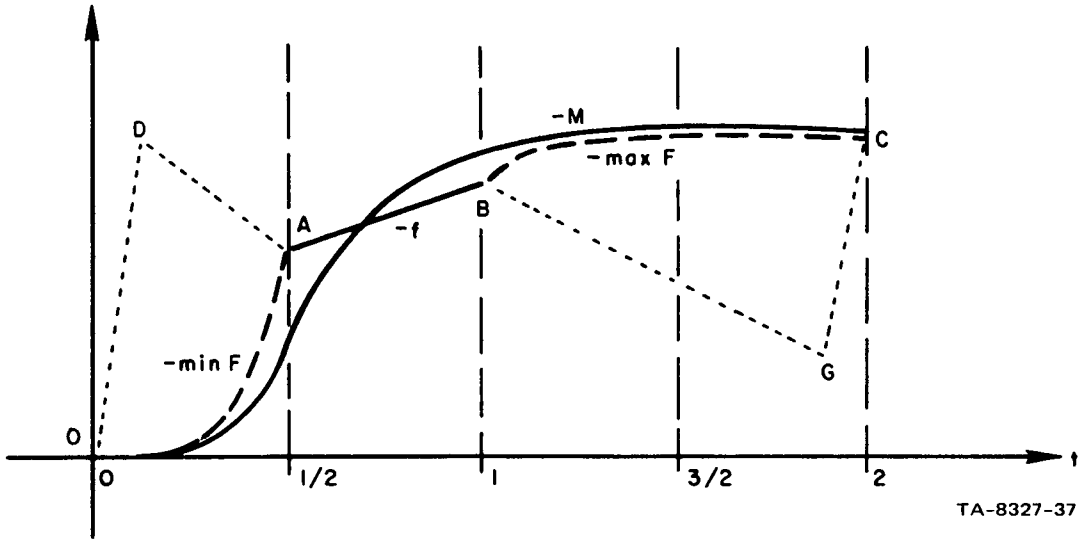

FIGURE 5-7 AUXILIARY FUNCTIONS

J. Conclusions

The approximate analysis of this section has been used to indicate possible patterns of avalanche regions in the space-time plane for the simplest case, the PIN diode. Estimates for the variation of current and voltage drop across the diode have been deduced without computation. The limitations on the current have been found, and first steps have been taken in selecting a current variation for efficient operation. Further efforts to refine the methods of pattern and current selection for the PIN diode and to extend them to diodes of other types are warranted.

C-2

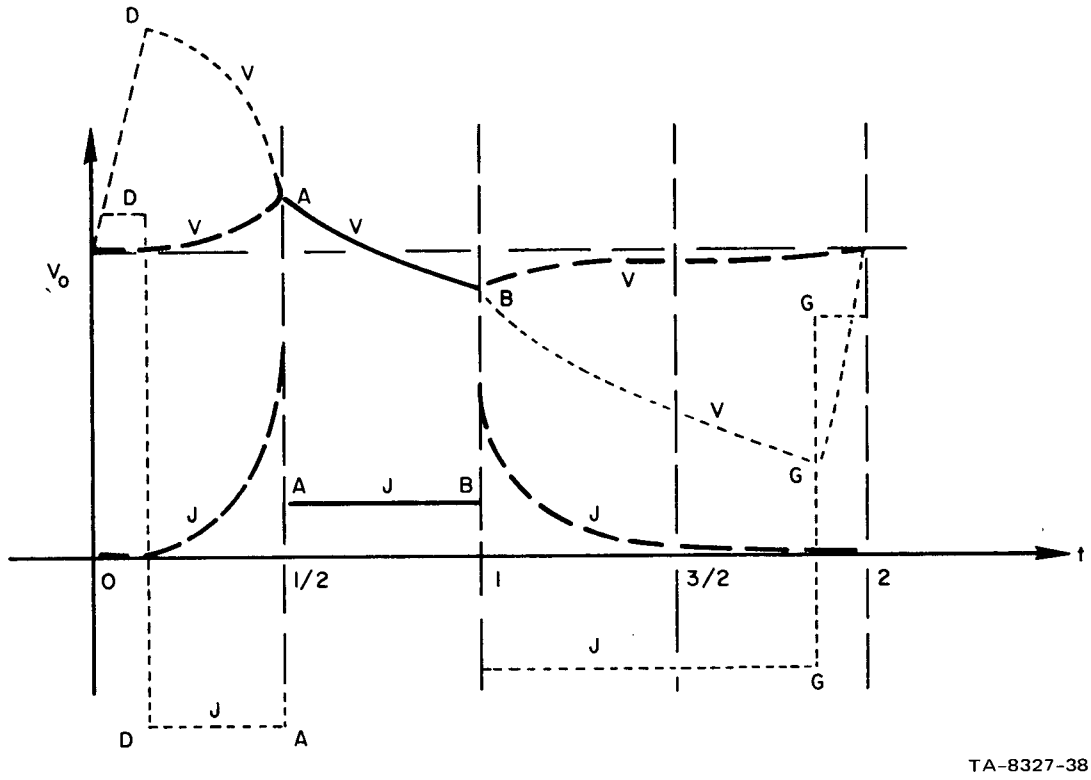

FIGURE 5-8 VOLTAGE ($V - V_o$) AND CURRENT J FOR THE TWO CASES—DASHED AND DOTTED

6. EXPERIMENTAL RESULTS

A. Summary of Experimental Work to Date

The principal objective of our experiments was to observe the effects on efficiency and output power of the various and independently variable vector impedances "seen" by an avalanche diode at each of several harmonically related frequencies.

The use of channel-dropping diplexers is appropriate for controlling loads that are separate and independent with respect to frequency. Accordingly, diplexers that dropped channels centered at 1500, 3000, and 6000 MHz were constructed and used with an avalanche diode having a breakdown voltage, V_B, of approximately 60 volts and an IMPATT frequency, f_{IMPATT}, of about 20 GHz. Experiments with this circuit were discontinued after preliminary results yielded only low efficiency at 1500 MHz and low output powers. In retrospect, it is seen that the pulsed bias supply then in use did not have the proper source impedance and was power limited. This experiment should be resumed with an appropriate bias supply which is now available.

A second experimental circuit was arranged for use with inexpensive diodes having $V_B \geq 160$ volts and known to oscillate very efficiently at a fundamental frequency near 750 MHz. The diplexers dropped channels centered at 750 and 2250 MHz while the RF circuit also included a stub that presented an open circuit to the diode at 1500 and 3000 MHz. The system was tried first with a bias supply now known to be inappropriate, and then with an almost ideal bias supply. In either case, the "high-conductivity state" was approached only feebly, and output efficiencies were too low to be of interest. Measurements showed that the circuits

contained too much loss, which prevented us from obtaining the required impedance transformations. The real part of the impedance presented to the diode in the desired frequency range was always greater than 10 ohms, regardless of tuning. For these diodes the real part of the circuit impedance at the fundamental frequency should apparently be less than 10 ohms when the real part of the circuit impedance at the second harmonic is relatively low.

Near the end of the contract, it was decided to set the diplexers temporarily aside and obtain information on the effects of harmonic tuning by indirect means. Two types of circuits were constructed, and the high-conductivity state (HCS) and accompanying high-efficiency oscillations (HEO) were obtained. The construction of these circuits allowed the vector impedance of the circuits to be measured and referred to the diode junction readily and with high accuracy. A great many different combinations of the settings of the tuning elements were used. All observations of HCS and HEO corresponded to low values to the real part of the circuit impedance for the first few harmonics. All corresponding values of the imaginary part of the circuit impedance were observed to be inductive for the first and second harmonics.

A few observations were also made with series and parallel combinations of avalanche diodes and with a novel and potentially useful arrangement in which a pair of diodes is in series for biasing purposes but in parallel with respect to the RF circuit.

B. Terminology and General Observations

This subsection lists some terminology for the purpose of simplifying and clarifying the discussion of the experimental results. Some experimental observations are also included that have not previously been published and that suggest future areas of investigation.

The reverse voltage required to draw a current from 1 to 100 μA was noted as the breakdown voltage, V_B. In general, we found that Fairchild FD-300 diodes that had $160 < V_B < 180$ volts gave the high-efficiency oscillations in the frequency range 650-900 MHz. In a batch of these diodes, this range of V_B is the lowest to be found since the manufacturer provides that V_B be not less than 150 volts. When diodes were placed in parallel, they were chosen to have, as nearly as possible, the same V_B.

Reverse bias was applied from a pulse supply that can be considered to be an ideal voltage source, V_0, with a series resistance R_{LL}. It was found advantageous to have, insofar as possible, R_{LL} variable. When $V_0 > V_B$, a "static breakdown" current, I_1, flows and $V_0 - V_1 = R_{LL}I_1$, where V_1 is the voltage across the diode junction. The point, (I_1, V_1), in Figure 6-1 will be called the "low-conductivity state" (LCS).

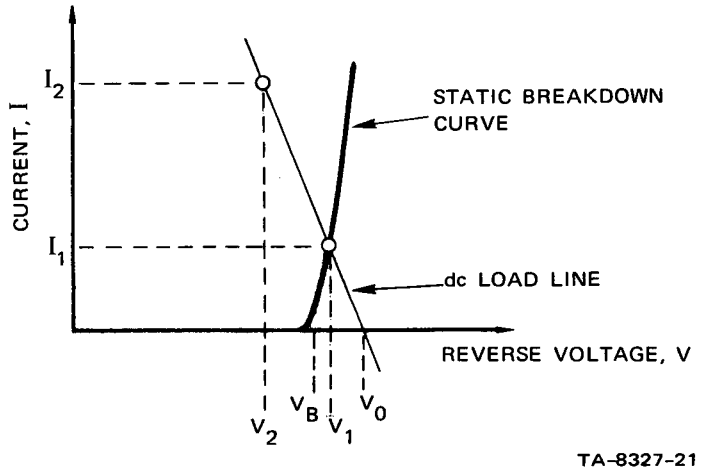

FIGURE 6-1 VOLTAGE AND CURRENT RELATIONS IN AVALANCHE-DIODE EXPERIMENTS

Certain critical tuning settings of the RF circuit created a condition whereby the diode spontaneously and rapidly (typically in 20 ns) switched to a high-conductivity state (HCS) defined by the point, (I_2,V_2), in Figure 6-1. For FD-300 diodes V_2 was typically about 20 percent less than V_1. The ratio of I_2 to I_1 was typically 5 to 1, but ratios from 1.2:1 to 12:1 have been observed. RF oscillations at low frequencies were obtained for both low-conductivity and high-conductivity states. The LCS oscillations were characterized by considerable noisiness in the RF pulse envelope whereas the HCS oscillations as seen in the pulse envelope were relatively free of noise. These two states of oscillation are illustrated in Figure 6-2. The LCS oscillations were weak, with typical efficiencies of 1.5 percent. Although a large I_2/I_1 ratio is associated with high RF efficiency, it does not guarantee high efficiency. In one locally optimized representative case noted, we had $I_2/I_1 = 7$, but the RF output efficiency was less than 0.1 percent, or more than 10 times weaker than with some LCS oscillations. Frequency also does not distinguish the two states, since the frequency of oscillation has been observed to increase typically by only 1.3 percent when a diode spontaneously switches from LCS to HCS if V_0 or the RF tuning is unchanged. Following application of the bias pulse, the LCS oscillations have negligible power but continue to grow until some time later (typically 100 ns) as shown in Figure 6-2(a). These oscillations are moderately sensitive to I_1 and are very much less sensitive to RF circuit tuning than are HCS oscillations.

A better-known hallmark of the HCS is that the rapid transition from the LCS to the HCS occurs after an interval, t_i. We have observed t_i to be as low as 40 ns or as high as 300 ns. Lower efficiencies, η, and lower I_2/I_1 ratios are generally, but not always, associated with longer values of t_i, whereas high η and I_2/I_1 are observed to occur along

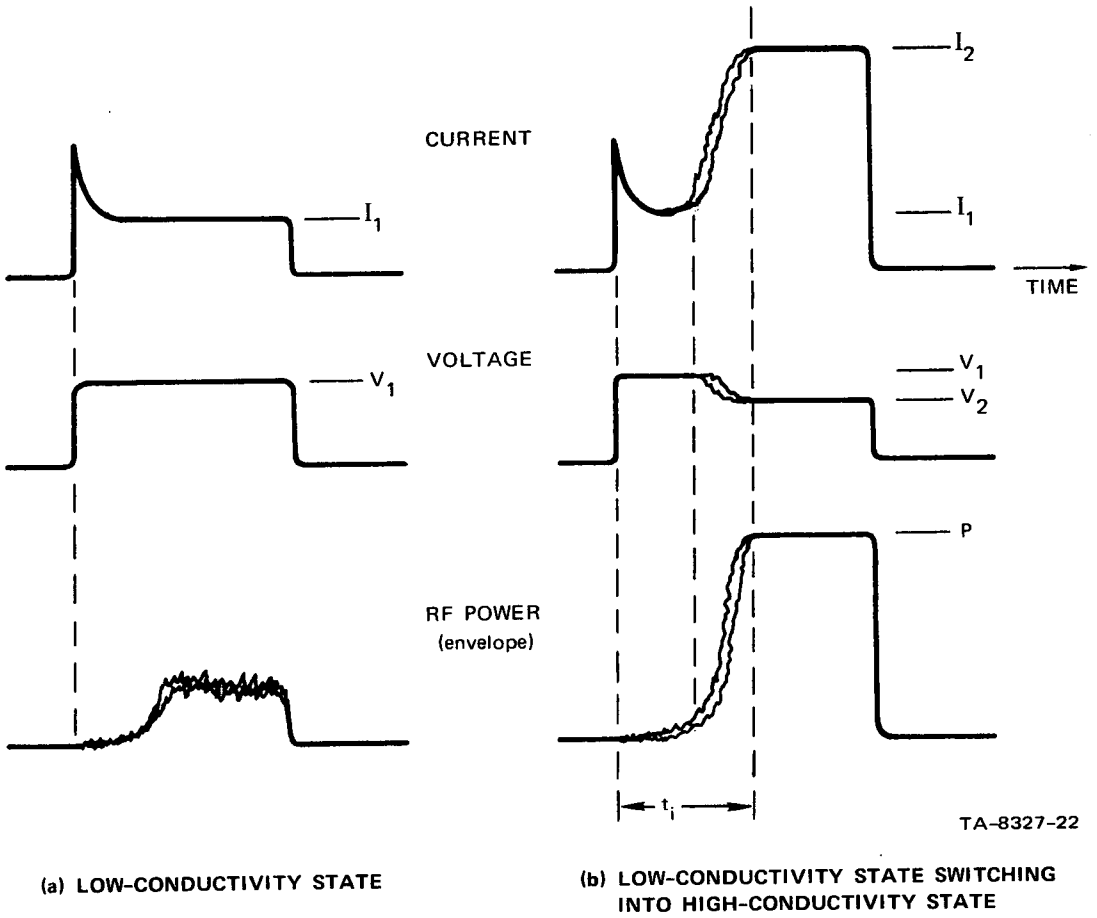

FIGURE 6-2 WAVEFORMS OBSERVED IN PULSED AVALANCHE-DIODE EXPERIMENTS

with all values of t_i. For a given R_{LL}, t_i usually first decreases and then increases as V_o is increased. Otherwise, we have not yet been able to identify which properties of the RF circuit or bias circuit determine whether t_i will be large or small. Furthermore, t_i is not constant from pulse to pulse, and the statistical spread in t_i is itself variable. Generally, but not always, the percentage spread is low when t_i is low. Frequently, but not always, t_i will increase substantially, and with no change in I_1, I_2, V_1, V_2, or P, when a FD-300 diode is chilled with Freon spray. Similarly t_i may decrease when the diode is heated. This suggests that t_i is related to the time

required for the diode to reach a thermal equilibrium consistent with the RF oscillations permitted by the circuit. In Section 2 we showed theoretically that the period of oscillation is strongly dependent upon the magnitude of the diode saturation current. But the saturation increases with the increased diode temperature. The experimental observation of t_i being temperature dependent appears to be consistent with theory. Additional experiments where the diode is placed in a controlled thermal environment are warranted to confirm this point.

Events occurring during the interval t_i are of interest. We have been able to determine experimentally that the RF oscillations are LCS in character and typically, only 1.3 percent lower in frequency than that generated in the HCS. These oscillations grow in magnitude until the transition to the HCS occurs. Only the first few harmonics of the fundamental frequency have been observed, and they were relatively small. Whether or not high-frequency "IMPATT" oscillations trigger the change of state, as supposed by some, is still uncertain. The construction of our circuits, however, is such that a high-Q resonance at the IMPATT frequency is unlikely.

It was observed also that the change in states sometimes failed to occur on a fraction of the pulses. On occasion this fraction was large. When high-efficiency performance from a given diode is accompanied by a high percentage of state-switch misses, another RF circuit can sometimes give the identical performance but without the state-switch misses. Investigation of the parameters affecting this instability effect would be of value.

Some of the effects of V_0 and R_{LL} on oscillator performance have been studied. Experimentally, it was observed that the efficiency and output power were unaffected by small changes in R_{LL}. An increase in R_{LL} from 20 to 30 ohms, for example, could be compensated by increases

in V_o, V_1, and I_1, and a change in t_i, but no change in I_2, V_2, and the output power. Larger changes in R_{LL} give different results. An increase from R_{LL} = 20 to 50 ohms or more led to a decrease in the ultimate RF power and efficiency obtainable. Perhaps, during the LCS some junction temperature is established that affects the RF efficiency after the HCS is reached. With the pulse supply used, the lowest value of $R_{LL} = (V_1 - V_2)/(I_2 - I_1)$ obtainable was about 18 ohms; hence we do not yet know whether an optimum value of R_{LL} less than this exists.

The effective dc resistivity of the HCS, $R_2 \equiv V_2/I_2$, was also noted. For FD-300 diodes, the range $35 < R_2 < 60$ ohms was observed, with the best η obtained for R_2 = 40 ohms. There is a trend for lower values of R_2 to be obtained at higher η, but many exceptions have occurred.

C. Details of Experimental Circuits

1. First Diplexer Circuit

The first circuit used with channel-dropping diplexers had the components shown in Figure 6-3. The two diplexers shown schematically were designed, constructed, and tested for the frequencies 1500 and 3000 MHz (fundamental and second harmonic) with a "maximally flat" fractional bandwidth of 0.2. A third, analogous, diplexer was prepared for the frequency 6000 MHz to be used to control either the fourth harmonic in the above case or the second harmonic for a diode having a fundamental oscillation at 3000 MHz.

The diplexers are of a complementary-impedance design, combining, in series, interdigital bandpass filters and parallel-coupled-strip band-stop filters. Adequate selectivity is obtained with two reactive elements (n = 2) per filter, and construction is achieved with

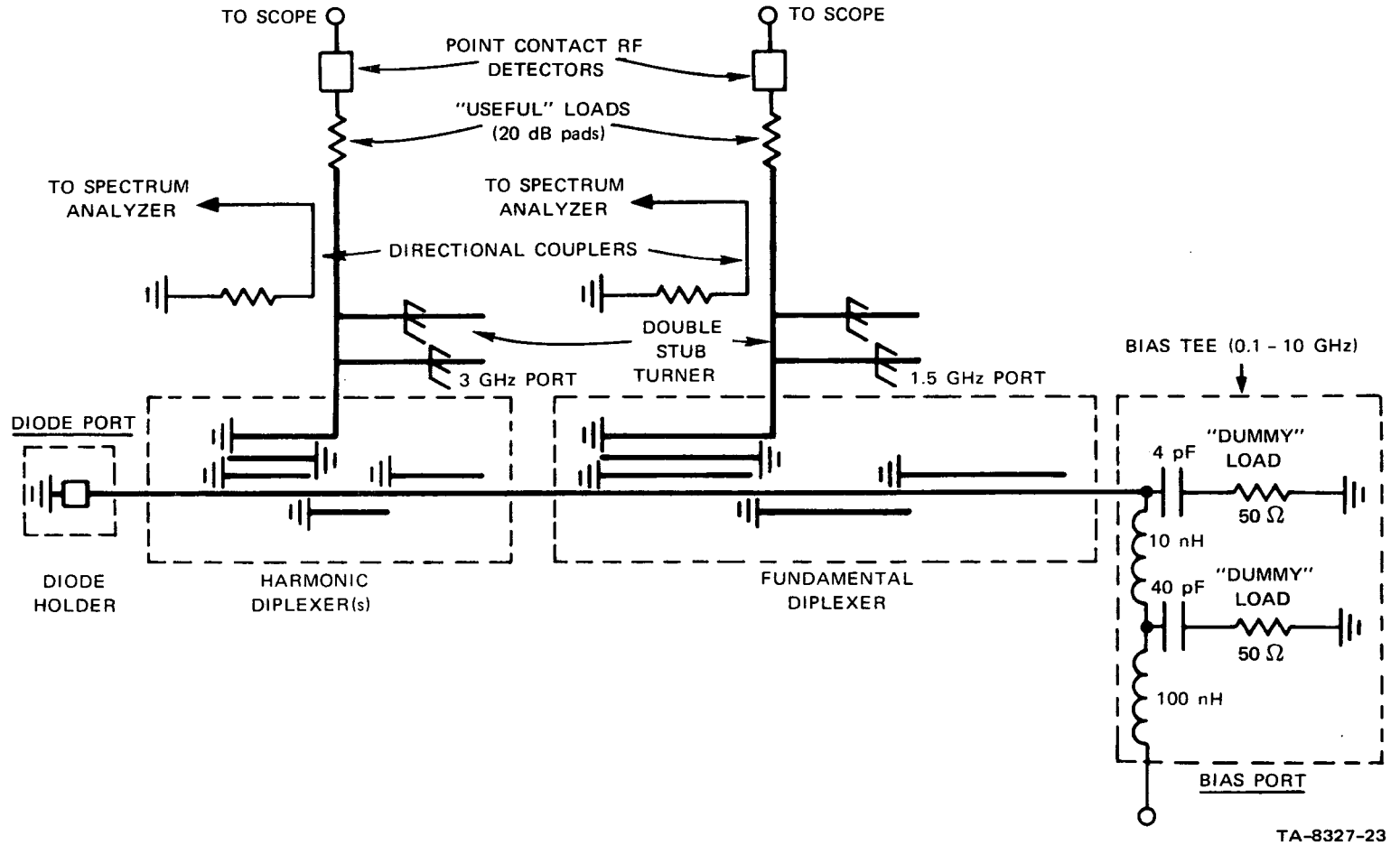

FIGURE 6-3 FIRST EXPERIMENTAL SETUP FOR PULSED OPERATION OF AN AVALANCHE DIODE WITH RF CHANNEL SEPARATION AT TWO (or more) FREQUENCIES

round rods between ground planes and OSM connectors. Computer programs were used to select coupled-rod diameters and spacings, and the Hewlett-Packard network analyzer was used in tuning up the filters.

The circuit included a new bias-T designed to present a match over a two-decade frequency band extending from well below the lowest frequency for which the diode might exhibit negative resistance to well above the frequency of the highest harmonic of interest. Thus, in the band of each critical frequency the avalanche diode could "see" only the load connected to the channel-dropping arm of the respective diplexer, while at all other frequencies it "saw" a "match." This bias-T is combined with the dummy load for the diplexer and is therefore uncritical since it is intended to be dissipative at the outset. The ultra-wide-band operation of this bias-T was realized with microstrip conductors and physically very small lumped reactive elements. Commercial bias networks were not acceptable because of insufficient bandwidth, inadequate peak voltage rating, and excessive capacitance relative to the short, fast-rise pulses to be used.

The system was calibrated initially by replacing the diode by a coaxial connector and placing resistive terminations at the 1500- and 3000-MHz ports. The combined residual VSWR referred to the diode port was below 1.3 in the critical ranges 1350-1650 MHz and 2700-3300 MHz. In addition, the VSWR was below 1.3 in the low range 100-600 MHz, provided that the bias supply looked substantially resistive. The VSWR did not exceed 1.9 in the high range 3900-7200 MHz, although the 1500-MHz diplexer had spurious pass bands 300 MHz wide centered at 4500 and 7500 MHz.

The bias-pulse voltage waveform was monitored with conventional probes whereas the diode-current pulse envelope was monitored with a ferrite-core transformer of novel design. Pulse lengths of 100 to

400 ns were used at a PRF of the order of 1 kHz. The bias supply combined a dc "pre-bias" supply with a low-voltage pulse in a "dc restorer" circuit. We now know that this supply was inappropriate for several reasons, including inadequate current capacity and lack of resembalance to a voltage source with finite R_{LL}. In addition we found that because $V_2 < V_B$, the diodes exhibited surface breakdowns when a "pre-bias" was combined with a low-voltage pulse.

Some Varian experimental TRAPATT diodes were used in the circuit configuration shown in Figure 6-3. These diodes typically had $V_B \approx 60$ volts and $f_{IMPATT} \approx 20$ GHz. Oscillations were obtained at the desired frequency of 1500 MHz although sometimes the fundamental was at 4500 MHz, which represented a spurious response of the fundamental diplexer. The low efficiency and noisiness of the power output suggest that the diode was not operating in the HCS. This was further indicated by the fact that I_2/I_1 was less than about 1.2. It is reasonable to suppose that satisfactory performance would have been obtained with a proper bias supply and that useful data could now be obtained with the configuration of Figure 6-3.

2. Second Diplexer Circuit

It was decided to work with Fairchild FD-300 diodes, which are very inexpensive. From a large batch of these diodes one can select diodes having V_B of any desired value from about 165 V to over 300 V. Others have obtained TRAPATT oscillations in the 500-to-1000-MHz range using these diodes.[13,14] The diodes are packaged in glass, with thin-wire pigtails and an S-shaped contact spring on one side of the silicon chip. Thus, these diodes are limited by low thermal dissipation capacity both during a pulse and from pulse to pulse.

It was also decided to control four harmonic impedances as follows. The diode would see adjustable impedances at 750 MHz (n = 1) and 2250 MHz (n = 3) through the use of a triplexer and suitable double-stub tuners for each of these two channels. The triplexer was built by SRI under Contract NAS 12-2165 and is described in the report NASA CR-111784. The design is based on a three-reactive-element Chebyshev-form fractional bandwidth of 0.286. At 1500 MHz (n = 2) and 3000 MHz (n = 4) the diode would "see" an open circuit. This was achieved by placing an open-circuited series stub next to the diode.

The complete arrangement is shown schematically in Figure 6-4. Because of the series open-circuited stub it was necessary to design a new bias-T that would not seriously load the RF circuit. A schematic of the bias circuit is shown in Figure 6-4, including the resistances that were added for damping when LC resonances in the bias network were observed. The circuit was checked out on the network analyzer and found to be satisfactory except for some loss between the diode port and the triplexer. Some of this loss was in the stub assembly, which was built in microstrip. The rest of the loss, which was most noticeable below 650 MHz, was due to a small coupling to the dissipative elements in the bias structure.

The equipment was operated first with a bias supply now known to be unsuitable in a variety of ways, and finally with a supply that has been most satisfactory. The pulse current and voltage capacity of the bias supply are adequate for series and parallel combinations of FD-300 diodes, and the supply acts as a voltage source with an internal resistance of typically 18 ohms. Generally, external series resistance was added to optimize R_{LL}.

Oscillations were obtained at the expected TRAPATT frequency, but they were inefficient and noisy. The oscillations were probably

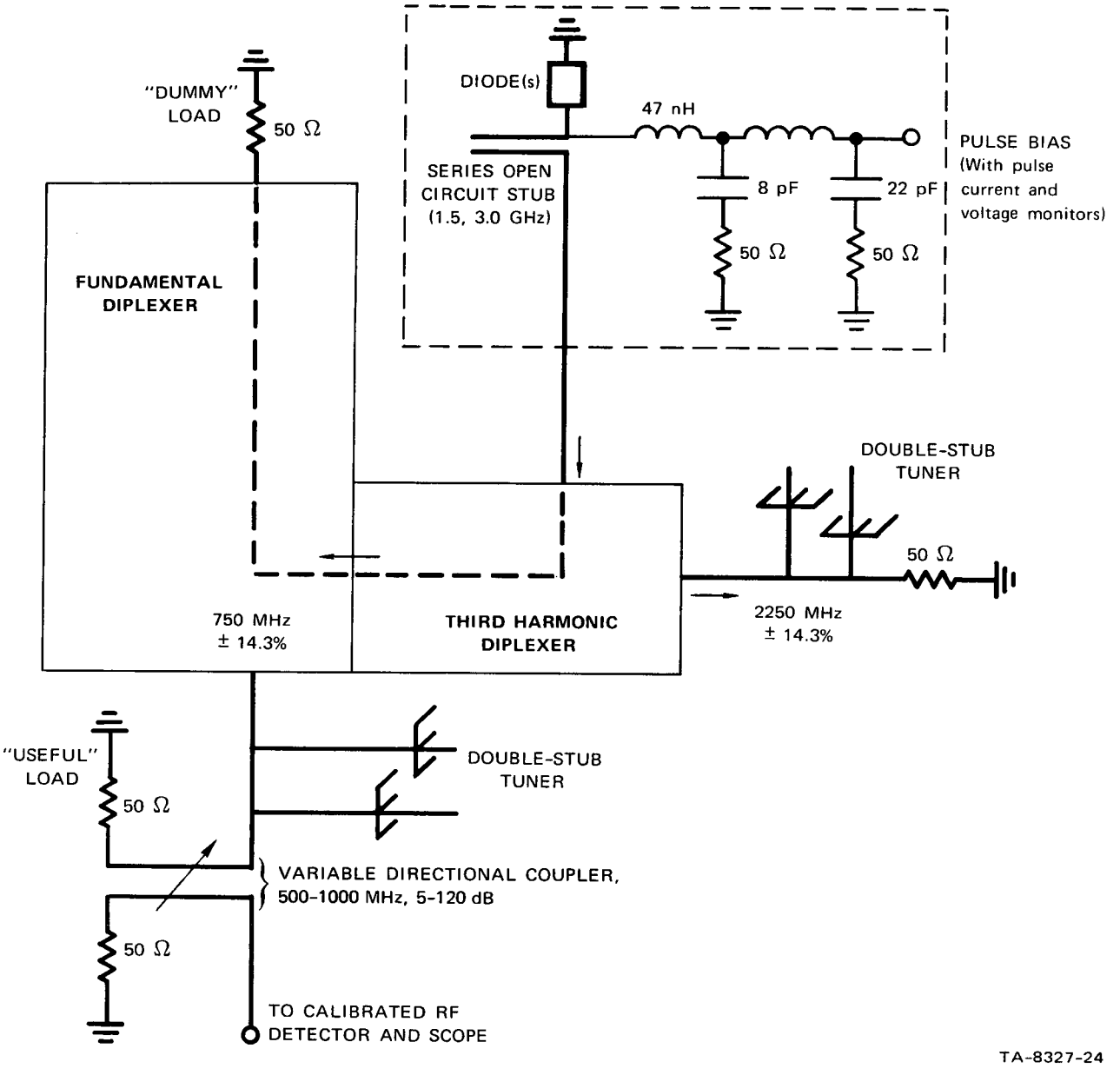

FIGURE 6-4 SECOND EXPERIMENTAL SETUP FOR PULSED OPERATION OF AVALANCHE DIODES WITH SEPARATE IMPEDANCE CONTROL (Two fixed, two variable) AT FOUR (Harmonic) FREQUENCIES

in the LCS in that if a "jump-up" in current was observed at all, it corresponded to $I_2/I_1 \leq 1.2$. Occasionally, we observed a modulation at about 20 MHz superposed on the pulse waveforms of I, V, and the RF envelope of 750 MHz in the region $t > t_i$. Similar observations have been reported by others.[15] Microwave generation was also observed in even cheaper Amperex A-13 diodes. These diodes have thicker pigtails and no S-spring, but many exhibited excess leakage resistance. Even cheaper 1N4454 diodes exhibited low-frequency oscillations. This is a new observation not previously reported.

A possible explanation for the low efficiencies observed was suggested from a Smith-chart plot of the impedances looking into the diode port of the circuit of Figure 6-4. In the band 643 to 857 MHz it was found that there was a small but critical "forbidden zone" in the form of a ring on the Smith chart which roughly covered the region $5 < \text{VSWR} < \infty$. That is, regardless of the positions of the double-stub tuners, the region $0 < \text{Re}[Z] < 10$ ohms was unattainable because of circuit losses. The stub tuners were found not to be the principal source of loss since measurements indicated that they could give a VSWR as high as 25:1 or Re[Z] as low as 2 ohms. The losses for the fundamental band were partly in the diplexer, but mainly in the series stub and bias-T assembly. Recently a new design for the bias circuit and circuits at the second and fourth harmonics has been developed which should reduce these losses. The circuit of Figure 6-4 with the new bias circuit should provide useful knowledge of the TRAPATT mode as originally proposed.

3. Avalanche-Diode Circuit Using Only a Double-Stub Tuner

Some experiments were made with FD-300 diodes in circuits without independent harmonic tuning. If the circuit impedances as seen

by the diode are readily measurable on a network analyzer, then information on harmonic tuning can be obtained indirectly. The simplicity of these circuits permits one to readily gain experience with the high-efficiency mode of operation and to measure the diode performance.

Figure 6-5 shows the diode holder, which used a bypass capacitor for the bias input. This method of applying bias has proved to be the most useful method for pulse operation where we are not limited by thermal dissipation. The bypass capacitance can be as large as desired, subject to distortion tolerance on the bias pulse. It is possible that this capacitance may affect the speed of the LCS-to-HCS transition, Figure 6-2(b). Our capacitor was formed by clamping a 0.5-inch × 0.5-inch plate over dielectric tape (typically, 0.001-inch mylar). The corresponding capacitance was roughly 100 to 200 pF, depending on the dielectric and the clamping pressure.

It was useful to measure the impedance looking into the diode holder terminals with the diode forward biased sufficiently (typically 30 mA) to "short out" the junction but not the diode package inductance and the holder parasitics. The holder assembly then looked, relative to 50-ohm coax, like a low-loss short-circuited stub of length ℓ, where ℓ varied with frequency as given in Figure 6-5. Then if the vector impedance of some RF load circuit to the left of the reference plane is known, one has only to translate the reference plane through the distance ℓ to refer this impedance to the diode junction. This procedure was used to prepare the impedance plots on the following pages.

The essentials of the rest of the RF circuit are shown in Figure 6-6. The procedure was to monitor the pulsed waveforms of I and V and the envelope of the fundamental power. The RF signal was detected by a calibrated point-contact diode which had a sensitivity close to 50 mV output across 100 ohms for 0 dBm input. Fundamental and harmonic

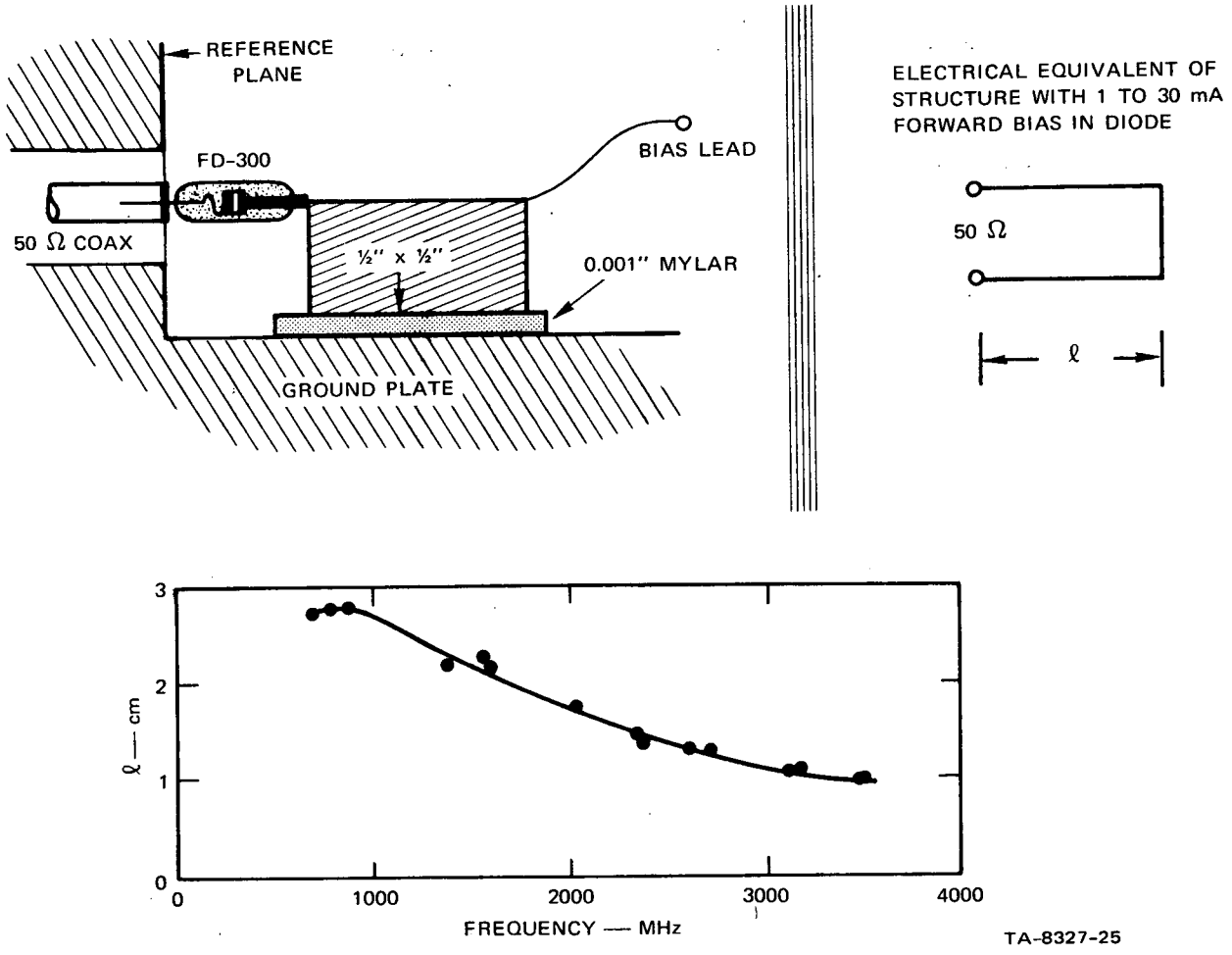

FIGURE 6-5 PASSIVE PROPERTIES OF FD-300 DIODE PACKAGE IN A GIVEN HOLDER

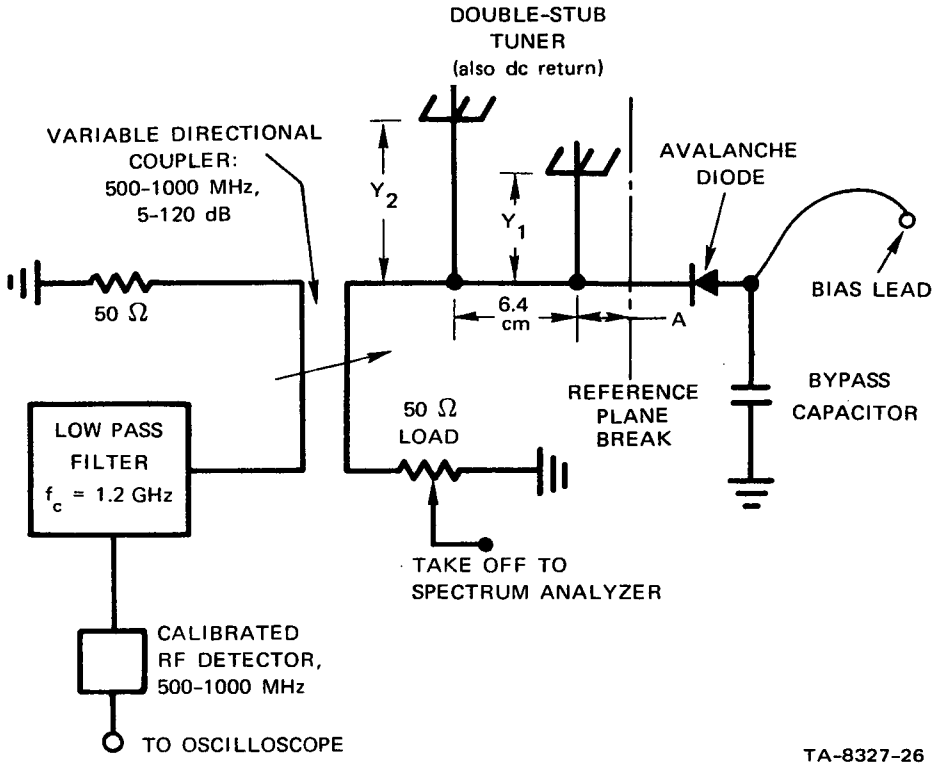

FIGURE 6-6 THIRD EXPERIMENTAL SETUP FOR PULSED OPERATION OF AVALANCHE DIODES WITH DOUBLE-STUB-TUNER CIRCUIT

power spectra were also monitored. After many trials, a single relatively "superior" diode was chosen, and data were taken for a limited number of fixed values of A while optimizing the RF output power at the fundamental frequency by varying Y_1, Y_2, and V_0. R_{LL} was found not to be critical when kept near its minimum value. Variation of V_0 usually yielded only a single maximum whereas all possible variation of Y_1 and Y_2 yielded numerous maxima, which may be referred to as "local maxima." One of these would be a "grand maximum." V_1, V_2, I_1, I_2, and tuner settings were recorded along with the peak fundamental power output (P_1) at the fundamental frequency, f_1. Computations included $R_2 = V_2/I_2$, $R_{LL} = (V_1 - V_2)/(I_2 - I_1)$, and fundamental mode efficiency $\eta_1 = P_1/V_2I_2$. Finally, the RF circuit was broken at the

indicated reference plane and the circuit impedances measured with the network analyzer at harmonics 1 through 4.

A selection of representative data (17 cases) is given in Figure 6-7 and Table 6-1. In no case was the Re[Z] > 20 ohms at any of the four harmonics. For n = 1 and n = 2, the Im[Z] was almost always inductive in contrast to the theoretical results of Section 2 for the TRAPATT mode. The major exception to the "inductive Im[Z]" rule is Case G, where tuning is relatively uncritical and Im[Z] is substantially capacitive for all four harmonics. In addition, Re[Z] tends to be higher than in the other cases, especially at n = 1. Case G is included for theoretical interest since it represents the LCS and not the HCS despite the same (within 1.5 percent) low frequency of oscillation.

Case D is of some interest because the HCS was clearly obtained, but the RF output was even less than can be obtained in the LCS. Apparently, wide RF swings of junction current and voltage occurred but their relative phases were such that very little power was delivered to the load.

Case L was noted as having the shortest observed t_i, but this feature seems to be uncorrelated with anything in the impedance plots. The same seems true of Case F, in which all three pulse waveforms developed a 14-MHz modulation once the HCS was reached. Cases H and K exhibited the most power and efficiency although state switching did not occur on all bias pulses. The efficiencies obtained compare well with those of Chaffin and EerNisse[14] but are somewhat less than was typical for Kostishack[13] for single diodes. The impedance-plot indications for cases H and K are as follows:

- At n = 1, relatively high Re[Z] among the cases presented (4 ohms)

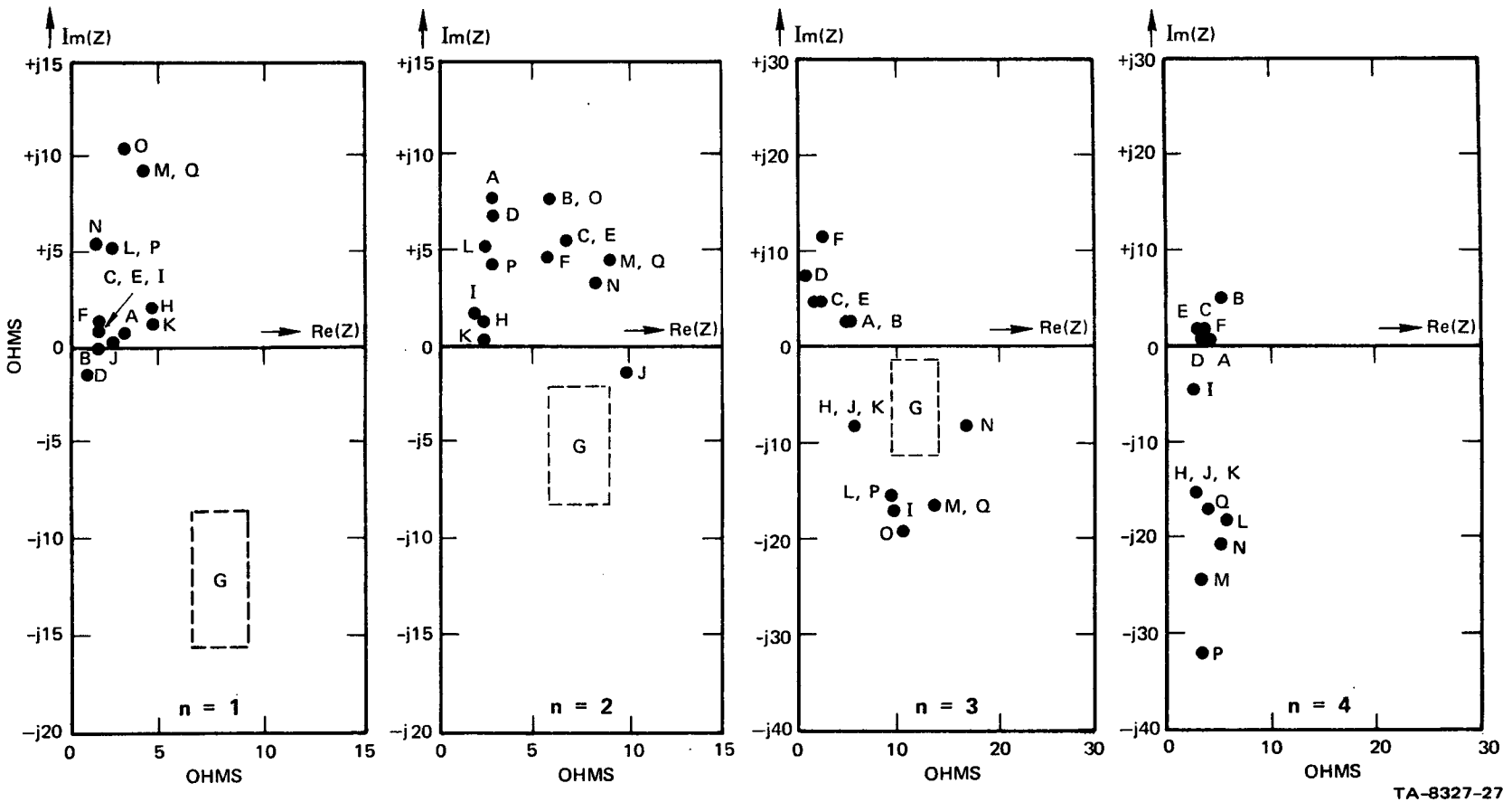

FIGURE 6-7 IMPEDANCE PLOTS (Referred to Diode Junction) FOR CIRCUIT OF FIGURE 6-6 TUNED FOR LOCAL MAXIMA OF POWER WITH SINGLE FD-300 DIODE NO. 54

Table 6-1

OPERATING DATA FOR FD-300 AVALANCHE DIODE NO. 54 IN DOUBLE-STUB-TUNNER CIRCUIT

(Case G is LCS, all others are HCS)

Case	Fundamental Frequency	Fundamental Peak Power	Fundamental Mode Efficiency				Remarks
	f_1 (MHz)	P_1 (watts)	η_1 (percent)	I_2 (A)	V_2 (V)	R_2 (Ω)	
A	680	22.4	5.2	3.08	140	46	
B	680	5.0	1.3	2.7	140	52	
C	680	3.2	0.8	2.77	140	51	
D	680	0.25	0.06	3.24	140	43	Lower P_1 and η_1 than for LCS
E	680	10.0	2.6	2.77	140	51	
F	680	6.3 pk		2.3 pk		61	Has 14-MHz envelope modulation
G	670	0.4 to 1	0.16 to 0.7	0.8	190	240	LCS, not HCS ($I_2 = I_1$, etc.)
H	860	70.0	14.0	3.54	140	40	Best efficiency
I	865	1.3	0.25	3.7	140	38	
J	860	10.0	2.3	3.16	140	44	Maximum t_i
K	860	63.0	13.0	3.5	140	40	Best efficiency
L	780	11.0	2.2	3.5	140	40	Minimum t_i
M	790	10.0	2.9	2.46	140	57	
N	780	2.0	0.7	2.16	140	65	
O	790	4.5	1.1	3.0	140	47	
P	780	10.0	2.0	3.6	140	39	
Q	790	13.0	3.3	2.8	140	50	

- At n = 1, only slightly inductive Im[Z]
- At n = 2, 3, 4, relatively low Re[Z]
- At n = 2, almost no reactance in Z
- At n = 3, 4, capacitive Im[Z].

4. Simple Tunable Avalanche-Diode Circuit

Another experiment was conducted to evaluate further the effects of harmonic tuning by indirect means. The RF circuit used is shown in Figure 6-8 and was related to that used by others.[13,14] The circuit includes a movable short circuit, in a 50-ohm transmission line, on one side of the point where the diode is connected to ground via the series bypass capacitor. On the other side of the diode, going toward the load, a variable, lumped, shunt capacitor was placed at a variable location. Thus, three RF tuning variables were available.

In Kostishack's work the tuning capacitor was about 1/9 fundamental wavelength away from the diode, and the movable short was

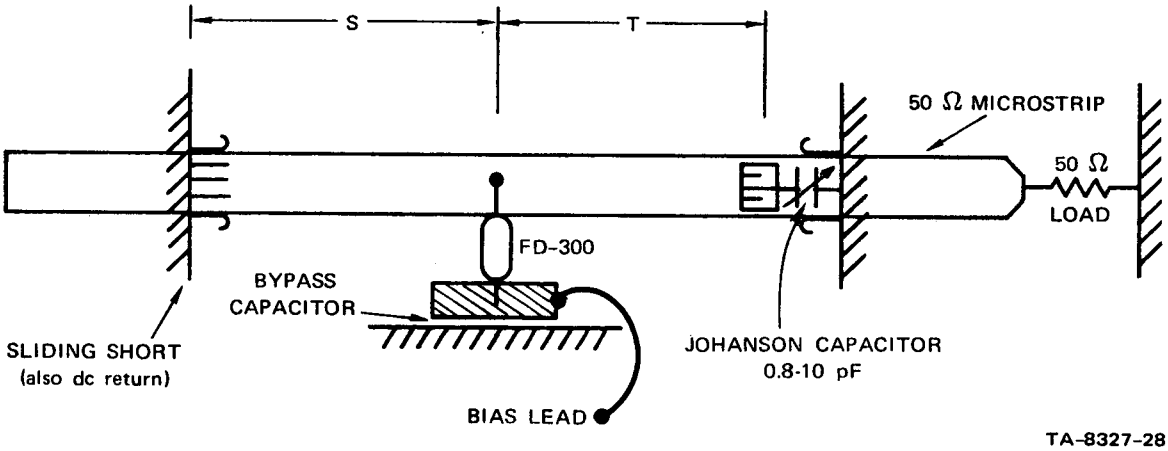

FIGURE 6-8 ESSENTIAL CONFIGURATION OF "FORTUITOUSLY EFFICIENT" AVALANCHE-DIODE CIRCUIT (In Microstrip)

located at approximately 1/6 fundamental wavelength from the diode.* Using the mechanical parameters recorded by Kostishack, and making some simplifying assumptions about diode pigtails, we made computations of the impedances presented to the diode:

At 570 MHz, $Z_1 = 16.5 + j20$ ohms

At 1140 MHz, $Z_2 = 200 + j25$ ohms

At 1710 MHz, $Z_3 = 0.05 + j25$ ohms

At 2280 MHz, $Z_4 = 20$ ohms.

In addition to the very high Re[Z] at n = 2, an inductive Im[Z] at n = 1 and 2 is to be noted. The latter fact is theoretically surprising, but it does agree with our experimental observations to date.

We built a version of this circuit in 50-ohm microstrip, rather than coaxial line. Microstrip was chosen primarily for ease in construction. The sliding short and movable variable capacitor were not really suited to microstrip design. The short was imperfect and there was inductance in series with the capacitor. These problems were not serious, however, for the type of measurements we were interested in making. The bypass capacitor was the same as used in the previous circuit. With this circuit, we were unable to obtain any stable, efficient, HCS oscillations where the dimensions S and T were of the order of 0.1 to 0.2 of a fundamental wavelength. Efficient, stable, HCS oscillations were observed only when $S \approx T \approx 0.45$ of a fundamental wavelength. The efficiency compared with the best observed when the same diode was used in the circuit of Figure 6-6. The stability was improved (i.e., no state-switch failures on some pulses) and t_i was

*Private communication.

generally at a minimum. Typical operating data for FD-300 diode No. 54 are:

f_1 = 850 MHz

P_1 = 50 watts (neglecting radiation)

P_2 more than 30 dB weaker and P_3 still weaker

$t_i \approx$ 50 ns

I_1 = 0.77 A

I_2 = 3.4 A

V_1 = 200 V

V_2 = 140 V

R_{LL} = 23 Ω

R_2 = 41 Ω

$\eta_1 \approx$ 10.5 percent.

When another diode (No. 61) having the same V_B was added in parallel, the combination exhibited the best performance with no change in the RF tuning adjustments. The fundamental frequency shifted to 825 MHz, t_i increased to 150 ns, P_1 increased by 1 to 2 dB, and η_1 increased to 13 percent. I_2 increased to only 4.2 A, which means each diode had much less current. Adding a third comparable diode (No. 30) gave no further change other than a slight increase in f_1.

The impedances in our circuit were readily measurable on the network analyzer. Referred to its junction, the diode "saw" the following impedances:

At n = 1, Z_1 = 2 + j13 ohms

At n = 2, Z_2 = 7.5 + j10 ohms

At n = 3, Z_3 = 12.5 - j25 ohms

At n = 4, Z_4 = 175 - j100 ohms.

5. Avalanche Diodes in Combination

In addition to what has already been mentioned, some further experimentation was done with combinations of FD-300 diodes. These data are only preliminary. A series combination of two diodes was tried in the circuit of Figure 6-4, but the best performance observed was unstable, noisy, and inefficient. Parallel combinations of diodes with comparable V_B's usually yielded improved stability, and less noise, with only a small increase in total I_2 and consequently less current per diode. The overall efficiency was generally reduced (except as noted previously). It is possible that with a circuit having a high impedance at n = 2 the opposite might be true. Kostishack observed increased overall efficiency and more noise with diodes in parallel.[13]

A novel hook-up of two diodes was suggested and investigated in part. As shown in Figure 6-9(a), the two diodes are biased in series, but to the RF circuit they appear in parallel. If the "DC Block" in Figure 6-9(a) is a series open-circuit stub, this circuit will achieve the original intentions of the circuit of Figure 6-4 (viz., forcing a high impedance to be seen by the diode at certain harmonics regardless of tuning further down the line) without requiring any troublesome bias chokes or inductors. At present, this is seen as the principal application for the diode arrangement of Figure 6-9(a).

To evaluate this bias scheme, we connected two diodes with comparable V_B's as shown in both Figures 6-9(a) and (b). A commercial broad-band "DC Block" was used, having, perhaps, as much as 0.2-dB loss. The double-stub tuner was optimized to give maximum output power in the fundamental. Tentative data are as follows:

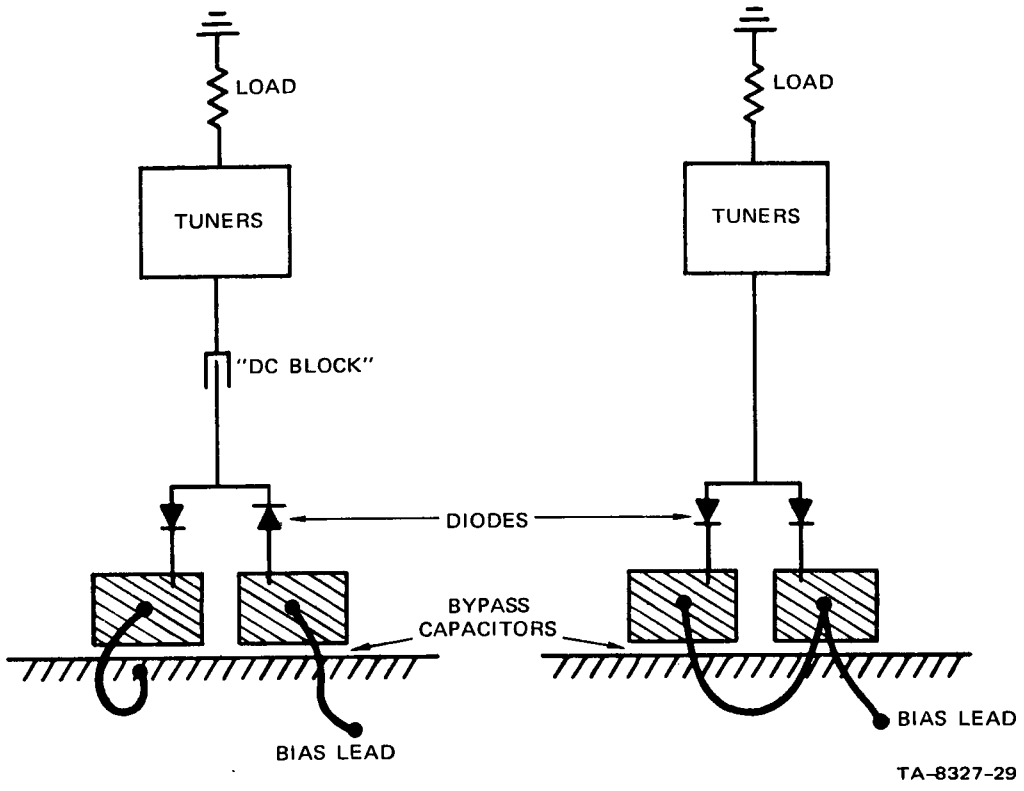

(a) BIASING IN SERIES, PARALLELING FOR RF

(b) CONVENTIONAL PARALLELING

FIGURE 6-9 NOVEL HOOKUP OF TWO AVALANCHE DIODES

	Figure 6-9(a)	Figure 6-9(b)
f_1	= 600 MHz	635 MHz
P_1	= 5 W	6 W
η_1	= 0.7 percent	2 percent
V_2	= 320 V (across 2 diodes)	140 V
I_2	= 2.3 A	2.2 A (2 diodes)
Remarks:	Noisy, with lots of state-switch failures	Clean, stable HCS ourput

The data are too incomplete for comment. Future investigation should use an improved DC Block or the series open-circuit stub

mentioned earlier. The diodes should also be selected such that each has a similar I_2 operating point for maximum efficiency at a given frequency.

7. CONCLUSIONS

The theoretical understanding of high efficiency oscillations in an avalanche diode has been increased by examining three modes of oscillation and by developing approximate analytical solutions for each mode. A semianalytical solution for TRAPATT oscillations in a PIN avalanche diode was obtained by considering seven different phases of one cycle and assuming a square-wave current driving the diode. It has been shown that a traveling avalanche zone does not form as in the P^+NN^+ structure. The resultant voltage waveform is qualitatively similar to that obtained for a P^+NN^+ diode for an assumed square-wave current. The highest efficiencies were obtained for the largest drive currents and the smallest saturation currents. In many instances the square-wave drive current does not correspond to the diode being embedded in a passive circuit.

Based on the analytical solution, an approximate computer model of TRAPATT oscillations in a PIN avalanche diode was developed. This model has a computer running time at least two orders of magnitude less than more exact computer models. The model was used to calculate the diode voltage waveform and operating characteristics for several different assumed diode current waveforms. A square-wave current was approximated by using the first few terms of its Fourier series. It was found that both the period of oscillation and the dc-to-RF conversion efficiency decreased from those of a corresponding square wave. The higher harmonics are necessary for high efficiency because they allow the current to rise rapidly and drive the diode far into avalanche before appreciable charge is generated. Subsequently a dense plasma

is formed, forcing the diode voltage to be very low while the current remains high. Equally important for high efficiency is that the current be zero or nearly zero over the second half of a period so that the diode voltage remains high over this half of the cycle.

There are numerous voltage and current waveforms consistent with the device physics of an avalanche diode that corresponds to high-efficiency operation at the fundamental frequency. Not all such sets of waveforms, however, correspond to the device being embedded in a passive microwave circuit with only a dc source. The results of Section 2 show, qualitatively at least, that high-efficiency oscillations are possible with currents containing only one or two harmonics.

A second mode of high efficiency oscillations which is very similar to the ordinary TRAPATT mode was described and a semianalytical solution developed for the voltage for a rectangular current waveform. Portions of a cycle of oscillation were shown to be identical with those of the ordinary TRAPATT mode, but during avalanche the external current was assumed to be small. No calculations have been made for this mode although it is believed that it may correspond to experimental observations of moderately high and high efficiency oscillations.

Another significant result obtained in this report is the development of a model of high efficiency oscillations in a PIN diode for extremely large current densities which causes avalanche to occur over a major portion of a half cycle. This mode has not been discussed in the literature before. We showed that the output power of the device increases proportionally with the magnitude of the current with only a relatively small decrease in dc to rf conversion efficiency. In practice operation in this mode would require circuits with lower impedances and better heat dissipation.

An approximate solution for the voltage waveform in a PIN diode was also derived using an idealized step function for the ionization coefficient. The utility of this approximate model is that it can be used to indicate possible patterns of avalanche regions in the space-time plane. Analytical solutions can then be written for each region and the solutions matched at the boundaries between the avalanching and nonavalanching regions. Estimates of the current and voltage variation across a diode were deduced without computation for one permissible pattern. It was shown that within limitations the current waveform could be selected for efficient device operation.

Experimental observations of high efficiency oscillations were made using inexpensive diodes. The highest efficiencies and output powers were comparable to those reported by others for these diodes except for the anomalous results reported by Kostishak.[13] Simpler circuits than those originally proposed for independent harmonic tuning were used. The efficiencies obtained with the channel dropping filters for harmonic tuning were typically less than a few percent. These results, however, are inclusive because the circuit losses were too large and the bias supply inadequate for these early measurements. A disadvantage of using filters to separate the harmonics for independent tuning is that the tuning elements are a long distance away from the diode. The tuning becomes more critical and the losses are increased. Ideally, impedance matching for each harmonic should be accomplished next to the diode for optimum efficiency.

The measured circuit impedances up to at least four harmonics of those circuits which gave highest efficiencies did not correspond to the theoretical results for TRAPATT oscillations obtained in Section 2 of the report. This can be explained by the fact that many different voltage and current waveforms are possible; all of these lead to high

efficiency operation. In our analyses we assumed current waveforms composed of a few harmonics and calculated the corresponding voltage waveform which always had several higher harmonics. An equally valid method would be to assume a voltage waveform composed of one or a few harmonics and calculate the corresponding current waveform which may be rich in harmonic content. The latter corresponds to circuits with very low impedances at the higher harmonics. This is more representative of the experimental observations. On the other hand, analysis of Kostishack's[13] circuit indicates that the impedances at the even harmonics are large, which corresponds more closely with the theoretical results of Section 2.

8. RECOMMENDATIONS

In as much as the experiments with tuning at multiple frequencies were inconclusive, it is recommended that these be repeated with the improved bias supply now available. It is also recommended that simpler circuits be designed which take into account the desired impedances at some of the higher harmonics but do not provide flexibility in tuning. The impedance matching could be designed to be close to the diode and the loss could be kept small in these circuits. By building a limited number of these circuits, one could verify the theoretical results obtained to date.

In the course of the experimental work several observations were made which led to some interesting theoretical and experimental questions. On any one bias pulse the time that the diode was in a low conduction state before switching into high efficiency oscillations appeared to be temperature dependent. For pulse applications this delay time would be important. Controlled experiments should help to identify the critical parameters affecting this delay time.

It was also noticed that from bias pulse to bias pulse the diode did not always begin to oscillate at the same time. In fact, on some pulses the diode did not break into oscillation at all. These effects may also be thermal in nature. A significant problem in the high efficient modes of operation is the noisy nature of the oscillations. It is recommended that a significant theoretical and experimental effort be directed toward understanding the noise properties of high efficiency oscillations in avalanche diodes.

Although the theoretical results obtained in this report are significant, they are not complete. First, more extensive calculations should be made of the second high efficiency mode and the mode with multiple avalanche discussed in this report. These calculations could be compared with the ordinary TRAPATT mode and guidelines developed for optimum operation and corresponding circuit design. The simple but economical computer program for TRAPATT oscillations in a PIN diode should be extended to include other doping distributions and nonequal ionization coefficients and carrier velocities. A similar economical computer program should be developed to calculate the diode current when the voltage waveform is specified.

Accurate and detailed computation of the operating parameters of an avalanche diode oscillating in a high efficiency mode require a complex computer program like UNSAT developed for this contract. However, the running time is extensive when the charge carrier and field gradients are large as they are in the TRAPATT mode. However these gradients usually exist only over a small portion of the diode depletion region. It may be possible by more elaborate programming to incorporate a variable step size in the spatial coordinate. Where the gradients are large the step size would be small and where they are small the step size would be large. This technique would permit accurate calculations more economically.

Appendix A

NORMALIZED VARIABLES

Below is the normalization used and the values each variable should be multiplied by to obtain unnormalized values.

Unit	Expression	Value
Length	w	10^{-3} cm
Time	w/v_s	10^{-10} second
Charge Density	N_o	10^{-15} cm^3
Current	qv_sN_o	1.6×10^3 A/cm^2
Field	wqN_o/ϵ	1.6×10^5 volts/cm
Unit Charge	q	1.6×10^{-19} coulombs
Voltage	w^2qN_o/ϵ	160 volts
Impedance	$w^2/\epsilon v_s$	0.1 ohms-cm^2
Power	$(qwN_o)^2 v_s/\epsilon$	2.56×10^5 watts/cm^2

Appendix B

AN ECONOMICAL COMPUTER PROGRAM FOR TRAPATT OSCILLATIONS

In this appendix we describe an approximate time-domain model for TRAPATT oscillations in a PIN avalanche diode. During these portions of a cycle when the E-field is effectively uniform, Eqs. (2-8) and (2-10) of Section 2 express the dynamics of the total internal charge and the terminal voltage of the diode. When a trapped plasma has formed and is being removed, the electric field increases from E_p in the plasma to a larger value at the edges of the depletion layer because of the residual charge. Let x be the distance from the right-hand edge of the depletion layer to the corresponding edge of the trapped plasma. It is also the distance from the left-hand edge to the plasma. Then, during the field depression phase of the TRAPATT cycle, x and the diode terminal voltage are given by the following two equations.

$$\frac{dx}{dt} = v \quad , \tag{B-1}$$

$$V = n_r x^2 + E_p \quad . \tag{B-2}$$

To a first approximation the residual charge, n_r, is equal to J/v_s if the time variations are not too rapid. This has been verified by more accurate computer simulations using program UNSAT. Thus, Eq. (B-2) becomes

$$V(t) = \frac{J(t)}{v_s} x^2 + E_p(t) \quad . \tag{B-3}$$

During the plasma extraction phase, the edges of the plasma move at a plasma velocity, v_p; thus Eqs. (B-1) and (B-3) become

$$\frac{dx}{dt} = v_p = \frac{J}{Q_p} \quad , \tag{B-4}$$

$$V(t) = \frac{J(t)}{v_s} x^2 + E_p(t) \quad , \tag{B-5}$$

where $E_p(t)$ is obtained by inverting the expression for $v_p = \frac{E}{E+0.1}$. Equations (B-1) through (B-5) are valid when $Q > J/v_s$. When the charge density is so small that the particle current (at a saturated velocity) is less than the external current, the E-field is nearly uniform across the depletion layer, and Eqs. (2-17) and (2-19) are applicable.

A computer program (Called modified SMPAL) was written which integrates Eqs. (2-17) and (2-19) numerically and uses Eqs. (B-1) and (B-3) or (B-4) and (B-5) as appropriate during a cycle. Note that in this formulation the more exact expression for the ionization coefficient can be used as well as an analytic expression for the velocity as a function of the electric field.

The validity of modified SMPAL was verified by comparing the results with a more exact computer simulation, UNSAT. Figure B-1 shows the charge generation, G, as computed by both UNSAT and modified SMPAL assuming that the diode current was constant. The generation predicted by the modified SMPAL is too large. This is a consequence of assuming that the charges drifting out of the depletion layer can be modeled by an exponential decay. In the more exact solution, UNSAT, when the diode is biased below avalanche, there is some very small but finite charge generated which increases the charge density over that corresponding to the saturation current. On the other hand, in modified SMPAL the

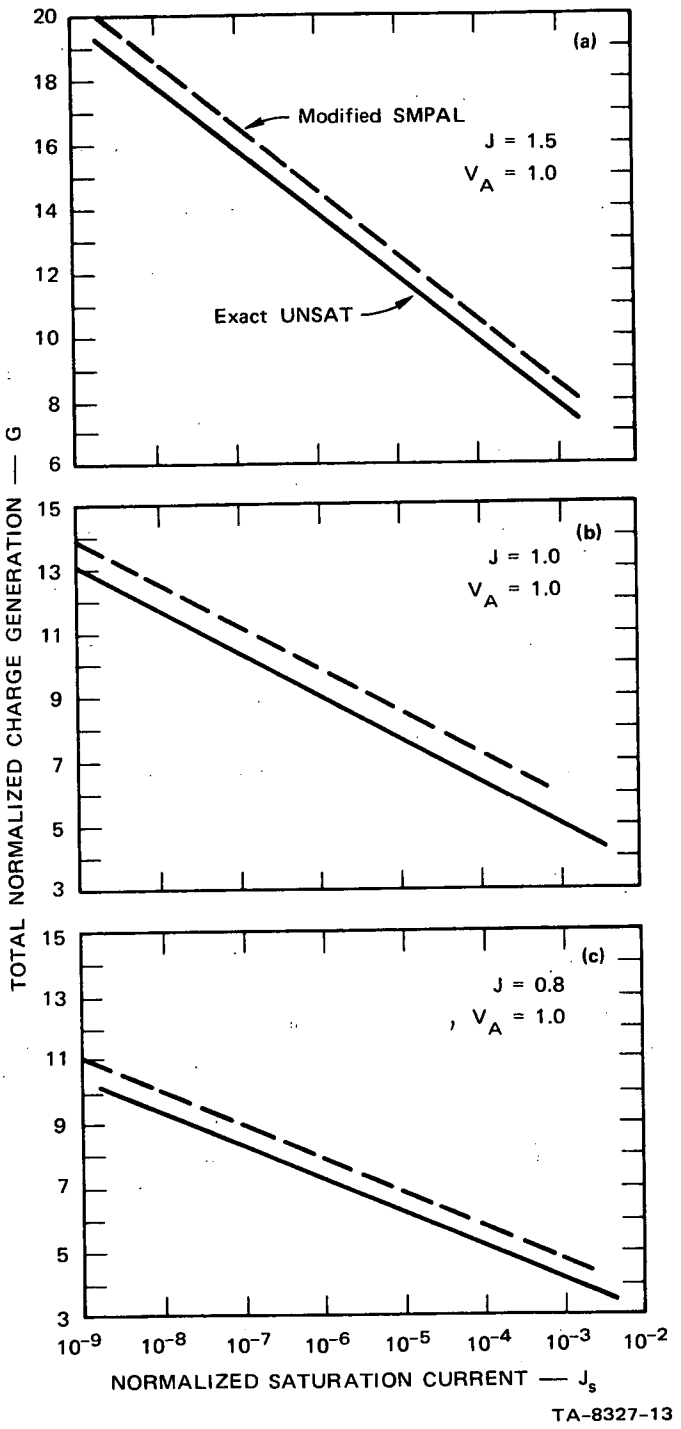

FIGURE B-1 TOTAL CHARGE GENERATED IN A PIN DIODE AS COMPUTED BY THE COMPUTER PROGRAMS UNSAT AND MODIFIED SMPAL FOR A CONSTANT CURRENT

charge decays when α is less than unity. Therefore, the charge in modified SMPAL will initially decrease from the saturation level when we start with the E-field below avalanche. With a smaller charge density (equivalently saturation current) the diode eventually charges up to a higher voltage, increasing the total charge generated. We can compensate for the differences in generated charge in the two programs by using a larger value of J_s in modified SMPAL than the corresponding value in program UNSAT. By doing this we are able to compare the voltage waveforms computed by both programs during the initial charge-up and generation phases of a TRAPATT cycle. Figure B-2 shows the voltage waveforms during the generation and field depression phases of a TRAPATT cycle as computed by modified SMPAL and UNSAT for two different current levels. The saturation currents used in each program were obtained by choosing the same value of generation for each and using the corresponding values

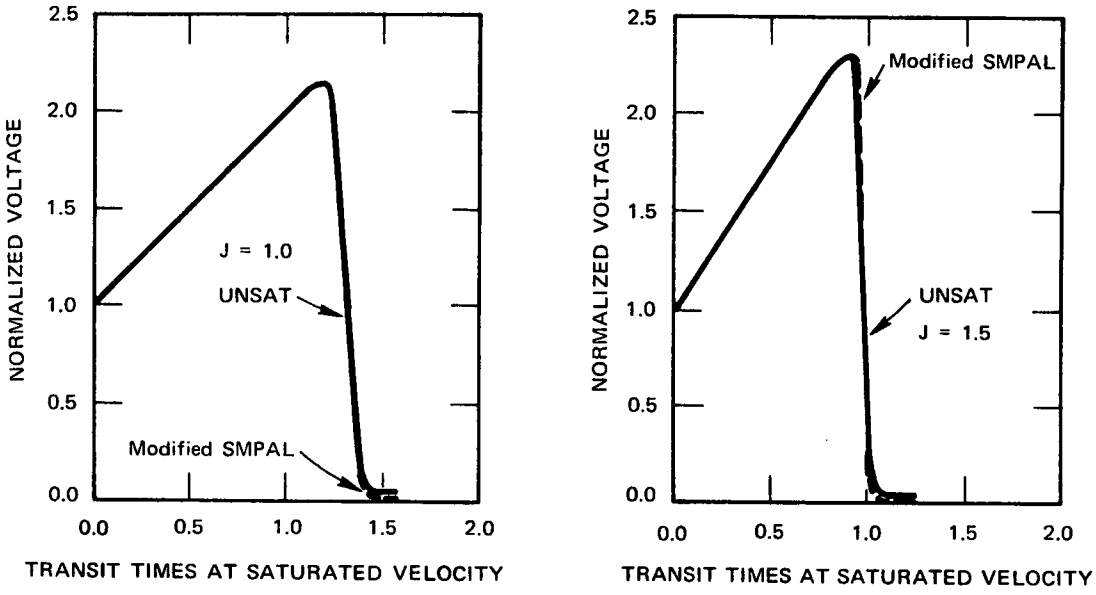

FIGURE B-2 COMPARISON OF THE TERMINAL VOLTAGE OF A PIN DIODE DURING THE INITIAL CHARGE-UP AND GENERATION PHASES OF A TRAPATT CYCLE AS COMPUTED BY PROGRAMS UNSAT AND MODIFIED SMPAL

of J_s given by the respective curves in Figure B-1. The agreement between the results from the two programs is excellent. The waveforms were not compared over an entire TRAPATT cycle because the exact solution was too expensive to run.

REFERENCES

1. H. J. Prager, K.K.N. Chang, and S. Weisbrod, "High-Power, High-Efficiency Silicon Avalanche Diodes at Ultra-High Frequencies," Proc. IEEE (Letters), Vol. 55, pp. 586-587 (April 1967).

2. R.L. Johnston, D.L. Scharfetter, and D.J. Bartelink, "High Efficiency Oscillations in Germanium Avalanche Diodes Below the Transit-Time Frequency," Proc. IEEE (Letters), Vol. 56, pp. 1611-1613 (September 1968).

3. A.S. Clorfeine, R.J. Ikola, and L.S. Napoli, "A Theory for the High-Efficiency Mode of Oscillation in Avalanche Diodes," RCA Review, Vol. 30, pp. 397-421 (September 1969).

4. B.C. DeLoach, Jr., and D.L. Scharfetter, "Device Physics of TRAPATT Oscillators," IEEE Trans. on Electron Devices, Vol. ED-17, pp. 9-21 (January 1970).

5. M.W. Muller and H. Guckel, "Negative Resistance and Filamentary Currents in Avalanching Silicon p^+-i-n^+ Junctions," IEEE Trans. on Electron Devices, Vol. ED-15, No. 8, pp. 560-568 (August 1968).

6. D.L. Scharfetter and H.K. Gummel, "Large Signal Analysis of a Silicon Read Diode Oscillator," IEEE Trans. on Electron Devices, Vol. ED-16, pp. 67-77 (January 1969).

7. C.P. Snapp, L.F. Eastman, and C.A. Lee, "Multifrequency Effects and High-Efficiency Oscillations in Avalanche Diodes," Cornell University Technical Report, RADC-TR-70-102, pp. 66-80 (July 1970).

8. K.G. McKay, "Avalanche Breakdown in Silicon," Physical Review, Vol. 94, pp. 877-884 (15 May 1954).

9. R. Courant and D. Hilbart, Methods of Mathematical Physics, Vol. 2, Chapter 5, Section 5 (Interscience, New York, 1962).

10. A. Erdelize, Tables of Integral Transforms, Vol. 1, Chapters 4 and 5 (McGraw-Hill, New York, 1954).

11. G.N. Watson, A Treatise on the Theory of Bessel Functions, Section 3.31 (Cambridge, 1948).

12. G.L. Matthaei and E.G. Cristal, "Theory and Design of Diplexers and Multiplexers," in Advances in Microwaves, Vol. 2, pp. 296-304 (Academic Press, Inc., N.Y., 1967).

13. D.F. Kostishack, "UHF Avalanche Diode Oscillator Providing 400 Watts Peak Power and 75 Percent Efficiency," Proc. IEEE (Letters), Vol. 58, p. 1282 (August 1970).

14. R.J. Chaffin and E.P. EerNisse, "A Poor Man's TRAPATT Oscillator," Proc. IEEE (Letters), Vol. 58, pp. 173-174 (January 1970).

15. R.L. Johnston and D.L. Scharfetter, "Low-Frequency High-Efficiency Oscillations in Germanium IMPATT Diodes," IEEE Trans. on Electron Devices, Vol. ED-16, No. 11, pp. 905-911 (November 1969).

16. D. Parker, "TRAPATT Oscillations in a PIN Avalanche Diode," (to be published in IEEE Trans. on Electron Devices, May 1971).

17. D. Parker, "TRAPATT Oscillations with a Half-Wave Rectified Sine Wave Current," (to be published in Proc. IEEE (Letters), 1971).